AD-A108 777 RCA LABS PRINCETON NJ F/G 7/4

HIGH-ENERGY ION IMPLANTATION FOR MULTIGIGABIT-RATE GAAS INTEGRA--ETC(U)

OCT 81 S G LIU, E C DOUGLAS, C P WU N00014-78-C-0367

UNCLASSIFIED PRRL-81-CR-32 NL

1 of 2

AD

A108777

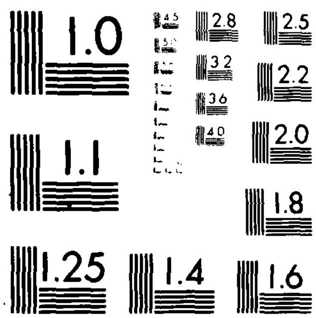

MICROCOPY RESOLUTION TEST CHART
NATIONAL BUREAU OF STANDARDS 1963 A

8

12

LEVEL V

AD A108777

HIGH-ENERGY ION IMPLANTATION FOR MULTIGIGABIT-RATE GaAs INTEGRATED CIRCUITS

RCA Laboratories
Princeton, New Jersey 08540

OCTOBER 1981

FINAL REPORT

for the period 1 May 1978 to 30 June 1981

Prepared for
Office of Naval Research
Arlington, Virginia 22217
Contract No. N00014-78-C-0367
Contract Authority: NR 383-046

UNCLASSIFIED

SECURITY CLASSIFICATION OF THIS PAGE (When Data Entered)

REPORT DOCUMENTATION PAGE		READ INSTRUCTIONS BEFORE COMPLETING FORM
1. REPORT NUMBER	2. GOVT ACCESSION NO. AD-A108	3. RECIPIENT'S CATALOG NUMBER 777
4. TITLE (and Subtitle) HIGH-ENERGY ION IMPLANTATION FOR MULTIGIGABIT-RATE GaAs INTEGRATED CIRCUITS		5. TYPE OF REPORT & PERIOD COVERED Final Report (5-1-78 to 6-30-81)
		6. PERFORMING ORG. REPORT NUMBER PRRL-81-CR-32
7. AUTHOR(s) S. G. Liu, E. C. Douglas, C. P. Wu, C. W. Magee, and S. Y. Narayan		8. CONTRACT OR GRANT NUMBER(s) N00014-78-C-0367
9. PERFORMING ORGANIZATION NAME AND ADDRESS RCA Laboratories Princeton, New Jersey 08540		10. PROGRAM ELEMENT, PROJECT, TASK AREA & WORK UNIT NUMBERS PE 62762N RF 54-582-001 NR 383-046
11. CONTROLLING OFFICE NAME AND ADDRESS Office of Naval Research Arlington, Virginia 22217		12. REPORT DATE October 1981
		13. NUMBER OF PAGES 164
14. MONITORING AGENCY NAME & ADDRESS (if different from Controlling Office)		15. SECURITY CLASS. (of this report) Unclassified
		15a. DECLASSIFICATION/DOWNGRADING SCHEDULE N/A

16. DISTRIBUTION STATEMENT (of this Report)

Approved for public release; distribution unlimited.

17. DISTRIBUTION STATEMENT (of the abstract entered in Block 20, if different from Report)

18. SUPPLEMENTARY NOTES

19. KEY WORDS (Continue on reverse side if necessary and identify by block number)

High-energy ion implantation
Multigigabit-rate GaAs ICs
Semi-insulating GaAs
Laser annealing

20. ABSTRACT (Continue on reverse side if necessary and identify by block number)

This Final Report describes results of an investigation of the implantation and activation of donors in semi-insulating (SI) GaAs under Contract No. N00014-78-C-0367. These investigations include implantation of ^{28}Si up to an energy of 1.2 MeV and annealing of implanted layers by (1) laser irradiation, (2) electron beam, and (3) radiation from a halogen lamp. The highlights of this report are summarized below.

DD FORM 1 JAN 73 1473

UNCLASSIFIED

SECURITY CLASSIFICATION OF THIS PAGE (When Data Entered)

299CC0

20. (1) A substrate pretreatment technique has been developed that has resulted in enhanced activation and/or mobility for the implanted n-GaAs layer. The pretreatment consists of ^{40}Ar implantation into SI GaAs substrates at appropriate energy and fluence prior to implantation of ^{28}Si and subsequent thermal annealing.

(2) Uniformly doped 0.2- to 1.0-μm n-layers having mobilities of 4700 to 4500 cm^2/V-s with carrier concentrations of 0.5-2x10^{17} cm^{-3} and uniformly doped 1-μm n^+-layers having a mobility of 3000 cm^2/V-s with a carrier concentration of 1x10^{18} cm^{-3} were produced by multiple implantation and capless thermal annealing under arsenic overpressure.

(3) Studies of Cr redistribution using SIMS analysis in capless-annealed Si implants in SI GaAs substrates show a strong dependence of Cr redistribution on implant dose. No significant redistribution was found for doses typically used for FET fabrication. At higher dose levels, pulsed-laser-irradiated samples show lower Cr redistribution than thermally annealed samples. Studies on ^{40}Ar-implanted samples showed Cr-redistribution effects similar to that of ^{28}Si-implanted GaAs.

(4) Investigation of $^{28}Si^+$ and $^{32}S^+$ implanted capless-annealed GaAs at the low-implant energy (<300 keV) shows that carrier concentration is limited to about 3x10^{18} cm^{-3} at the high-dose level and about 5x10^{16} cm^{-3} at the low-dose level. A cutoff fluence of ~2x10^{12} cm^{-2} at 200-keV was observed typically in Bridgman Cr-doped GaAs substrates used for implant.

(5) The surface of the as-implanted SI GaAs substrates exhibits electrical conduction as a result of lattice disorders. The dependence of the sheet conductivity on implantation dose was determined experimentally. The conductivity provides a convenient way to monitor the as-implanted GaAs.

(6) High-dose Si-implanted GaAs was annealed using high-power pulsed laser and electron beams. Electrical activation of high-dose-implanted samples is many times higher in laser-annealed samples than for those thermally annealed.

(7) Unalloyed ohmic contacts were formed on laser-irradiated GaAs using AuGe/Ni or Ti/Pt/Au metallization. The crystallinity of laser (or electron beam) irradiated Si-implanted GaAs was studied using reflection high-energy diffraction (RHEED) analysis.

(8) Impurity distribution in as-implanted, thermally annealed, and laser annealed samples has been investigated by SIMS analysis. The amount of impurity redistribution depends on the energy and dose of implantation and on the energy density of the laser pulse used to anneal the sample.

(9) Si-implanted GaAs samples were successfully annealed with good mobility and activation using a short-duration (<10 s) radiant pulse produced by a quartz halogen lamp.

(10) The success in producing high-quality n-GaAs layers by direct implant of ^{28}Si into SI GaAs was demostrated in a concurrent program by fabrication of high-performance GaAs FET operating up to 26 GHz.

PREFACE

This Final Report describes the research carried out at the Microwave Technology Center of RCA Laboratories during the period 1 May 1978 to 30 June 1981 in a program sponsored by the Office of Naval Research under Contract No. N00014-78-C-0367. F. Sterzer is the Center's Director and S. Y. Narayan is the Project Supervisor. The Project Scientist is S. G. Liu. Other Members of Technical Staff who contributed to the program are C. P. Wu, E. C. Douglas, and C. W. Magee. The Associate Staff contributing to this program are F. Kolondra, S. Jain, and F. C. Duigon. S. Manasian and J. Nering of Fusion Energy Corporation, Princeton, NJ, were responsible for the Van de Graaff generator used for high-energy implantation. J. T. McGinn and J. H. Thomas of RCA Laboratories carried out the RHEED and Auger analyses, respectively.

The authors express their appreciation to M. N. Yoder of ONR (Contract Monitor) for his advice and encouragement throughout the course of this program.

TABLE OF CONTENTS

TABLE OF CONTENTS (Continued)

TABLE OF CONTENTS (Continued)

LIST OF ILLUSTRATIONS

LIST OF ILLUSTRATIONS (Continued)

LIST OF ILLUSTRATIONS (Continued)

LIST OF ILLUSTRATIONS (Continued)

LIST OF ILLUSTRATIONS (Continued)

LIST OF ILLUSTRATIONS (Continued)

LIST OF ILLUSTRATIONS (Continued)

LIST OF TABLES

LIST OF TABLES (Continued)

SECTION I

INTRODUCTION

This report describes our work during the past 38 months on the ONR-sponsored program started in May 1978 [1]. The objectives of the program are to: (1) investigate high-energy ion implantation of donors into GaAs for multigigabit-rate GaAs integrated-circuit (IC) development and (2) to study the use of high-power lasers and other techniques for removing lattice damage and activating implanted species. GaAs ICs require the selective definition of n-layers in semi-insulating (SI) GaAs for the fabrication of active devices such as FETs, TELDs, and Schottky-barrier diodes [2-8]. In order to fabricate such device elements, a capability for realizing n-layers with doping ranging from 10^{16} to $5x10^{18}$ cm^{-3} and thicknesses from 1 to 0.15 μm is required.

Until the inception of this program, the major effort on ion implantation into GaAs has been at energies less than 500 keV, which limits the implant depth to typically less than several hundred nanometers. During this program, high-energy implantation of Si into SI GaAs at energies of 30 to 1200 keV has

1. S. G. Liu, E. C. Douglas, and C. P. Wu, "High-Energy Ion Implantation for Multigigabit-Rate GaAs Integrated Circuit," Annual Report, May 15, 1978 to May 14, 1979, also May 15, 1979 to June 30, 1980, under Contract No. N00014-78-C-0367.
2. B. M. Welch, F. H. Eisen, and J. A. Higgins, "Gallium Arsenide Field Effect Transistors by Ion Implantation," J. Appl. Phys. 45, 3685 (1974).
3. E. Stoneham, T. S. Tan, and J. Gladstone, "Fully Ion-Implanted GaAs Power FETs," 1977 IEDM Digest, p. 330.
4. R. A. Murphy et al., 1974 IEEE S-MTT Int. Symp., New York, p. 345.
5. C. O. Bozler et al., "High-Efficiency Ion-Implanted Lo-Hi-Lo GaAs IMPATT Diodes," Appl. Phys. Lett. 29, 123 (1976).
6. T. Mizutani and K. Kurumada, "GaAs Planar Gunn Digital Devices by Sulfur Ion-Implantation," Electron. Lett. 11, 639 (1975).
7. L. C. Upadhyayula, S. Y. Narayan, and E. C. Douglas, "Fabrication of 3-Terminal Transferred-Electron Logic Devices by Proton Bombardment for Device Isolation," Electron. Lett. 11, 201 (1975).
8. B. M. Welch and R. C. Eden, "Planar GaAs Integrated Circuits Fabricated by Ion Implantation," Technical Digest, Int. Elec. Devices Meeting, 1977, p. 205.

been investigated [9-10]. Projected ranges and straggles have been measured by secondary ion-mass spectrometry (SIMS). Based on these measurements, we have produced up to ~1-μm-thick n-type GaAs layers at doping levels of $\sim 5\times10^{16}$ to $1\times10^{18}\,cm^{-3}$ by multiple-energy Si implantation. These results are described in Section III.

One of the major problems of ion implantation into GaAs is that the material begins to dissociate at the commonly used anneal temperatures which are in the 800 to 1000°C range. In order to prevent problems associated with dissociation, an encapsulant is normally used on the implanted wafer during annealing.

We have developed an operationally simple postimplantation annealing process without encapsulation on the wafer [1,9]. The anneal is carried out under an arsenic overpressure which prevents decomposition of GaAs and results in an excellent surface morphology. In a concurrent company-sponsored program, we have used wafers with ^{28}Si implanted directly onto commercially available SI GaAs substrates to fabricate power MESFETs that operate at frequencies as high as 26 GHz [11]. The implantation and annealing process and the results on Si and S implantation into GaAs substrates at energy levels below 300 keV are presented in Section II.

The damage caused by implantation can be removed by using annealing techniques other than furnace annealing, viz, the laser beam, [12-15], the

---

9. S. G. Liu, E. C. Douglas, C. P. Wu, C. W. Magee, S. Y. Narayan, S. T. Jolly, F. Kolondra, and S. Jain, "Ion-Implantation of Sulfur and Silicon in GaAs," RCA Review 41, 227 (1980).
10. S. G. Liu, E. C. Douglas, C. W. Magee, F. Kolandra, and S. Jain, "High-Energy Implantation of Si in GaAs," Appl. Phys. Lett. 37, 79 (1980).
11. G. C. Taylor, S. G. Liu, and D. Bechtle, "Ion-Implanted K-Band GaAs Power FET," IEEE/MTT Intnl. Microwave Symp. Digest, June 1981.
12. E. I. Shtyrkov, I. B. Khaibullin, M. M. Zaripov, M. F. Galyatudinov, and R. M. Bayazitov, "Local Annealing of Implantation Doped Semiconductor Layers," Sov. Phys. Semicond. 9, 1309 (1976).
13. W. L. Brown, J. A. Gdovchenko, K. A. Jackson, L. C. Kimerling, H. J. Leamy, G. L. Miller, J. M. Poate, J. W. Rodgers, G. A. Rozgonyi, T. T. Sheng, T. N. C. Venkatesan, and G. K. Celler, "Laser-Annealing of Ion-Implanted Semiconductors," Proc. on Rapid Solidification Proc. - Principles and Technologies, Reston, VA, Nov. 1977.
14. R. T. Young, C. W. White, G. J. Clark, J. Narayan, W. H. Christie, M. Murakami, P. W. King, and S. D. Karmer, "Laser Annealing of Boron-Implanted Silicon," Appl. Phys. Lett. 32, 139 (1978).
15. S. U. Compisano, I. Catalano, G. Foti, E. Rimini, F. Eisen, and M. A. Nicolet, "Laser Reordering of Implanted Amorphous Layers in GaAs," Solid-State Electron. 21, 485 (1978).

electron beam [16], or the radiation pulse techniques [17]. Very high carrier concentrations have been obtained in high-dose implanted GaAs after annealing by high-power pulsed laser beams [18,19]. We have measured activation efficiencies in laser-annealed Si-implanted GaAs that are more than an order of magnitude higher than for samples annealed thermally. Ohmic contacts have been formed on laser-irradiated GaAs surfaces without subsequent treatment [20]. These results are described in Section VII, which also includes the following: the optical absorption study in Si-implanted GaAs before and after laser irradiation, the depth distribution of impurity concentration using SIMS measurements, and studies on the surface morphology and crystallinity of laser and electron-beam-annealed GaAs wafers.

Redistribution of Cr in thermally annealed SI GaAs substrates with or without implanted impurities has been reported recently [21-24]. We have studied the dependence of Cr redistribution on fluences in thermally annealed SI GaAs substrates that were implanted with Si at energies of 200 and 600-1000 keV [9]. Similar studies were made on inert Ar-implanted and thermally annealed GaAs and have shown similar Cr-redistribution dependence on the implant dose. A broad, well-defined Cr-depletion channel forms below the wafer surface when the SI GaAs wafer is appropriately implanted with Ar and annealed. These results are described in Section VI.

---

16. J. L. Tandon and F. H. Eisen, "Pulsed Annealing of Implanted Semi-Insulating GaAs," AIP Conf. Proc. 50, 616 (1979).
17. M. Arai, K. Nishiyama, and N. Watanabe, "Radiation Annealing of GaAs Implanted with Si," Jpn. J. Appl. Phys. 20, L124 (1981).
18. S. G. Liu, C. P. Wu, and C. W. Magee, "Annealing of Ion-Implanted GaAs with Nd:Glass Laser," AIP Conf. Proc. 50, 603 (1979).
19. B. J. Sealy, M. H. Badawi, S. S. Kular, and K. G. Stephens, "Electrical Properties of Laser-Annealed Donor-Implanted GaAs," Electron. Lett. 14, 720 (1978).
20. S. G. Liu, C. P. Wu, and C. W. Magee, "Annealing of Ion-Implanted GaAs with a Pulsed Ruby Laser," Symp. Proc. on Laser and Elec. Beam Processing of Materials, Academic Press, 1980, p. 341.
21. A. M. Huber, G. Morillot, and N. T. Linh, "Chromium Profiles in Semi-Insulating GaAs after Annealing with a Si_3N_4 Encapsulant," Appl. Phys. Lett. 34, 858 (1979).
22. R. G. Wilson, P. K. Vasuder, D. M. Jamba, C. A. Evans, Jr., and V. R. Deline, "Chromium Concentrations, Depth Distributions and Diffusion Coefficient in Bulk and Epitaxial GaAs and in Si," Appl. Phys. Lett. 36, 215 (1980).
23. J. Kasahara and N. Watanabe, "Redistribution of Cr in Capless-Annealed GaAs Under Arsenic Pressure," Jpn. J. Appl. Phys. 19, L151 (1980).
24. C. A. Evans, Jr. and V. R. Deline, "Redistribution of Cr During Annealing of ^{80}Se-Implanted GaAs," Appl. Phys. Lett. 35, 291 (1979).

Last but not least, we have studied Si implantation into SI GaAs substrates pretreated with high-energy ^{40}Ar implants and developed a substrate pretreatment technique that can have a major impact on the successful development of GaAs integrated circuits for microwave and multigigabit-rate logic applications. This pretreatment technique consists of ^{40}Ar implantation into SI GaAs substrates at appropriate energy and fluence prior to implantation of ^{28}Si and subsequent furnace anneal. This substrate pretreatment has demonstrated improved activation efficiency and/or mobility for low-dose ($2x10^{12}$ cm^{-2} at 200 keV) Si-implanted furnace-annealed n-layers. Normally, at this low Si-implant fluence level, referred to as the activation threshold, the implanted/annealed layer in the Cr-doped SI substrate has very low activation efficiency and very poor mobility. This ^{40}Ar pretreatment also enhances activation and/or mobility in medium-dose ($6x10^{12}$ cm^{-2}, 200 keV) implanted n-layers. This effect has, to different extents, been observed in Bridgman, LEC Cr-doped, LEC undoped, and Cr-O-doped SI GaAs substrates. Details of implanted n-layers on these substrates, with or without Ar pretreatment, are described, respectively, in Sections V and IV. Possible mechanisms for activation/mobility enhancement are discussed.

SECTION II

LOW-ENERGY (<300 keV) IMPLANTATION IN GaAs

This section describes ion-implantation of sulfur, silicon, and selenium into GaAs substrates and the thermal-annealing process following implantation. To produce an *n*-type layer on GaAs, implantation of S, Se, Te, Si, Sn, and Ge have been used and have been reported previously [25-27]. An annealing step is essential to anneal out the lattice defects caused by the impact of high-energy impurity atoms. To prevent dissociation of GaAs at the surface of the wafer, the sample is usually encapsulated during the high-temperature annealing. Various dielectric materials such as SiO_2 [28], Si_3N_4 [2], Al_2O_3 [29], AlN [30], the combination of SiO_2 and Si_3N_4 [31], or aluminum metal [32], have been used as encapsulants. The annealing temperature varies from 800 to 1100°C with dielectric encapsulation and is 700°C with Al encapsulation [32]. Annealing without encapsulation either in vacuum, sealed ampoule, or in a controlled atmosphere [33,34] has also been reported. In this section, we describe an operationally simple, capless-annealing process developed during this program.

---

25. F. H. Eisen et al., "Sulfur, Selenium, and Tellerium Implantation in GaAs," Inst. Phys. Conf. Proc. 28, 64 (1976).
26. R. K. Surridge and B. J. Sealy, "A Comparison of Sn-, Ge-, and Te-ion-implanted GaAs," J. Phys. D: Appl. Phys. 10, 911 (1977).
27. J. K. Kung, R. M. Melbon, and D. H. Lee, "GaAs FETs with Silicon-Implanted Channels," Electron. Lett. 13, 187 (1977).
28. A. G. Foyt, J. P. Donelly, and W. T. Lindley, "Efficient Doping of GaAs by Se^+ Ion Implantation," Appl. Phys. Lett, 14, 372 (1969).
29. W. K. Chu et al., Proc. 3rd. Intnl. Conf. on Ion Imp., Plenum Press, New York, 1973.
30. R. D. Pashley and B. M. Welch, "Tellurium-Implanted N^+ Layers in GaAs," Solid State Electron. 18, 997 (1975).
31. A. Lidow and J. F. Gibbons, "A Double-Layered Encapsulant for Annealing Ion-Implanted GaAs Up to 1100°C," Appl. Phys. Lett. 31, 158 (1977).
32. B. J. Sealy and R. K. Surridge, "A New Thin Film Encapsulant for Ion-Implanted GaAs," Thin Solid Films 26, L19 (1974).
33. A. A. Immorlica and F. H. Eisen, "Capless Annealing of Ion-Implanted GaAs," Appl. Phys. Lett. 29, 94 (1976).
34. D. H. Lee, R. M. Malbon, and J. M. Whelan, "Characteristics of Implanted N-type Profiles in GaAs Annealed in a Controlled Atmosphere," Ion-Implanted Semiconductors, ed. by F. Chernow et al., Plenum Press, New York, 1976.

A. SUBSTRATES

Cr-doped, SI (100)-oriented GaAs substrates were mostly used for our ion-implantation experiments. Studies were also made for implantation into vapor-phase-grown, high-resistivity epitaxial layers.* Semi-insulating substrates were obtained from various sources: Laser Diode (Metuchen, NJ), Morgan (Garland, TX), Sumitomo (Osaka, Japan), Mitsubishi-Monsanto, Metals Research (Royston, England), Crystal Specialties (Monrovia, CA), and Westinghouse (Pittsburgh, PA). The substrates are grown either by Bridgman or LEC (Liquid Encapsulated Czochralski) method and are Cr doped, undoped, or Cr/O doped. Ion-implantation results depend strongly on the quality of the substrate material. Some substrates may convert to either p-type or n-type following high-temperature annealing even in the absence of implanted ions. Substrate qualification is therefore desirable prior to implantation. A normal qualification test consists of implanting the sample with Ar (atomic weight close to that of silicon) and then annealing the sample at a given temperature and duration (typically 800 to 950°C for 15 to 30 min). A qualified SI substrate shows no conversion or activation following annealing.

Before ion implantation the SI substrates require careful cleaning and etching to produce a damage-free surface. The wafers were cleaned in organic solvents followed by DI-water rinsing and a 5- to 10-min etch in a solution of $H_2SO_4:H_2O_2:H_2O$ (4:1:1). The solutions were freshly mixed and cooled to room temperature. After being etched, the wafers were rinsed in DI water (>14 Mohm) and spun dry. The etching was done in a tilted rotating beaker to provide a uniformly etched surface. The layer removed was approximately 3 to 6 μm. In cases where implantation through a dielectric layer is required, the wafer surface is either coated with a chemical-vapor-deposited SiO_2 layer or a reactively sputtered Si_3N_4 layer. The layer thickness is 500 to 700 Å.

B. ION-IMPLANTATION OF $^{28}Si^+$, $^{32}S^+$, and $^{80}Se^+$ INTO GaAs

Low-energy ion-implantation experiments were performed in the 300-keV machine at RCA Laboratories. Silane (SiH_4) was used as the source gas in the rf ion source for Si implantation, solid sulfur or H_2S in the rf ion source was

*VPE layer grown by S. T. Jolly, RCA Laboratories, Princeton, N.J., Contract No. N00014-77-C-0542.

used for S implantation, and hydrogen selenide (H_2Se) was used as a source gas for Se implantation. The beam current during Si implantation is typically 0.1 μA for low-dose (10^{12} to 10^{13} cm^{-2}) and up to 10 μA for high-dose (10^{15} cm^{-2}) implants. A typical implantation at 200 keV with a dose of $1x10^{14}$ cm^{-2} and a beam current of 10 μA takes about 1 min. The maximum beam-current level attainable for S implantation at 200 keV is about 5 μA. Implantation was studied with fluences in the range between $1x10^{12}$ and $3x10^{15}$ cm^{-2} and energies between 40 and 250 keV

High-energy (>300 keV) implantations were performed using a 3-MeV Van de Graaff machine. Silane (SiH_4) was used as the source gas in the ion source for Si implantation. The implantation energy ranged from 500 to 1200 keV. Details on high-energy implantation are described in Section III.

C. POSTIMPLANT ANNEALING - A CAPLESS ANNEALING PROCESS

We have developed a capless annealing process [1,9] for ion-implanted GaAs wafers. The anneal is carried out at a temperature between 800 and 900°C under an arsenic overpressure in an open quartz tube. The system allows ∿1.5-in.-diameter wafers to be annealed up to a temperature of 1000°C. The arsenic overpressure was maintained by a constant flow of 75 ml of 7.5% AsH_3 in 2 liters of H_2. The introduction of AsH_3 differs from a previously reported capless process [33,34] and was developed independently from the work of Kasahara et al. [35]. Under this condition, the AsH_3 partial pressure at 850°C was approximately 2 Torr, which corresponds to an arsenic overpressure over two orders of magnitude higher than the equilibrium partial pressure [36]. The arsenic overpressure prevents decomposition of GaAs and results in an excellent surface morphology.

Most of our work on capless annealing of implanted GaAs under arsenic overpressure was carried out at 800 to 850°C. Studies were also made on annealing Si-implanted GaAs up to 900°C keeping arsenic overpressure constant. The arsenic partial pressure [36] was controlled by varying the flow rate of

---

35. J. Kasahara, M. Arai, and N. Watanabe, "Effect of Arsenic Partial Pressure on Capless Anneal of Ion-Implanted GaAs," J. Electrochem. Soc. 126, 1997 (1979).
36. J. R. Arthur, "Vapor Pressures and Phase Equilibria in the GaAs System," J. Phys. Chem. Solids 28, 2257 (1967).

the AsH_3/H_2 mixture passing through the annealing furnace. Results will be described later.

Anneal experiments were also performed on wafers encapsulated with a Si_3N_4 layer. A typical layer thickness was 2000 to 3000 Å, and annealing was carried out in a N_2 atmosphere. Both plasma-deposited Si_3N_4 layers and reactive-sputtered Si_3N_4 layers were tested. The plasma Si_3N_4 encapsulated samples showed blisters following an 850°C, 30-min annealing in a N_2 atmosphere, while samples encapsulated with sputtered Si_3N_4 showed no sign of blistering up to 1000°C. An accumulation of Cr at the surface was observed in Si_3N_4 encapsulated samples after thermal annealing, while no accumulation was observed in low-dose implanted, capless-annealed GaAs samples. This is further discussed in Section IV.

The laser annealing of ion-implanted semiconductors has been investigated as an alternative for the thermal annealing of lattice disorders created by high-energy irradiation. This technique is attractive for its simplicity, potential capability of annealing small local areas, and annealing without encapsulation of the semiconductor surface. During this program, both a high-power Q-switched Nd:glass laser and a ruby laser were used in the study of lattice reordering in Si-implanted GaAs samples. Details are described in Section VII.

D. CHARACTERIZATION OF IMPLANTED LAYERS

1. Impurity Concentration Profile

The depth distribution of the implanted atoms in GaAs was measured by secondary ion-mass spectrometry (SIMS). The machine at RCA is capable of measuring concentrations down to $\sim 5 \times 10^{15}$ cm^{-3}. This was accomplished by monitoring negatively charged secondary ions produced by cesium positive ion bombardment [37,38]. Contamination from the vacuum system was avoided by performing all analyses at pressures of 4×10^{-10} Torr.

37. P. Williams, R. K. Lewis, C. A. Evans, and P. R. Hanley, "Evaluation of a Cesium Primary Ion Source on an Ion Microprobe Mass Spectrometer," Anal. Chem. 49, 1399 (1977).
38. C. W. Magee, "Depth Profiling of n-Type Dopants in Si and GaAs Using C_s^+ Bombardment Negative Secondary Ion Mass Spectrometry in Ultra-High Vacuum," J. Electrochem. Soc. 126, 600 (1979).

Figures 1, 2, and 3 illustrate SIMS profiles of a S-implanted, a Si-implanted, and a Se-implanted sample, respectively. The implant schedules are 1×10^{15} cm^{-2} at 250 keV for sulfur, 5×10^{14} cm^{-2} at 200 keV for silicon, and 1.6×10^{14} cm^{-2} at 200 keV for selenium. The distribution is approximately Gaussian except with a broad tail. More SIMS data for Si implantation in GaAs are presented in Section III.

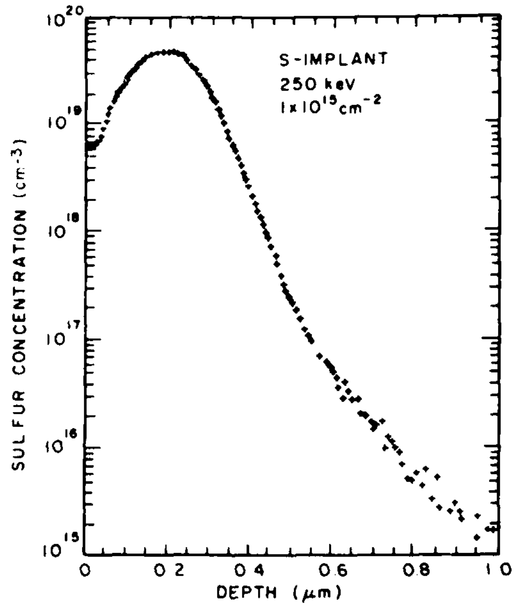

Figure 1. Impurity profile of S-implantation in GaAs measured by SIMS.

The impurity redistribution caused by thermal annealing was studied using SIMS. The depth profiles of the Si and Se atoms after the samples are thermally annealed (825°C, 20 min) are included, respectively, in Figs. 2 and 3. No impurity redistribution was observed in the Si-implanted, thermally annealed sample, while the Se-implanted thermally annealed sample showed a kink at a concentration of $\sim10^{19}$ cm^{-3}.

Quite a pronounced impurity redistribution was measured in a high-impurity concentration, Si-implanted, thermally annealed sample. Figure 4 illustrates the SIMS profile of a Si-implanted GaAs sample before and after thermal annealing (825°C, 20 min). The sample was implanted at 70 keV with a dose of 3×10^{15} cm^{-2}. The peak impurity concentration was 3.2×10^{20} cm^{-3}. The shoulder extends

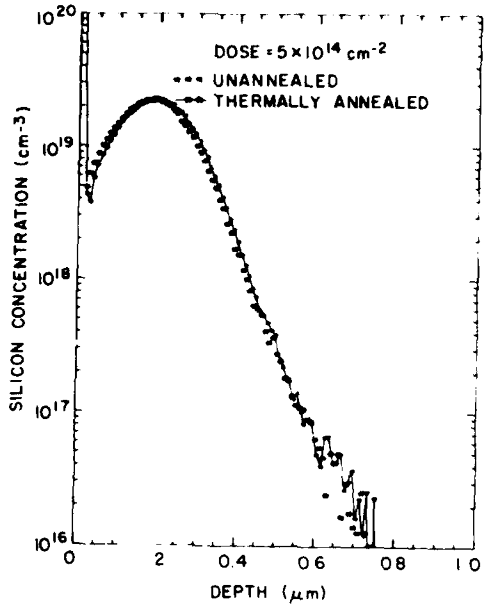

Figure 2. SIMS profile of a Si-implanted GaAs sample before and after thermal annealing, 200 keV, $5x10^{14}$ cm^{-2}.

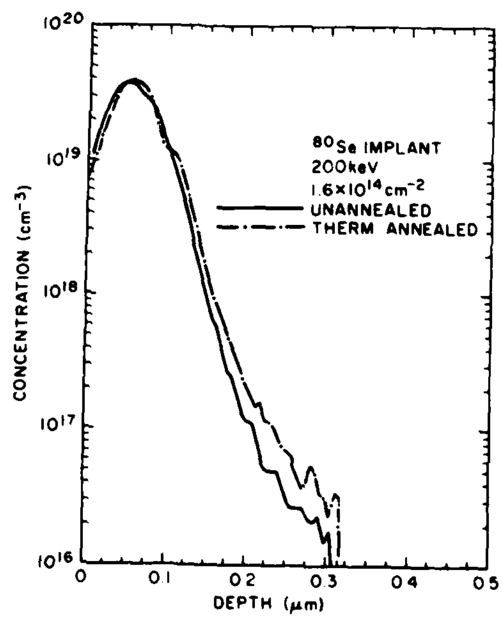

Figure 3. SIMS profile of a Se-implanted GaAs sample before and after thermal annealing, 200 keV, $1.6x10^{14}$ cm^{-2}.

to a depth of ~0.4 μm which approximately coincides with the peak of the electrically active electron density profile (shown by a dotted line).

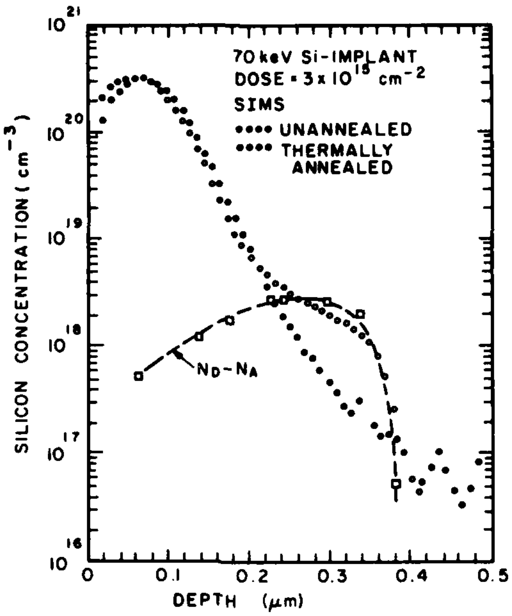

Figure 4. SIMS profile of a Si-implanted GaAs sample before and after thermal annealing, 70 keV, $3x10^{15}$ cm^{-2}.

These results are believed to be caused by damage-enhanced diffusion of unprecipitated silicon, similar to that being reported in Se-implanted GaAs [39]. Experiments here further demonstrated the dependence of anomalous broadening on the implantation conditions, which affect the degree of damage in the sample.

2. Electrical Conductivity of Ion-Implantation-Created Disordered Layers

The surface of an as-implanted SI GaAs substrate exhibits an electrical conduction as a result of lattice disorders. The sheet conductivity is a function of implantation dose. This phenomenon has been discussed by Y. Kato et al. [40].

39. A. Lidow, J. F. Gibbons, V. R. Deline, and C. A. Evans, Jr., "Solid Solubility of Selenium in GaAs as Measured by Secondary Ion Mass Spectrometry," Appl. Phys. Lett. 32, 572 (1978).
40. Y. Kato et al., "Electrical Conductivity of Disordered Layers in GaAs Crystal Produced by Ion Implantation," J. Appl. Phys. 45, 1044 (1974).

The sheet resistances of as-implanted GaAs were measured by the four-point-probe technique. Ohmic characteristics were obtained with probes on as-implanted GaAs surfaces. Figures 5 and 6 show the variation of sheet resistance vs implantation dose for S and Si implants into a number of SI GaAs substrate materials. There are several interesting features that are common to both the S and Si implantations. First, in the dose range of approximately 2×10^{12} to 3×10^{13} cm^{-2}, the sheet resistance decreases with increasing dose, according approximately to

$$\rho_s = 3.08 \times 10^{23} \times N^{-1.39} \tag{1}$$

for S implantation, and

$$\rho_s = 7.46 \times 10^{28} \times N^{-1.79} \tag{2}$$

for Si implantation.

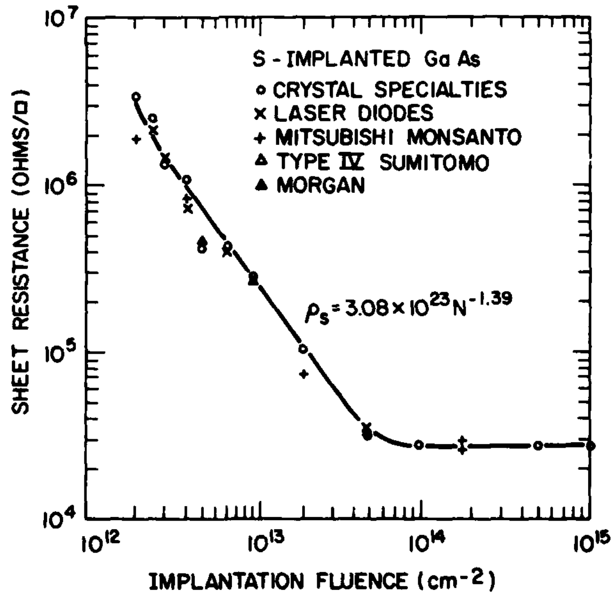

Figure 5. Sheet resistance vs implant dose measured on S-implanted unannealed GaAs.

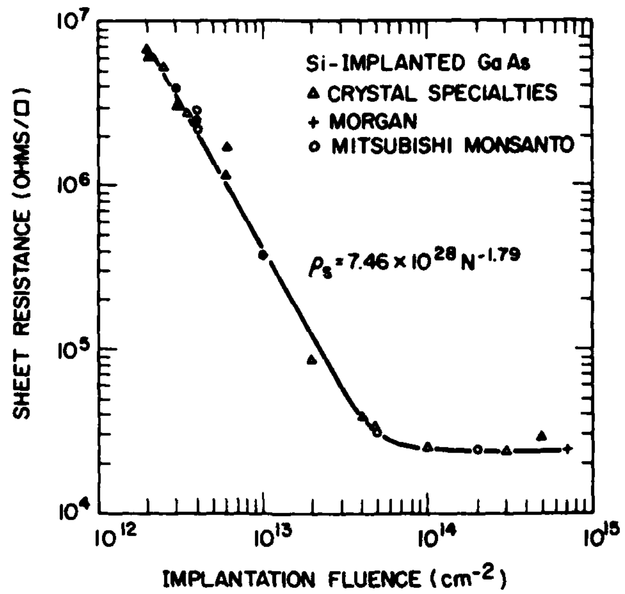

Figure 6. Sheet resistance vs implant dose measured on Si-implanted unannealed GaAs.

Secondly, above the dose level of about 5×10^{13} cm^{-2}, the electrical conductivity begins to saturate. A reduction in conductivity is observed as the dose increases beyond 10^{15} cm^{-2}. These general features are in agreement with Kato's result. The exponent dependence of ρ_s on N, given by Eqs. (1) and (2), however, is considerably less steep than Kato's (-1.39 and -1.79 vs -3).

It is interesting to note some qualitative correlations between the electrical conductivity of disordered layers following implantation and the electrically active carrier concentration (given in the next section) following the annealing process. Both show a dependence on the implant fluence with (1) an exponentially related region between dose levels, $\sim2\times10^{12}$ and $\sim3\times10^{13}$ cm^{-2} and (2) a saturation effect starting at a dose level of about 5×10^{13} cm^{-2}. The conductivity of the as-implanted layers may be utilized as a convenient way of monitoring implantation prior to the annealing process.

3. Mobility, Carrier Concentration, and Activation Efficiency at Various Dose Levels

Following implantation and annealing, the electrically active layer was characterized by van der Pauw measurements [41], which determine the Hall mobility, sheet carrier concentration, conductivity, and activation efficiency of the n-layer. A square or a clover-shaped mesa sample with four ohmic contacts at the corners of the sample was prepared for the measurement. Typical sample dimensions were 7x7 mm to 10x10 mm. The Hall mobility is given by

$$\mu_H = \frac{R_S}{\rho_s} \tag{3}$$

where R_S is the Hall coefficient and ρ_s is the sheet resistance. The Hall coefficient is given by

$$\rho_s = 10^8 \frac{\Delta V_{24}}{B\ I_{13}} \tag{4}$$

where I_{13} is the current, B is the magnetic flux density applied perpendicular to the surface of the sample, and ΔV_{24} is the voltage change with and without the magnetic field. The subscript numbers correspond to the four ohmic contacts, which are numbered in sequence, either clockwise or counterclockwise. The sheet resistance ρ_s is given by

$$\rho_s = \frac{\pi}{2\ \ln\ 2}\left(\frac{V_{34}}{I_{12}} + \frac{V_{23}}{I_{41}}\right) \cdot F \tag{5}$$

where F is a geometrical correction factor. A relation between F and the ratio (V_{34}/I_{12}) to (V_{23}/I_{41}) is given in ref. 41. From Eq. (3), the sheet carrier concentration N_s can be expressed as

$$N_s = \frac{1}{q\ R_S} \tag{6}$$

where q is the electronic charge ($1.6\text{x}10^{-19}$ C).

41. L. J. van der Pauw, "A Method of Measuring Specific Resistivity and Hall Effect of Discs of Arbitrary Shape," Philips Res. Rep. 13, 1 (1958).

The percentage activation efficiency for an implanted and annealed sample is given by

$$\eta = \frac{N_s}{N_s'} \tag{7}$$

where N_s' is the fluence (in cm^{-2}) used in the implantation.

Table 1 lists typical results on S implantation into SI substrates and into substrates with a vapor-phase epitaxially grown buffer layer. The implantations listed were for an energy level of 200 keV and a dose level between 4×10^{12} and 5×10^{14} cm^{-2}. Table 2 lists results on typical Si-implanted samples. All the samples listed were annealed at 825°C for 20 min using the capless process described earlier. The mobility values are in the 3000- to 4400-cm^2/V-s range, and the activation efficiencies are in the 20 to 80% range.

The activation is lower in high-dose implanted samples. The mobilities are generally higher ($\gtrsim$4000 cm^2/V-s) for implantations into a high-resistivity epitaxial buffer layer grown on a SI GaAs substrate, as shown in Tables 1 and 2. A direct implant into some substrates (e.g., sample A26, A28C) also gives an electron mobility of higher than 4000 cm^2/V-s at the $1\text{-}2 \times 10^{17}$ cm^{-3} doping density level.

The carrier concentration values listed in Tables 1 and 2 were approximately determined from

$$N_m = \frac{N_s}{\sqrt{2\pi}\ \Delta R_p} \tag{8}$$

which is an approximation to the Gaussian distribution:

$$N_s = \int_0^\infty N(x,E)\ dx = \sqrt{\frac{\pi}{2}}\ N_m\ \Delta R_p \left[1 + \left(\text{erf}\ \frac{R_p}{\sqrt{2}\ \Delta R_p}\right)\right] \tag{9}$$

where R_p and ΔR_p are, respectively, the projected range and standard deviation of the implanted atoms. The measured sheet electron concentration values were used for N_s in Eq. (8), and the ΔR_p was taken as 0.08 μm at the 200-keV energy level, which is close to that measured by SIMS. Some data computed by Gibbons

TABLE 1. S IMPLANTATION IN GaAs

SAMPLE NUMBER	SUBSTRATE	ENERGY (keV)	DOSE (cm^{-2})	MOBILITY ($cm^2/V\text{-}s$)	APPROX. CARRIER CONC. (cm^{-3})	ACTIVATION EFF (%)
62B	SI (MM-G103)	200	4.0×10^{12}	3318	8.4×10^{16}	41.8
63B	Cr-n^-/SI* (A-141)	200	5.0×10^{12}	4053	1.8×10^{17}	72.4
10A	SI (LD)	200	5.0×10^{12}	3220	1.8×10^{17}	73.6
10D	(5-μm)n^-/SI*	200	5.0×10^{12}	4005	1.7×10^{17}	67.2
45A	(3-μm)n^-/SI* (C265)	250	7.0×10^{12}	4364	1.4×10^{17}	40.9
45E	SI (MX)	250	7.0×10^{12}	4067	1.5×10^{17}	46.9
45F	(10-μm)Cr-n^-/SI* (A90)	250	7.0×10^{12}	4331	1.2×10^{17}	37.1
19X	SI (LD)	200	7.0×10^{13}	3219	3.7×10^{17}	73.0
14C	SI (LD)	200	1.5×10^{13}	3230	2.5×10^{17}	32.8
64A	SI (MMG102)	200	2.0×10^{13}	2899	5.8×10^{17}	58.3
57	SI (XS3761)	200	1.0×10^{14}	3201	1.5×10^{18}	30.6
50A	SI (XS3761F)	200	5.0×10^{14}	2891	1.7×10^{18}	6.7

*Vapor-phase high-resistivity epitaxial layer grown on SI substrate.

TABLE 2. Si IMPLANTATION IN GaAs

SAMPLE NUMBER	SUBSTRATE	ENERGY (keV)	DOSE (cm^{-2})	MOBILITY ($cm^2/V\text{-}s$)	APPROX. CARRIER CONC. (cm^{-3})	ACTIVATION EFF. (%)
A24A	6-μmn$^-$/SI* (D95)	200	3.0×10^{12}	4285	8.2×10^{16}	54.9
A35A	SI (XS3761)	200 70	3.0×10^{12} 1.5×10^{12}	3374	1.9×10^{17}	82.6
A35C	SI (XS3765F)	200 70	3.0×10^{12} 1.5×10^{12}	3630	1.7×10^{17}	76.8
A35D	5-μmn$^-$/SI* (D143)	200 70	3.0×10^{12} 1.5×10^{12}	4000	1.9×10^{17}	85.1
A28N	SI (XS3761F)	200	3.5×10^{12}	3740	1.6×10^{17}	90.3
A23A	Cr-n$^-$/SI* (A156)	200	4.0×10^{12}	3928	1.2×10^{17}	60.5
A3A	SI (MMG102)	200	4.0×10^{12}	3570	1.2×10^{17}	62.0
A26	SI (XS3765)	200 50	4.0×10^{12} 2.0×10^{12}	4000	1.5×10^{17}	60.5
A4B	SI (XS3761)	200	6.0×10^{12}	3222	1.9×10^{17}	64.7
A31	SI (XS3761)	200	2.0×10^{13}	2931	7.0×10^{17}	70.1
A6	SI (MMG102)	200	5.0×10^{13}	2049	1.1×10^{18}	37.0
A34	SI (XS3761F	200	1.0×10^{14}	2204	1.1×10^{18}	21.5
A44	SI (XS3761F)	70	1.0×10^{15}	1770	1.6×10^{18}	3.2

*Vapor-phase high-resistivity epitaxial layer grown on SI substrate.

et al. [42] on the R_p and ΔR_p of ^{32}S and ^{28}Si ions implanted into GaAs are reproduced in Table 3.

TABLE 3. LSS RANGE STATISTICS OF Si AND S IMPLANTATION IN GaAs

S in GaAs			Si in GaAs		
Energy (keV)	R_p (μm)	ΔR_p (μm)	Energy (keV)	R_p (μm)	ΔR_p (μm)
10	0.0094	0.0066	10	0.0103	0.0074
50	0.0375	0.0222	50	0.0424	0.0254
70	0.0518	0.0291	70	0.0592	0.0333
100	0.0740	0.0387	100	0.0850	0.0442
120	0.0891	0.0448	120	0.1025	0.0510
150	0.1121	0.0534	150	0.1291	0.0607
200	0.1509	0.0667	200	0.1739	0.0753
250	0.1901	0.0788	250	0.2187	0.0884
300	0.2292	0.0899	300	0.2632	0.1003
400	0.3067	0.1096	400	0.3507	0.1210
600	0.4569	0.1412	600	0.5181	0.1534
800	0.5996	0.1658	800	0.6750	0.1780
1000	0.7349	0.1856	1000	0.8225	0.1975

The mobility vs carrier concentration data of S- and Si-implanted samples were plotted in Figs. 7 and 8, respectively. Theoretical curves [43] of drift mobility with different compensation ratio values are also included in the plots. Most of our experimental data points are located between a compensation ratio of 1 and 2, indicating that material quality is acceptable.

42. J. F. Gibbons et al., Projected Range Statistics, 2nd. ed. (Halsted Press, A Div. of John Wiley and Sons, Inc., 1975).
43. D. L. Rode and S. Knight, "Electron Mobility in GaAs," Phys. Rev. B3, 2534 (1971).

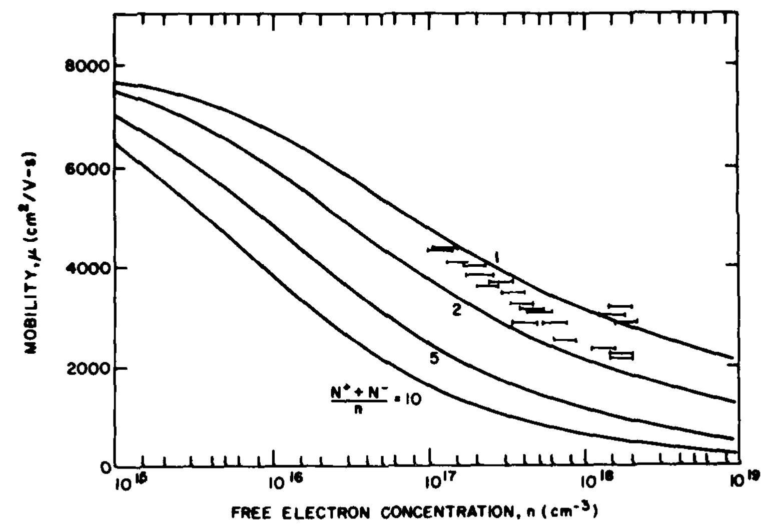

Figure 7. Mobility vs carrier concentration, S implanted in GaAs.

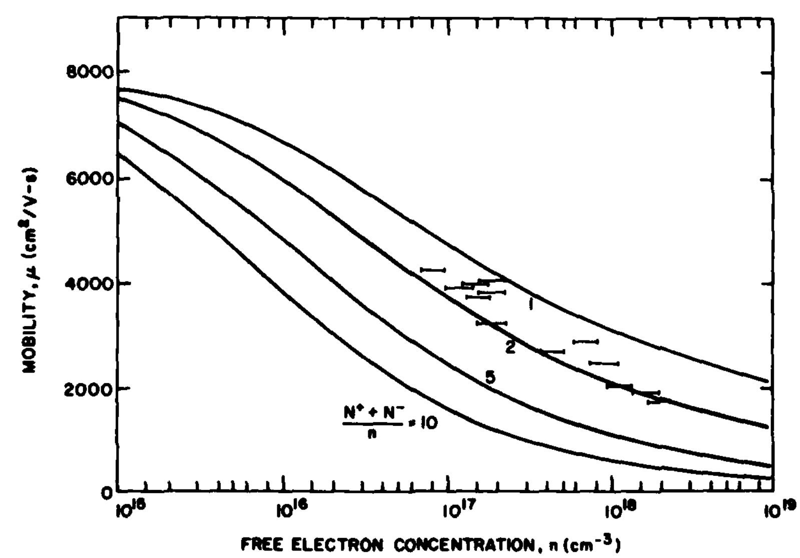

Figure 8. Mobility vs carrier concentration, Si implanted in GaAs.

Se implantations in GaAs were carried out at 200 keV and 120 keV with fluences between 3.5×10^{12} cm^{-2} and 1.6×10^{14} cm^{-2}, respectively. Preliminary measurements on capless-furnace-annealed samples showed mobilities between 2400 and 3500 $cm^2/V\text{-}s$ and activation between <1% and 25%. Both are low compared with Si-implanted n-layers. Se implants are being further investigated.

Experimental data of carrier concentration (electrically activated) as a function of implantation dose are shown in Fig. 9 for S implantation into GaAs and in Fig. 10 for Si implantation into GaAs. The samples were capless-annealed at a temperature of 825°C for 20 min. The implantation energy was 200 keV for all data points. Scattering of data points for different substrate materials

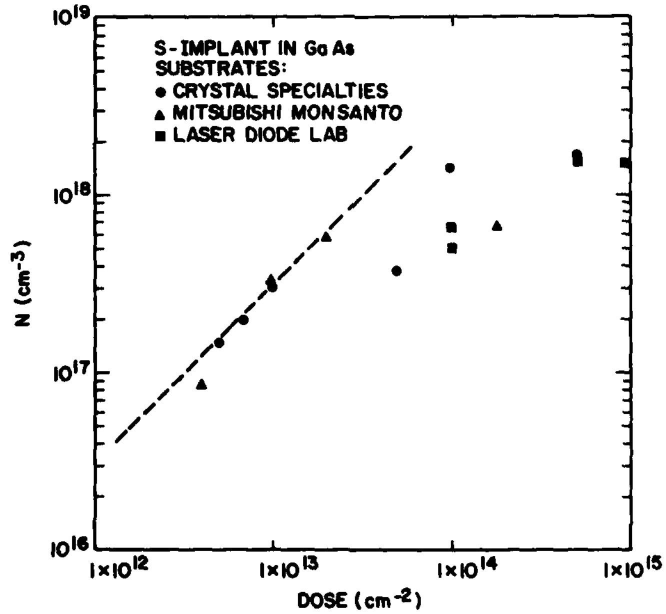

Figure 9. Carrier concentration as a function of implantation dose for S implantation into GaAs.

is present in the plot. The data in both the Si- and S-implantation cases indicate the following features: (1) In the range of fluence between $5x10^{12}$ and $3x10^{13}$ cm^{-2} for S implant and $2.5x10^{12}$ and $2x10^{13}$ cm^{-2} for Si implant, the carrier concentration varies approximately linearly with the fluence, and (2) the free carrier concentration increases at a much slower rate at a high fluence level. A thermal annealing of up to 1000°C for 20 min has been carried out for one sample as shown by the unfilled circle in Fig. 10. The sheet carrier concentration increases somewhat, but it still stays in the low increasing rate range. The high-temperature anneal was done in nitrogen atmosphere with 2000 Å of sputtered Si_3N_4 encapsulant.

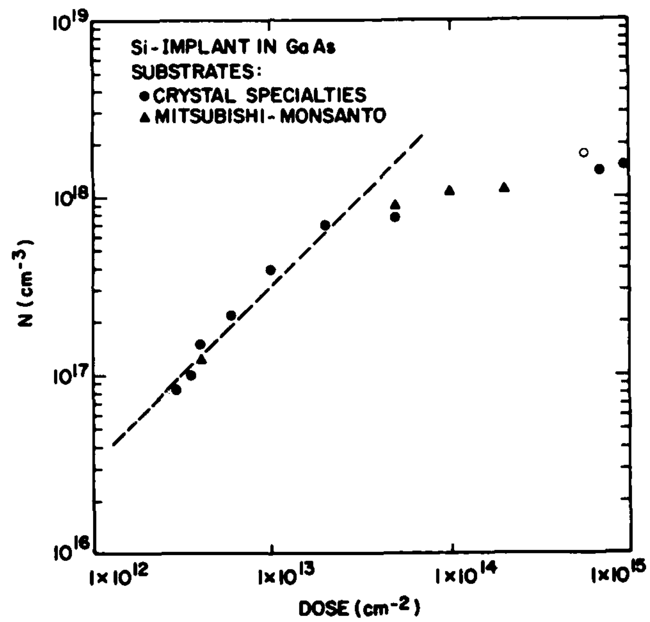

Figure 10. Carrier concentration as a function of implantation dose for Si implantation into GaAs.

To study the dependence of electrical properties of implanted n-layers on annealing temperatures, we implanted three samples from the same wafer at 200 keV with different Si doses ($2.5x10^{13}$, $2.5x10^{14}$, and $3x10^{15}$ cm^{-2}). The samples were annealed at 900°C for 20 min under arsenic overpressure. The measured mobilities of the three samples were 3030, 1900, and 1740 cm^2/V-s in the order of increasing carrier concentrations. The corresponding compensation factors are 1.1, 1.8, and 1.9, respectively.

Figure 11 compares the results of samples capless-annealed at 825 and 900°C. The data were plotted in terms of sheet carrier concentration (the activated charge density per unit area) as a function of implant dose. Figure 11 illustrates that the 900°C capless annealing produces electrical activations higher than those of 825°C capless annealing for implant doses higher than $\sim 10^{13}$ cm^{-2}. This result is substantiated in samples which received multiple Si implantations. The data from three 1000°C annealed samples (using sputtered Si_3N_4 as an encapsulant in N_2 atmosphere) are also included in Fig. 11 (shown by a dotted line). The activation is found to be lower than the 900°C capless annealing.

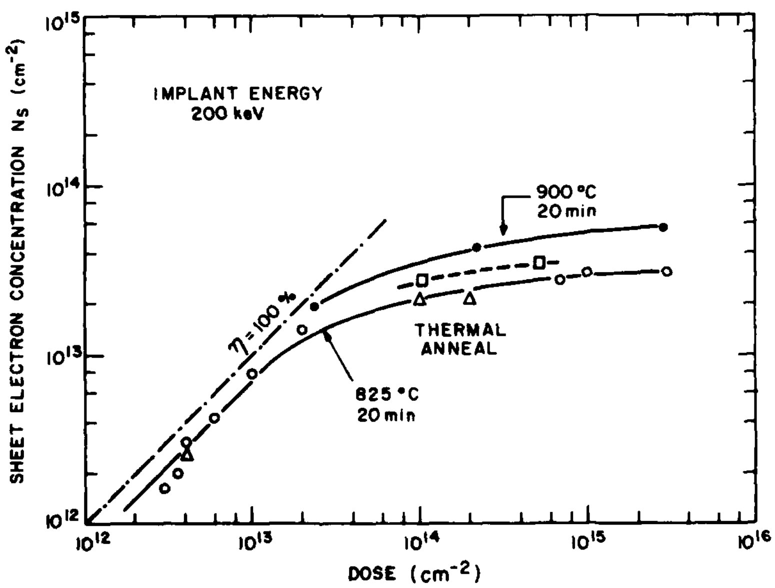

Figure 11. Sheet electron concentration as a function of dose for thermally annealed samples.

Table 4 lists the electrical properties of multiple-implanted samples which were capless-annealed under different conditions. The multiple-implant conditions of each wafer are listed in the second column. Note that in high-dose implanted wafers (C71, C72), the sheet resistance of a sample annealed at 900°C is about 60 Ω/□, which is half that annealed at 825°C. In low-dose implanted wafers (H58, H59), the sheet resistance does not change significantly at these two temperatures. An increase of ∿50% in arsenic overpressure at

TABLE 4. ELECTRICAL PROPERTIES OF Si IMPLANTS CAPLESS-ANNEALED UNDER DIFFERENT CONDITIONS

Sample No.	Implant Conditions (cm^{-2})	(keV)	Temp. (°C)	Time (min)	AsH_3 Pressure* (Torr)	μ (cm^2/V-s)	ρ_s (Ω/□)
C70	$2x10^{14}$	250	825	20	2.0	1760	94
	$1x10^{14}$	70	900	15	21.3	1690	74
C71	$3x10^{15}$	200	825	20	2.0	1650	125
	$1x10^{15}$	70	900	15	21.3	1690	59
C72	$1x10^{15}$	200	825	20	2.0	1790	124
	$5x10^{14}$	70	900	15	21.3	1540	55
	$7.2x10^{12}$	900	825	20	2.0	3860	75
	$5.8x10^{12}$	500	900	15	21.3	3720	77
H58	$4.3x10^{12}$	265	900	15	31.9	3760	72
	$1.6x10^{12}$	80					
	$7.2x10^{12}$	900	825	20	2.0	3510	71
	$5.8x10^{12}$	500	900	15	21.3	3880	71
H59	$4.3x10^{12}$	265	900	15	31.9	3870	74
	$1.6x10^{12}$	80					

900°C reduces the sheet resistance about 8% in the low-dose multiple-implanted sample under this high arsenic overpressure condition.

Further profiling measurements confirm that the lower sheet resistance is due to the higher carrier concentration in 900°C annealed samples. The depths of the n-layers and the mobilities were approximately the same for both the low (825°C) and high (900°C) temperature annealed samples.

4. Depth Distribution of Electron Concentration

From reverse-biased capacitance vs applied voltage data on a Schottky diode of known area, the depth distribution of charged carriers can be computed from [44]:

$$N = \frac{-C^3}{q\varepsilon A^2}\left(\frac{\partial C}{\partial V}\right)^{-1} \tag{10}$$

and

$$x = \varepsilon \frac{A}{C} \tag{11}$$

where C is the capacitance; V, the applied voltage; q, the electronic charge; ε, the dielectric constant ($\varepsilon/\varepsilon_o$ = 12.5 for GaAs); and A, the area of the Schottky diode. The C-V data may be taken point-by-point on a capacitance bridge or by using an automatic plotter which measures C-V and plotted N vs x on an x-y recorder directly. Data were measured on an automatic plotter which was calibrated against the point-by-point result.

The accuracy of the C-V technique is inherently limited in reproducing a shallow electron density profile with a steep doping density variation [45]. The inaccuracy occurs particularly close to the surface and toward the tail end. For most of the implantations performed, the ratio of $R_p/\Delta R_p$ is on the order of 2 (Table 3), which means a less steep variation in doping densities as compared to implantations in silicon. The C-V technique thus should provide information around the peak of the depth distribution which is useful as a guide to device fabrication.

In order to measure the carrier concentration of a thin layer an SI substrate, one often forms a Schottky diode and an ohmic contact on the surface of the active layer. Because making ohmic contact to GaAs usually requires a second metallization and sintering, an alternative way simply measures the capacitance between two circular Schottky diodes, one being forward-biased while the other is reverse-biased. Applying this technique,

44. C. O. Thomas, D. Kahng, and R. C. Manz, "Impurity Distribution in Epitaxial Silicon Films," J. Electrochem. Soc. 109, 1055 (1962).
45. C. P. Wu, E. C. Douglas, and C W. Mueller, "Limitations of the CV Technique for Ion-Implanted Profiles," IEEE Trans. Electron Devices ED-22, 319 (1975).

however, introduces an additional zero-bias capacitance connecting in series with the reverse-biased capacitance. This must be corrected according to

$$1/C = 1/C_r + 1/C_f \tag{12}$$

where C is the measured capacitance, C_r is the reverse-biased capacitance, and C_f is the forward-biased capacitance.

A technique was developed in preparing samples for C-V measurement that eliminates the above complexities. Figure 12 shows the patterns of Schottky contact made to the active implanted layer. The circular diodes are surrounded by large-area Schottky contacts forming a donut-shaped pattern. Because of the large-area Schottky contact, the capacitance C measured between the reverse-biased circular diode and the forward-biased Schottky contacts approximately equals C_r, since the second term in Eq. (12) can be neglected. No corrections are therefore required in measured capacitance data. Samples prepared in this manner are readily adaptable to the automatic C-V profile equipment.

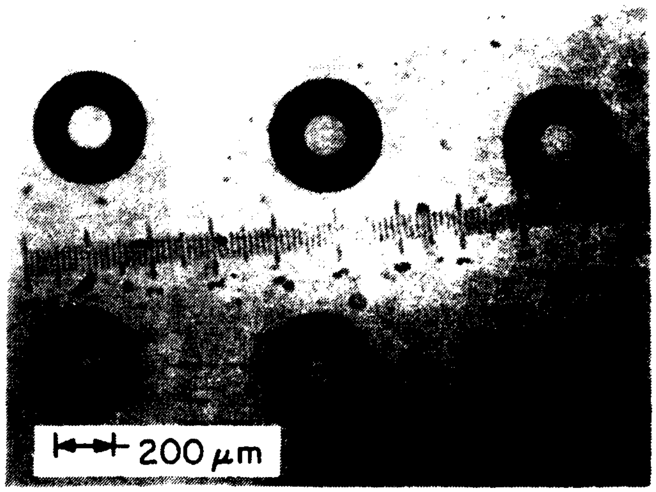

Figure 12. Photograph showing patterns of Schottky contact.

The Schottky patterns shown in Fig. 12 were easily produced by a single-step photolithography, followed by metallization and liftoff. Cr-Au (500 Å Cr/1500 Å Au), Ti-Pt-Au (500 Å Ti/500 Å Pt/1500 Å Au), or Al (2000 Å) metallization was used in forming Schottky contacts for C-V measurement. The diameter

of the circular dots is 0.152 mm (0.006 in.) which produces a zero-bias capacitance below 30 pF for a typical implanted layer. This capacitance value is within the limit of the automatic C-V profile equipment.

Figure 13 shows the carrier concentration density profile of a Si-implanted sample (A49A) as measured on the automatic C-V impurity profile equipment. The implantation dose and energy level are 3.5×10^{12} cm^{-2} and 200 keV, respectively.

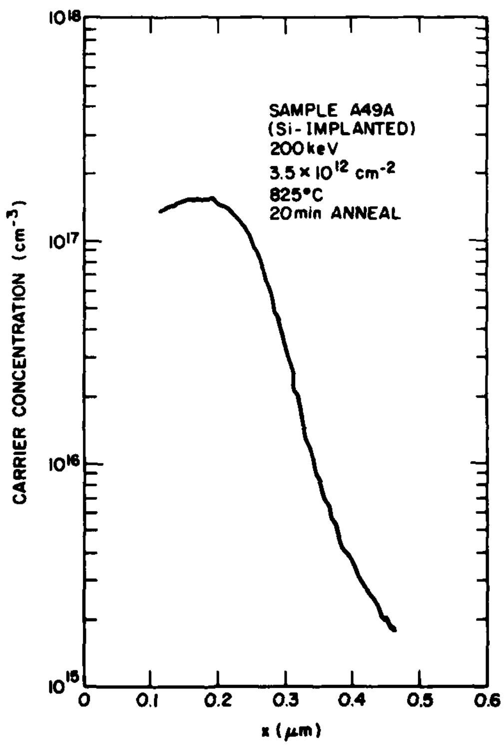

Figure 13. Carrier concentration profile for single-energy Si implant.

Figure 14 shows the carrier concentration density profile of a multiple-Si-implanted sample (A60B) obtained from C-V measurement. The dose and energy levels of the double implantations are 3×10^{12} cm^{-2}, 200 keV and 1×10^{12} cm^{-2}, 70 keV, which are designed to yield a nearly constant doping distribution. Figure 14 demonstrates that the implantation profile can be controlled by using multiple implants.

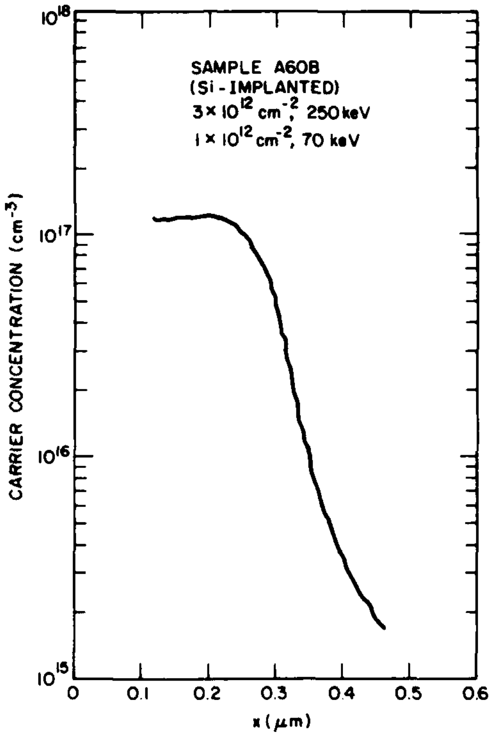

Figure 14. Carrier concentraction profile for dual Si implant.

The measured electron distribution of S-implanted GaAs is usually broader than for Si-implanted samples and deviates from a Gaussian distribution. This may be attributed to a significant diffusion effect during anneal. Figure 15 shows a measured curve with circles indicating the LSS distribution, including the thermal diffusion effect, normalized to match the peak of the measured curve. The diffusion coefficient corresponding to the 825°C anneal temperature was deduced from the matched curve to be $5x10^{-14}$ cm^2/s. Similar measurements on a number of samples show a range of between $2x10^{-14}$ and $5x10^{-14}$ cm^2/s under this anneal condition. This value compares favorably with those measured by Young and Pearson [46] and Asai and Kodera [47] on solid-state S diffusion into

46. A. B. Y. Young and G. L. Pearson, "Diffusion of Sulfur in GaP and GaAs," J. Phys. Chem. Solid 31, 517 (1970).
47. A. Asai and H. Kodera, "Electrical Properties of n-type Layers in GaAs prepared by Solid Sulfur Diffusion," Proc. of the 4th. Int. Symp., Boulder, CO, 1972, p. 130.

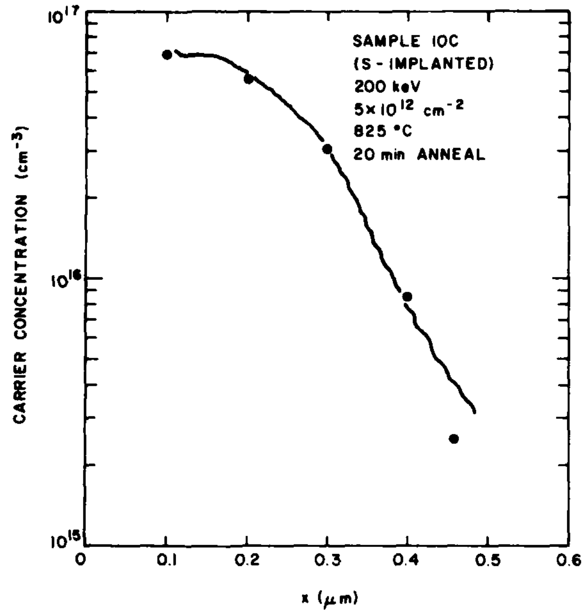

Figure 15. Measured electron density distribution of S-implanted GaAs.

bulk GaAs, but it is almost an order of magnitude lower than Kendall's result [48]. A similar match of LSS distribution was made to the measured profile on Si-implanted GaAs samples, and the diffusion effect was found to be negligible. The corresponding diffusion coefficient is less than or equal to 10^{-15} cm^2/s.

5. Electron Concentration and Hall Mobility Profile

The depth distribution of carrier concentration and mobility on some samples were determined by the use of layer removal technique combined with the van der Pauw measurement.

48. P. L. Kendall, Semiconductors and Semimetals, vol. 4, (Academic Press, New York, 1968).

The mobility, μ, and carrier concentration density, n, corresponding to the i-th chemically removed GaAs layer are given, respectively, by [49,50]:

$$\mu_i = \left[\left(\frac{R_s}{\rho_s^2}\right)_{i-1} - \left(\frac{R_s}{\rho_s^2}\right)_i\right] \Bigg/ \left[\left(\frac{1}{\rho_s}\right)_{i-1} - \left(\frac{1}{\rho_s}\right)_i\right] \tag{13}$$

$$n_i = \left[\left(\frac{1}{\rho_s}\right)_{i-1} - \left(\frac{1}{\rho_s}\right)_i\right] \Bigg/ q\, h_i\, \mu_i \tag{14}$$

where ρ_s is the sheet resistivity, R_S is the sheet Hall coefficient, h is the thickness of the chemically removed layer, q is the electrical charge, and the lower case index i and i-1 refer to the successive order of removed layer. The sheet resistivity, ρ_s, and Hall coefficient, R_S, are given, respectively, by Eqs. (5) and (4).

Figure 16 shows the carrier concentration and mobility profile of a S-implanted sample (49B) determined by the differential Hall-effect measurement. The sample was implanted with a dose of 10^{13} cm^{-2} at an energy level of 200 keV. The Cr-doped SI substrate was from Crystal Specialties. Postimplant annealing was done at 825°C for 20 min under AsH_3 overpressure as described earlier. The profile shows a maximum carrier concentration of 2.4×10^{17} cm^{-3} which agrees with that obtained by C-V measurement. The mobility profile varies from 3000 cm^2/V-s at the surface to over 4000 cm^2/V-s toward the SI substrate, which agrees with the measured effective Hall mobility of 3520 cm^2/V-s for the entire implanted layer.

49. R. Baron, G. A. Shifrin, and O. J. Marsh, "Electrical Behavior of Group III and V Implanted Dopants in Silicon," J. Appl. Phys. 40, 3702 (1969).
50. J. W. Mayer, L. Eriksson, and J. A. Devices, Ion Implantation in Semiconductors, (Academic Press, New York, 1970), p. 193.

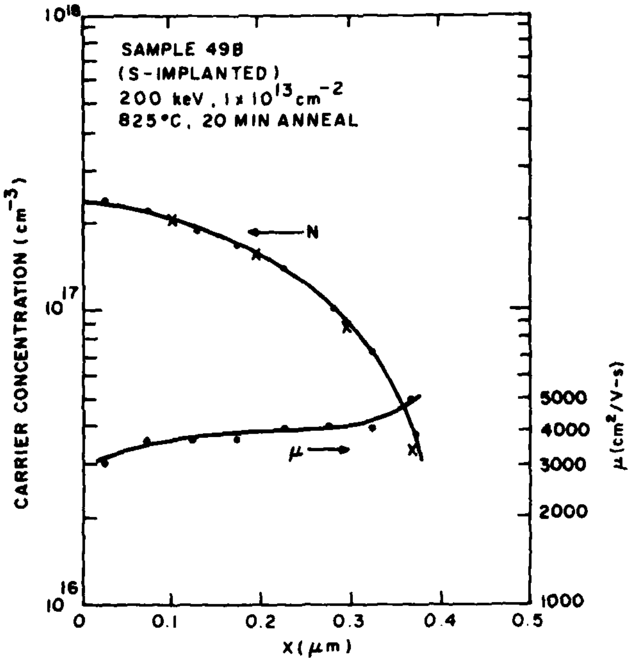

Figure 16. Carrier concentration and mobility profile of a S-implanted wafer, 70 keV.

The profile deduced from the C-V measurement after normalization in carrier concentration matches well with the profile measured by differential Hall-effect measurement. The normalized points are indicated as crosses in Fig. 16. Both cases are for S implantation at 200 keV but with a difference in implanted dosage.

The carrier concentration and mobility profiles on two high-dose Si-implanted GaAs wafers are shown in Figs. 17 and 18. The average mobility and sheet carrier concentration of the two wafers are measured to be, respectively, 1800 cm^2/V-s and 2.14×10^{13} cm^{-2} for sample A69 and 2120 cm^2/V-s and 2.26×10^{13} cm^{-2} for sample A82. Layers of GaAs were etched using $H_2SO_4:H_2O_2:H_2O$ in the ratio 1:1:50 at 0°C. This gave a reproducible etch rate of 4.4 Å/s.

E. CO-IMPLANTATION OF ^{28}Si AND ^{32}S IN GaAs

Co-implantation of ^{28}Si and ^{32}S into SI GaAs was investigated in an attempt to fabricate a high-quality n-layer. The idea is that since the ^{32}S

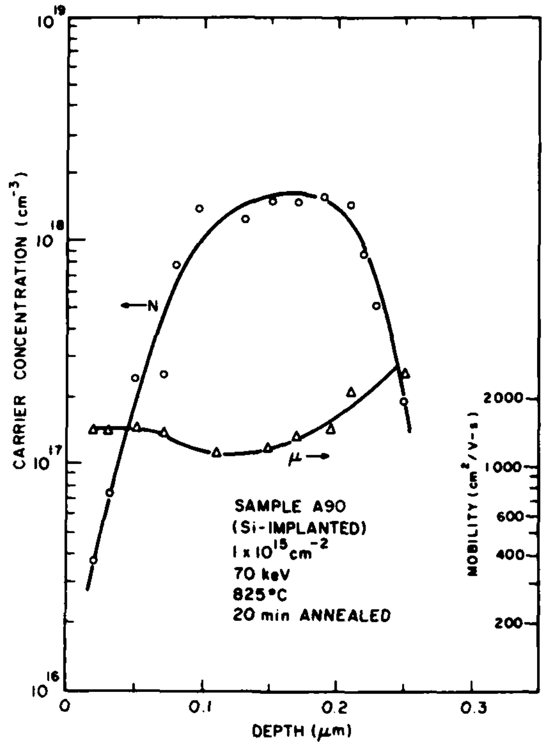

Figure 17. Carrier concentration and mobility profile of a Si-implanted wafer, 70 keV.

(column VI) occupies the As lattice sites, the amphoteric Si will be consequently preferentially located at the Ga sites as a donor, and hence an enhanced electrical activation should occur resulting in high-quality doped layers. The experiments performed, however, did not lead to conclusive results.

The first experiment was performed by co-implantation of ^{28}Si and ^{32}S at 200 keV into a Bridgman-grown, Cr-doped SI GaAs substrate. The implant fluences for ^{28}Si and ^{32}S were 4.5×10^{12} cm^{-2} and 2.3×10^{12} cm^{-2}, respectively. Figure 19 illustrates the electron density profiles of the co-implanted sample annealed at 825°C for 20 min and 900°C for 15 min. The activation efficiency increased from 63.2 to 83.5% and the mobility increased from 3490 to 3910 cm^2/V-s as the annealing temperature was increased from 825 to 900°C. This increment is generally not observed in Si-implanted GaAs at these low-dose levels. The AsH_3 flow rate was increased more than ten times [36] for capless annealing at 900°C to maintain the same arsenic overpressure used routinely at 825°C. Electron density profiles of Si- and S-implanted GaAs samples that were thermally

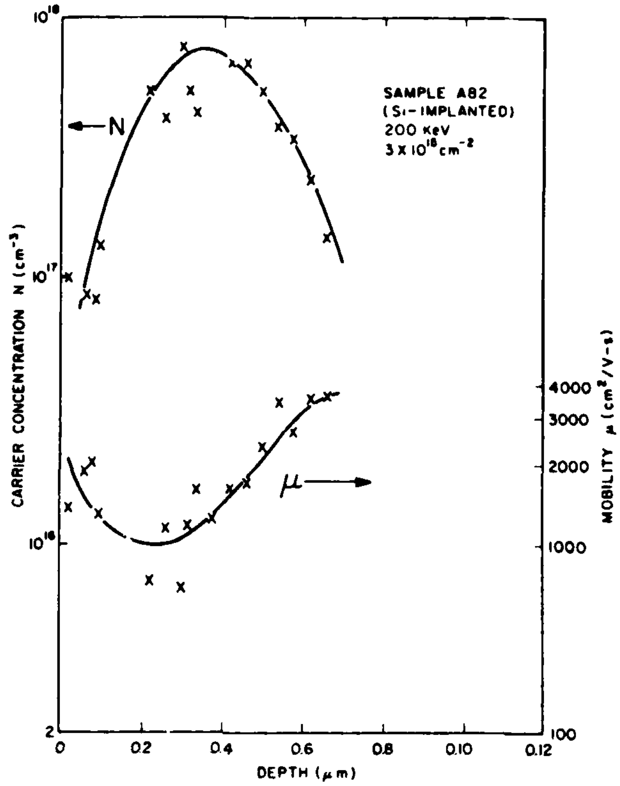

Figure 18. Carrier concentration and mobility profile of a Si-implanted wafer, 200 keV.

annealed at 825°C are also included in Fig. 19 for comparison. Both samples were implanted at 200 keV with doses of 3.5×10^{12} cm^{-2} for Si and 4.5×10^{12} cm^{-2} for S. The corresponding mobilities were 3060 and 3900 cm^2/V-s. Note that the implant energies are the same, but the doses do not equal those in the co-implanted sample. The profiles are included to show the shape of each electron density distribution.

The Si implant has a near Gaussian electron density profile indicating a very small thermal diffusion coefficient which has been determined previously to be $\leq 10^{-15}$ cm^2/s. The S implant has an electron density profile which increases toward the surface and is considerably deviated from Gaussian. The electron density profiles of the co-implanted wafer show a broader peak with higher activation and mobility when annealed at higher temperatures. These results are encouraging from a device point of view.

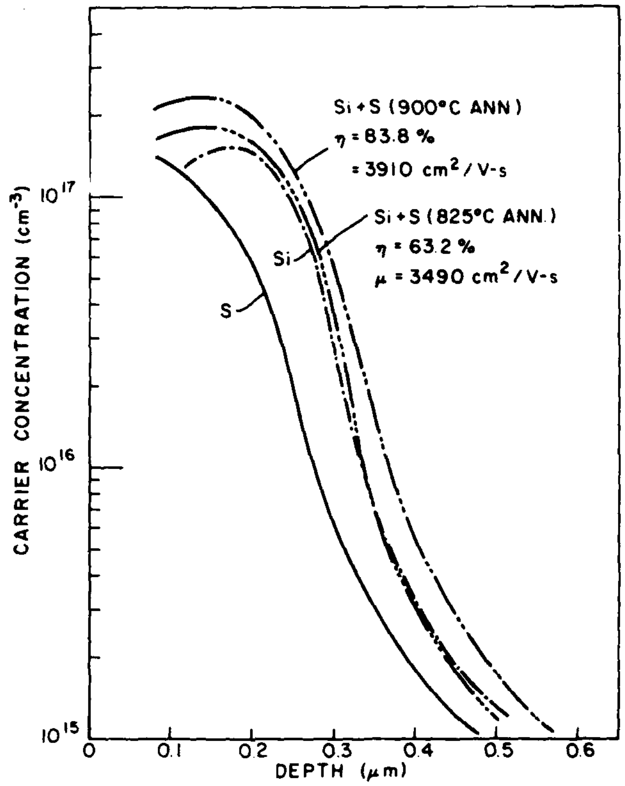

Figure 19. Electron density profiles of co-implanted (^{28}Si and ^{32}S) GaAs annealed at 825 and 900°C, respectively. Individual implants annealed at 825°C are also shown.

The co-implantation experiments were repeated using an undoped Cz/LEC substrate as well as Bridgman and Cz/LEC Cr-doped substrates. The samples were prepared so that the co-implants can be compared closely with single (Si) implants from the same substrate. It is postulated* that the co-implantation of Si/S in undoped GaAs substrates may produce a higher activation than that in Cr-doped substrates. This postulation is based on reports that Si implants in GaAs substrates with higher Cr content produce a higher activation, and this is interpreted on the basis of the presence of Cr on arsenic sites. Therefore, with S^+ as a co-implant into low Cr (undoped Cz/LEC), GaAs substrates would enhance the activation even further since S^+ occupies As sites as a donor.

*M. N. Yoder, private communication.

It should be pointed out that we have had similar results of higher activation for Si implants in Cr-doped Cz/LEC crystal than that found in undoped Cz/LEC. However, this occurs only when the Si-implant dose is relatively high ($\geq 5\times10^{12}$ cm^{-2}); i.e., above the implant threshold (2×10^{12} cm^{-2}) normally occurring in Cr-doped substrates. All implant energies are at 200 keV. Details of activation near the threshold dose level are discussed further in the following sections.

The repeated co-implantation experiments using the undoped and Cr-doped substrates were carried out as follows. A section of each wafer was implanted with ^{28}Si alone in order to make comparisons between the co-implants and single implants using the same substrate. Following implantation, all the wafers were annealed at 850°C for 30 min under arsenic overpressure. The electrical characteristics were then evaluated using van der Pauw measurements and C-V measurements.

Table 5 summarizes the implant schedules and the electrical properties using van der Pauw measurements for the single and co-implanted wafers. The fluences of the ^{32}S and ^{28}Si for the co-implants were 4.4×10^{12} cm^{-2} and 2.2×10^{12} cm^{-2}, respectively. Both were implanted at 200 keV. The fluences of the ^{28}Si for the single ion-implanted wafers were 4.4×10^{12} cm^{-2} and 2.2×10^{12} cm^{-2}, at 200 keV and 176 keV, respectively. The additional Si implant at 176 keV in this wafer was used to match the projected range of the ^{32}S implant at 200 keV in the co-implanted wafer so that the single- and co-implanted wafers can be closely compared.

Table 5 shows that the co-implanted wafers (S10A, S10B) result in a lower activation than the corresponding single implants (D49A, D49B). The undoped substrates (S10A, D49A) result in a lower activation than the corresponding Cr-doped substrates (S10B, D49B). Figure 20 shows the carrier concentration profiles of the four wafers. The higher carrier concentration of Si-implanted wafers (D49A, D49B) and the lower carrier concentration of undoped substrates (D49A, S10A) are consistent with the data shown in Table 5. These results appear contradictory to the predictions. The reasons are not clearly understood and remain to be further investigated.

TABLE 5. COMPARISON OF ELECTRICAL PROPERTIES OF ^{28}Si IMPLANTS AND ^{28}Si/^{32}S CO-IMPLANTS IN LEC SI GaAs SUBSTRATES

			Implant				
Sample	Substrate	Source	Energy (keV)	Dose (cm^{-2})	N_s (cm^{-2})	η (%)	μ (cm^2/V-s)
S10A	W14-18	^{28}Si	200	$4.4x10^{12}$	$2.93x10^{12}$	44.4	4630
	(Undoped)	^{32}S	200	$2.2x10^{12}$			
S10B	W15-10	^{28}Si	200	$4.4x10^{12}$	$3.71x10^{12}$	56.2	3840
	(Cr doped)	^{32}S	200	$2.2x10^{12}$			
D49A	W14-18	^{28}Si	200	$4.4x10^{12}$	$4.06x10^{12}$	61.5	3920
	(Undoped)	^{28}Si	176	$2.2x10^{12}$			
D49B	W15-10	^{28}Si	200	$4.4x10^{12}$	$4.41x10^{12}$	66.8	4150
	(Cr doped)	^{28}Si	176	$2.2x10^{12}$			

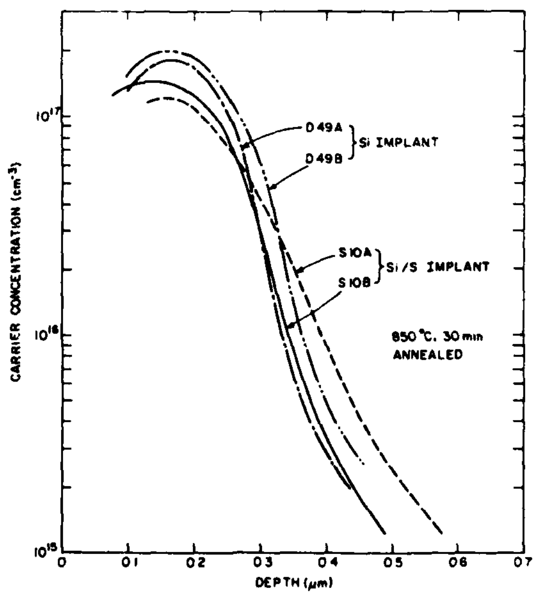

Figure 20. Comparison of electron density profiles of co-implanted (^{28}Si and ^{32}S) and Si-implanted GaAs.

SECTION III

HIGH-ENERGY (UP TO 1.2 MeV) IMPLANTATION

In this section, the progress made during this program in obtaining and implanting high-energy (up to 3 MeV) ion beams will be reviewed. Beams of ^{11}B and ^{28}Si have been produced and implanted into both Si and GaAs substrates. The profiles and range statistics of these implants have been analyzed using SIMS analysis, and based on the information obtained, uniformly doped ^{28}Si profiles ~1 μm deep have been produced in GaAs using multiple implants. This section discusses the production of implanted profiles, dopant activation analyses, mobility measurements, and electron density profiles on implanted (single or multiple) and annealed GaAs wafers.

A. HIGH-ENERGY Van de GRAAFF FOR HEAVY ION IMPLANTATION

The Van de Graaff machine used for the high-energy implant experiments was built by High Voltage Engineering Corp.* and was originally designed to produce proton beams at 3 MeV and ~1 mA. The machine was originally equipped with a duo-plasmatron source and operated with a cumbersome end-station (for wafer implantation) attached to the 25° magnet port.

To produce and implant heavy ion beams, a number of modifications were made to the Van de Graaff machine. First, the duo-plasmatron source was replaced with a cold-cathode-discharge heavy ion source, and the cold cathode source was in turn replaced with an rf-excited plasma source. Both the extraction optics on the machine and the high operating pressures required by the available cold cathode source made it unusable, hence the final selection of the rf source. The second major modification to the Van de Graaff machine was the construction of a new beam line attached to the 15° port rather than the 25° port of the analyzing magnet. Using the 15° port, a mass-energy (at mass x energy in MeV) product of ~33 could be achieved with the available analyzing magnet. The new beam line that was constructed contained x-y sweep plates and terminated in an end-station which holds a single wafer at a time. The implant

*High Voltage Engineering Corp., Burlington, MA.

area was originally 7.56 cm^2 (square) and later modified to a circular area of 13.07 cm^2 (4.08 cm in diameter). During the implant, the normal to the wafer was inclined at an angle of 7° relative to the direction of the incident beam. The vacuum in the beam line and end-station during the implant was maintained in the 10^{-6}-Torr region. The third modification to the Van de Graaff machine was the installation of a 4° beam deflection system ("dogleg") to eliminate the neutral particles in the beam. This eliminates some discrepancies found earlier between the implanted and the measured doses.

B. CALIBRATION IMPLANTS USING $^{11}B^+$ BEAM

The first experiments were performed using BF_3 as a source gas in the ion source and implanting $^{11}B^+$ ions into a silicon substrate. These conditions were chosen because the spectrum of BF_3 (i.e., the amplitude of the various ion components extracted from the source plotted as a function of the current in the analyzing magnet) is well known and has a distinctive set of $^{10}B^+$, $^{11}B^+$ peaks. The mass of the boron ion is also relatively small so that the machine could be exercised at higher energies. The mass-energy product (atomic mass x energy in MeV) for the machine is ∿33. We selected ^{11}B in silicon for the first tests because of the ability of SIMS analysis to readily measure the profile.

Figure 21 shows a SIMS plot of a 1-MeV ^{11}B implant that was made on the FEC* machine compared with a 60-keV ^{11}B implant that was made on the RCA Laboratories' implanter. The scanned area in the newly constructed beam line is 2.54 cm x 2.54 cm, and all portions of the system performed well during the implant.

To test the endurance of the machine for higher level implants, we made a series of implants at progressively higher energies as shown in the SIMS plots given in Fig. 22. Each implant required approximately 45 min of implant time using a beam current of ∿4 μA. These implants were carried out over a two-day period of essentially continuous running. Terminal overheating problems were experienced during these long tests, and suitable corrections were made to some of the cooling systems. Beam currents as high as 8 μA of ^{11}B were obtained, but lower values were used to prevent excessive end-station and wafer heating.

*Fusion Energy Corporation, Princeton, NJ.

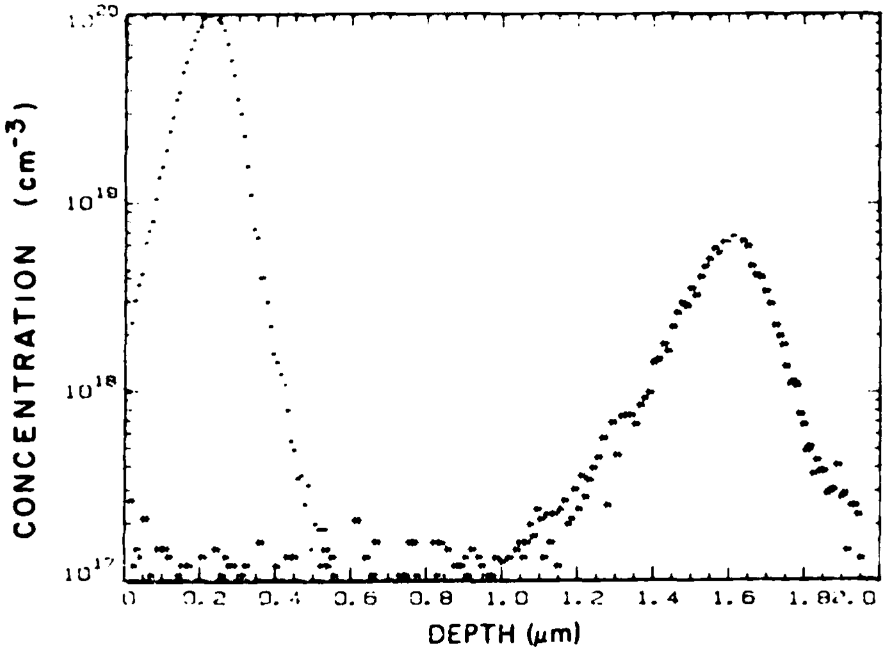

Figure 21. SIMS plots of a 60-keV ^{11}B implant performed on on the RCA Labs machine and a 1-MeV ^{11}B implant performed on the FEC Van de Graaff implanter.

(At 2 MeV and 8 μA, the average incident power density on target is ~2.5 W/cm^2.)

The measured value of the range R_p for the series of ^{11}B implants is given in Fig. 23. The value of the implant energy was calibrated by bombarding a lithium target with high-energy protons (obtained from the source operating with SiH_4). A resonant interaction occurs between the lithium target and the proton beam at 1.88 MeV which produces detectable neutrons. The machine is calibrated by comparing the reading on the machine energy dial with the occurrence of neutrons being emitted from the lithium target.

C. IMPLANTATION OF $^{28}Si^+$ INTO GaAs

1. Calibration

Having demonstrated with ^{11}B the ability of the Van de Graaff machine to produce heavy ion beams, we changed the source gas from BF_3 to SiH_4, and beams

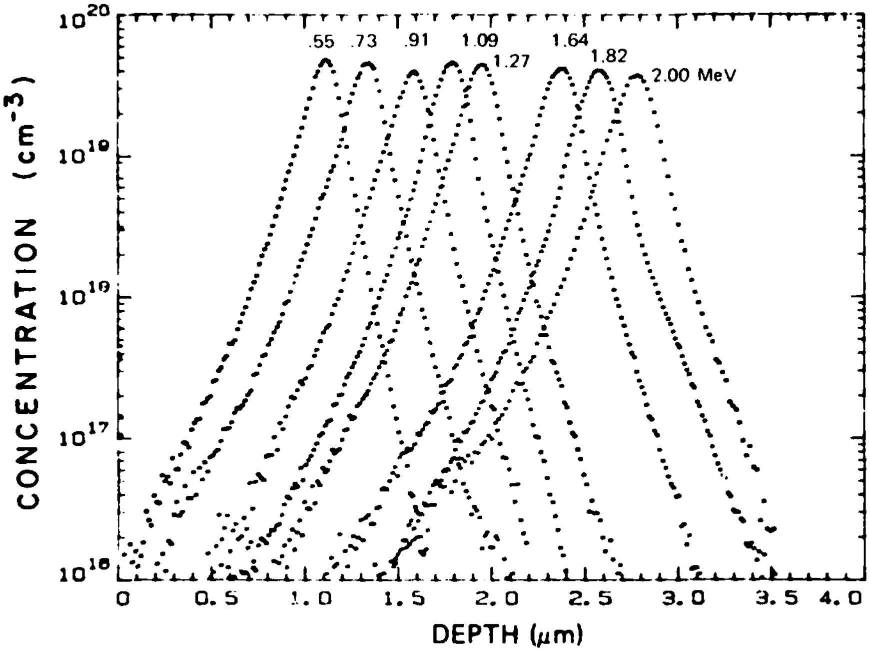

Figure 22. SIMS plots of a group of samples implanted with increasing energies using the FEC Van de Graaff implanter.

of $^{28}Si^{+}$ were produced and implanted into GaAs substrates. The results of the first test implants made at 600 keV are shown in the SIMS plot in Fig. 24. These results indicate that the magnet was properly adjusted to produce a Si beam.

The results of a series of implants made at a number of different implant energies ranging from 40 keV to 1.2 MeV are shown in Figs. 25 and 26. The lower range implants (40 to 280 keV) were performed on the implant machine located at RCA Laboratories and the higher range implants (0.7 to 1.2 MeV) were performed on the Van de Graaff implanter.

It is evident from Fig. 26 that the profiles are not Gaussian in shape but are noticeably skewed. A theory, developed by the statistician Karl Pearson [51,52] and applied to ^{11}B implants into Si at energies up to 800 keV by Hofker

51. M. G. Kendall and A. Stuart, The Advanced Theory of Statistics, (Charles Griffin, London, 1958), vol. 1, p. 148.
52. W. P. Elderton, Frequency Curves and Correlation, 4th ed. (Cambridge Univ. Press, 1953).

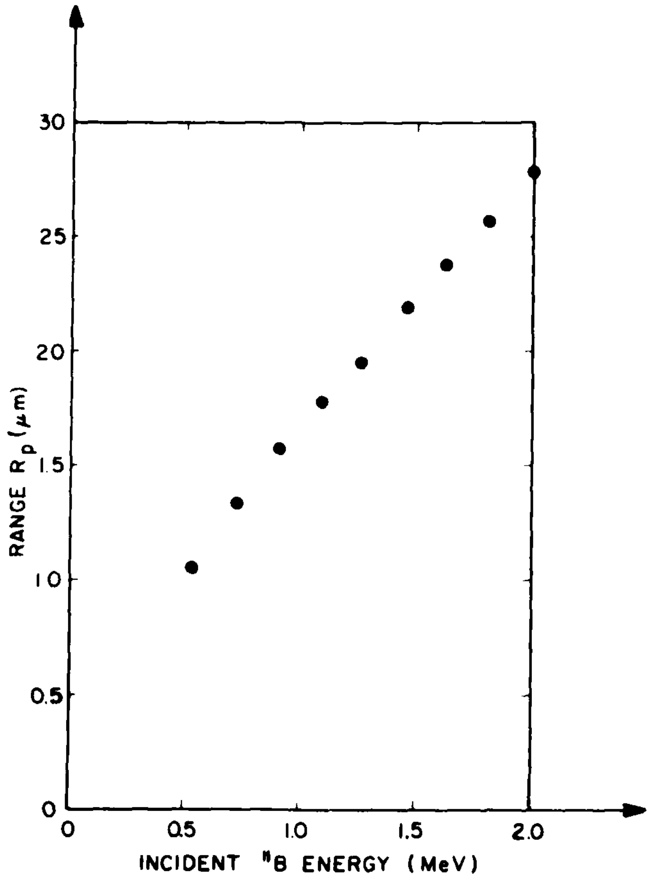

Figure 23. Measured value of the range R_p for the series of ^{11}B implants.

[53], makes use of the first four experimental moments to produce fits to the observed profile data. From these calculations, statistical information, such as the range R_p and straggle ΔR_p, can be obtained for skewed data.

The results of curve-fitting to the experimental data, based on the first four experimental moments, are shown in Figs. 27 to 29. Figures 27 and 28 show both log and linear plots of the experimental and calculated data using the formula described by Elderton [53]. Figure 29 shows a composite plot of the

53. W. K. Hofker, "Implantation of Boron in Silicon" Philips Research Supplements 8, 1975.

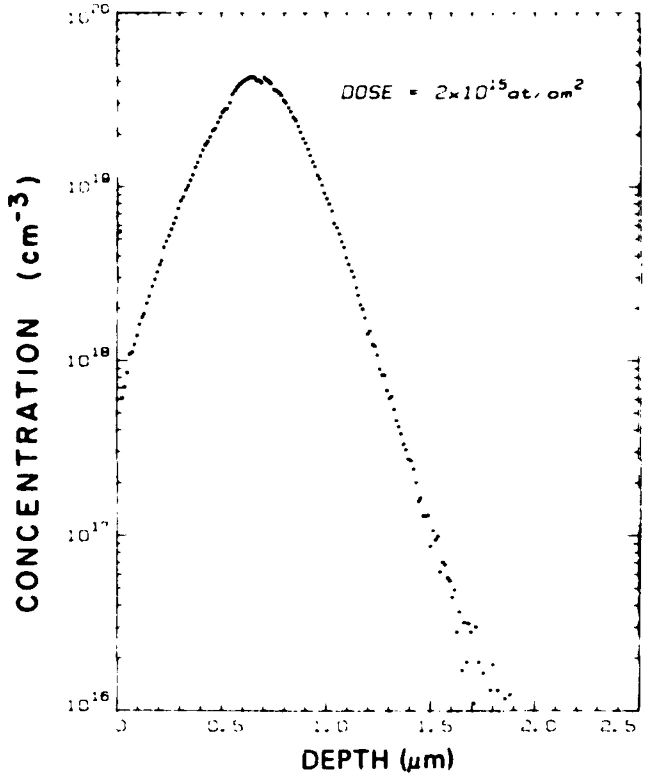

Figure 24. SIMS plot of the first $^{28}Si^{+}$ implant into a GaAs substrate using the Van de Graaff machine.

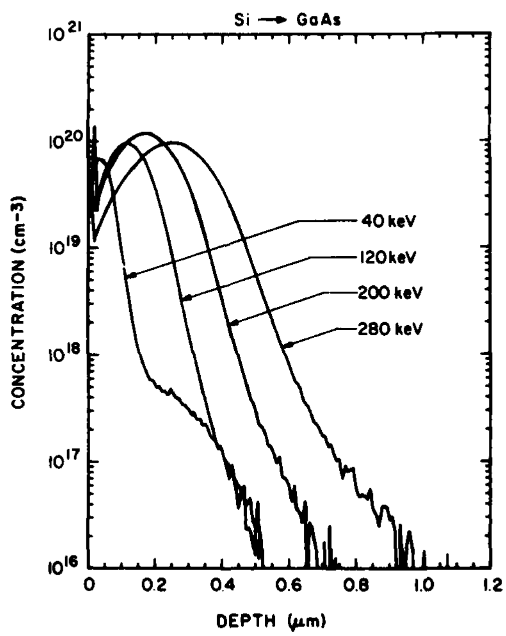

Figure 25. SIMS profiles of implants made at energies of 40, 120, 200, and 280 keV

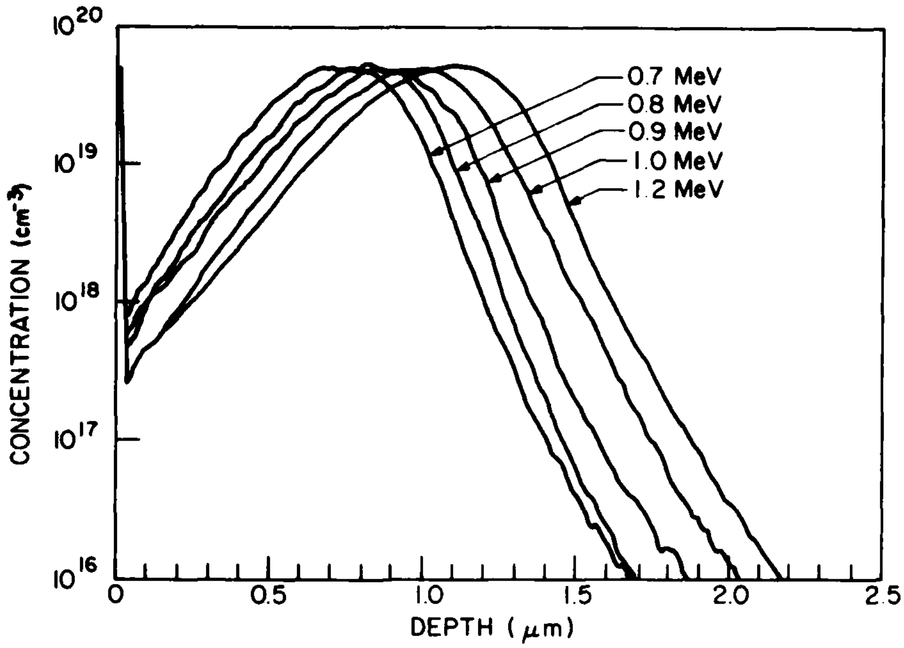

Figure 26. SIMS profiles of implants made at energies of 0.7, 0.8, 0.9, 1.0, and 1.2 MeV.

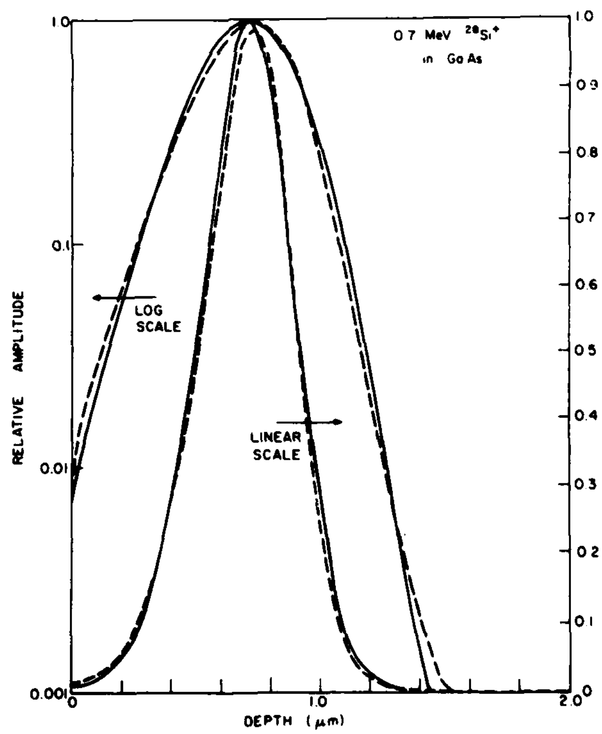

Figure 27. Curve-fitting to experimental data, 0.7-MeV $^{28}Si^{+}$ into GaAs.

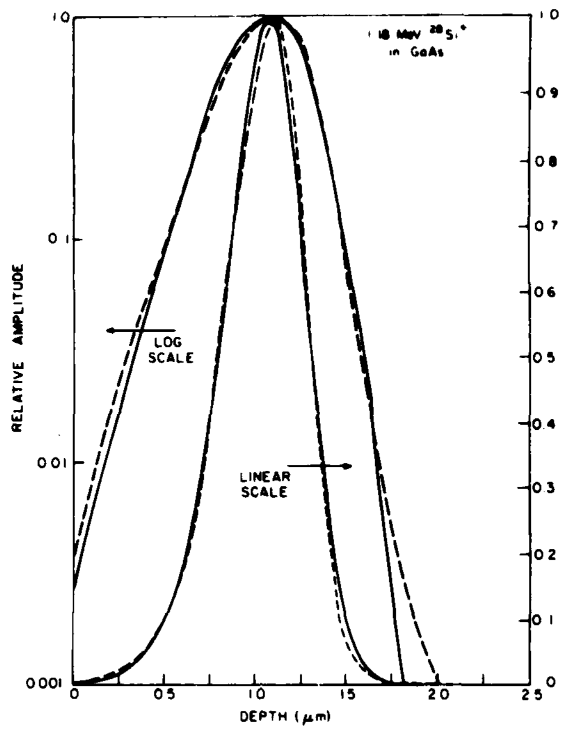

Figure 28. Curve-fitting to experimental data, 1.18-MeV $^{28}Si^+$ into GaAs.

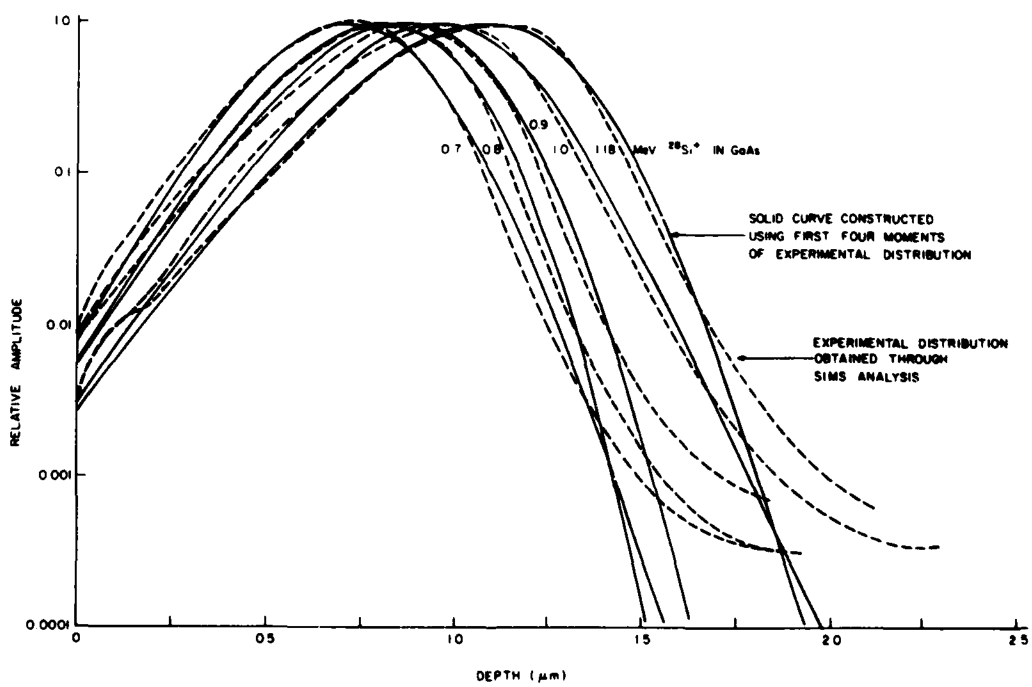

Figure 29. Composite plots of curves corresponding to the data given in Fig. 26.

curves corresponding to the experimental data given in Fig. 26. Figure 30 shows a reduction of the data to R_p and ΔR_p values corresponding to LSS Gaussian reduction techniques and first-four-moment Pearson techniques. It should be noted that the crossovers of the computed curves in Fig. 29 and the poor fit of the computed curves to the extended tails at both the shallow and deep portions of the curve indicate that care must be taken to ensure that excessive channeling is not present.

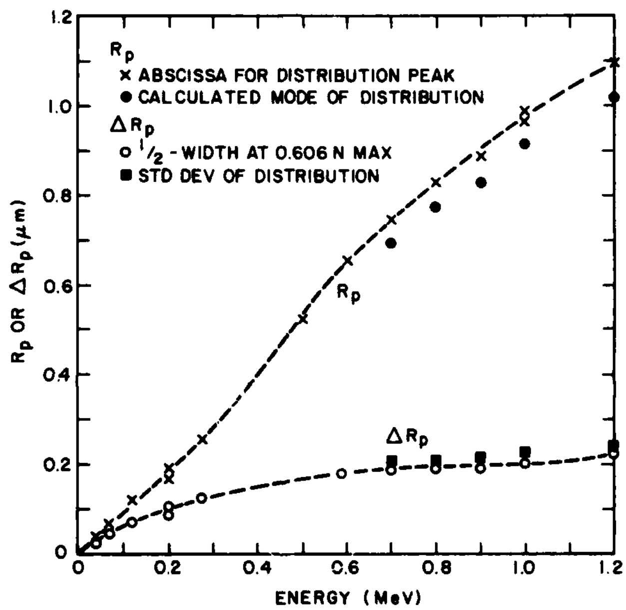

Figure 30. Reduction of data to R_p and ΔR_p values.

The effect of thermal annealing on the distribution of high-energy implanted Si atoms in GaAs is illustrated in Fig. 31. It shows the SIMS profiles of a 1-MeV Si-implanted GaAs wafer before and after thermal annealing. No silicon redistribution was detected after capless annealing under arsenic pressure at 825°C for 20 min.

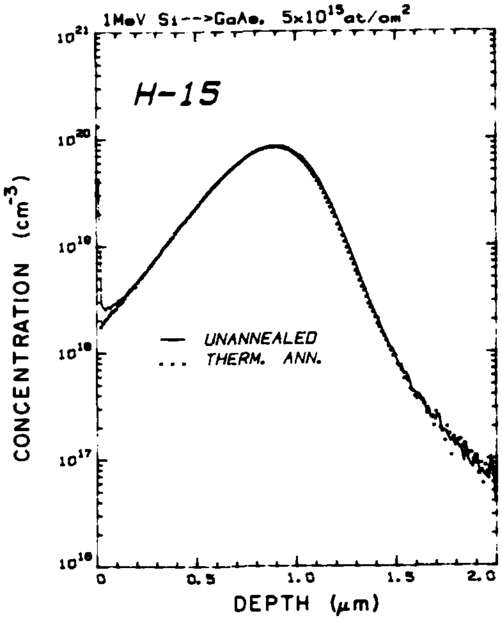

Figure 31. Impurity profiles of Si-implanted GaAs before and after thermal annealing at 825°C for 20 min.

2. Mobility, Carrier Concentration, and Activation Efficiency

Following thermal annealing, the electrical characteristics of the high-energy implanted n-layers were evaluated by the van der Pauw measurement. The measuring technique was briefly described earlier. Table 6 shows the measured sheet carrier concentration, N_s, sheet resistance, ρ_s, Hall mobility, μ, and the activation efficiency, η, on the 1-MeV Si-implanted GaAs. The implanted Si doses varied between 1.5×10^{13} and 5×10^{15} cm^{-2}. The mobilities and activation efficiencies obtained are either comparable to or better than those obtained with low-energy implantation at comparable dose levels (Table 2). The mobilities are in the range of 1690 cm^2/V-s for high-dose implanted samples to 4720 cm^2/V-s for low-dose implanted samples; the activation efficiencies are in the range of below 1% for high-dose implanted samples to ∿100% for low-dose-implanted samples. All the data shown in Table 6 are for samples capless-annealed at 825°C for 20 min.

The activation efficiency of heavily implanted samples increased at a higher annealing temperature. This result is shown in Table 7 where Si-implanted wafers were annealed at two different temperatures, 825 and 970°C.

TABLE 6. 1-MeV Si IMPLANTATION IN GaAs

Sample No.	Energy (keV)	Dose (cm^{-2})	N_s (cm^{-2})	ρ_s ($\Omega/\Box$)	μ ($cm^2/V\text{-}s$)	η (%)
H15	1000	$5.0x10^{15}$	$3.7x10^{13}$	85	2000	0.7
H39	1000	$3.0x10^{15}$	$3.6x10^{13}$	82	2120	1.2
H16	1000	$1.5x10^{15}$	$5.7x10^{13}$	65	1690	3.8
H38	1000	$1.0x10^{15}$	$6.3x10^{13}$	54	1830	6.3
H17	1000	$5.0x10^{14}$	$7.3x10^{13}$	49	1760	14.7
H18	1000	$1.5x10^{14}$	$4.6x10^{13}$	52	2620	30.8
H19	1000	$5.0x10^{13}$	$2.7x10^{13}$	70	3310	54.2
H20	1000	$1.5x10^{13}$	$1.1x10^{13}$	142	3980	73.5
H36	1000	$1.5x10^{13}$	$8.0x10^{12}$	167	4720	53.0
H37	1000	$1.0x10^{13}$	$1.0x10^{13}$	138	4530	100.0

TABLE 7. RESULTS OF Si-IMPLANTED WAFERS AT 825 AND 970°C

Sample No.	Energy (keV)	Dose (at./cm^2)	Anneal Temp (°C)	N_s (cm^{-2})	ρ_s ($\Omega/\Box$)	μ ($cm^2/V\text{-}s$)	η (%)
H10	900	$3.0x10^{15}$	825	$4.16x10^{13}$	83.5	1800	1.39
			970	$2.13x10^{14}$	22.2	1320	7.10
H11	1000	$3.1x10^{15}$	825	$3.73x10^{13}$	92.7	1807	1.20
			970	$1.47x10^{14}$	27.4	1554	4.74

The two samples annealed at 970°C produce a higher activation efficiency. The annealing was done in a N_2 atmosphere with samples encapsulated with 2000-Å-thick reactively sputtered Si_3N_4.

Figure 32 shows the measured sheet carrier concentration as a function of Si dose for samples implanted at 200 keV and 1 MeV, respectively, and annealed thermally at 825°C for 20 min. The 1-MeV implanted samples showed a substantially higher sheet carrier concentration in the dose range of $5x10^{13}$ to $2x10^{15}$ cm^{-2}. This result may be due to the fact that, at a given dose level, the 1-MeV implant results in a lower impurity concentration distribution than the 200-keV implantation, because of its higher straggle value. The drooping in the sheet carrier concentration at the high-dose level is not fully understood.

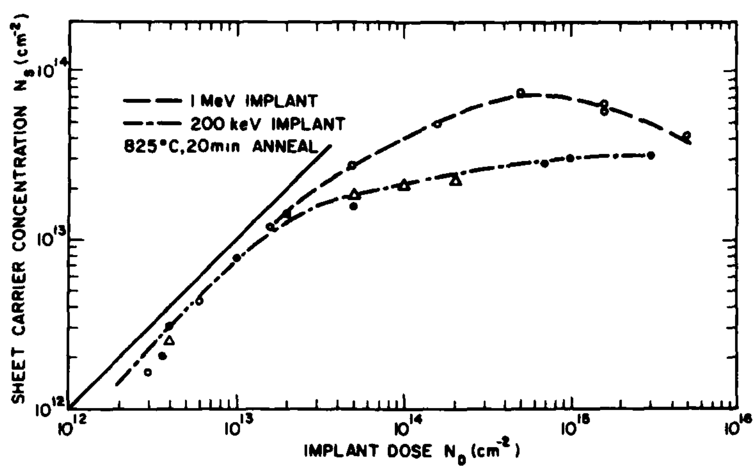

Figure 32. Measured sheet carrier concentration as a function of Si dose for samples implanted at 200 keV and 1 MeV.

3. Electron Density Profiles

The electron density profiles of high-energy implanted, thermally annealed samples were evaluated using differential C-V measurement in conjunction with controlled layer removal by chemical etching. Each controlled chemical etching step was between 500 and 1500 μm depending on the electron densities of the layer being removed. Large etching steps were used for low-density regions ($\leq 10^{17}$ cm^{-3}). Schottky-barrier diodes were formed either by evaporation of

aluminum on to the surface following each chemical etching step or pre-etch to different depths on divided sections on the sample, then followed by a single metallization; depth profiles were measured on automatic C-V profile equipment. An automatic Polaron profiler, which combines the step etching and doping profiling, has also been used.

Figure 33 shows the electron concentration distribution of Si-implanted, thermally annealed, SI GaAs samples measured using this technique. These samples were implanted at an energy level of 1 MeV, with fluences of $5x10^{14}$ (H19) and $1.5x10^{13}$ cm^{-2} (H20), respectively. The heavily printed line segments represent the C-V measurement data recorded by the automatic C-V profile machine. An impurity profile measured by SIMS on a high-dose ($3.7x10^{14}$ cm^{-2})-implanted, unannealed sample (H17) is included in Fig. 33 for comparison.

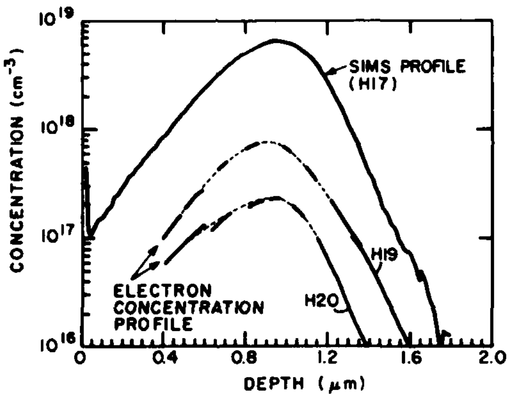

Figure 33. SIMS profile and electron density profiles of 1-MeV Si-implanted thermally annealed GaAs.

4. Electron Density and Hall Mobility Profile

Figure 34 shows the carrier concentration and mobility profiles of a 1-MeV, $1x10^{13}$-cm^{-2} Si-implanted, capless-annealed GaAs sample (H37). The carrier concentration profile is composed of both the van der Pauw and the differential C-V measurements. It is interesting to note the high mobility (μ_{av} = 4520 cm^2/V-s) associated with this implanted sample. In particular, the

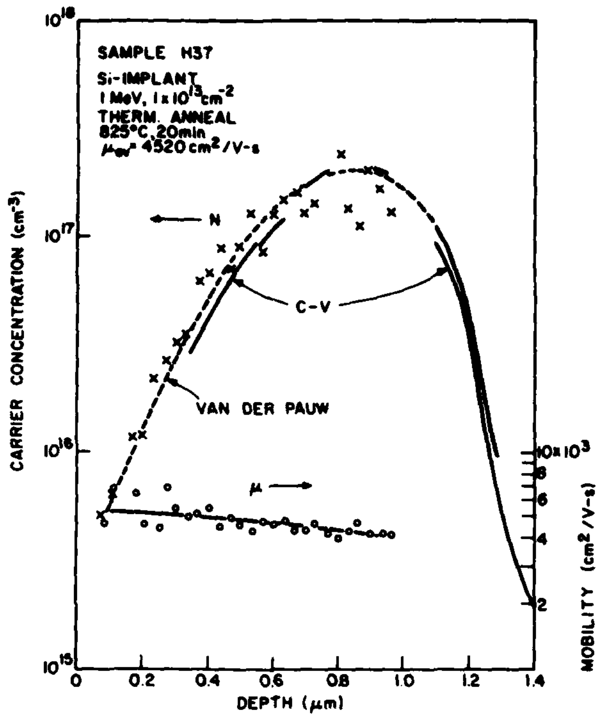

Figure 34. Carrier concentration and mobility profiles of sample H37.

mobility is maintained at a high level of $\sim$5000 cm^2/V-s as the doping density decreases to $\sim 10^{16}$ cm^{-3} toward the sample surface. This result was not observed in low-dose ($<3\times10^{12}$ cm^{-2}), low-energy ($\sim$200 keV) implantation experiments. We speculate that this result may be related to the Cr redistribution in the SI GaAs substrate following implantation and annealing. As shown in Section IV, the Cr distribution depends on the amount of implant dose. In sample H37 (1 MeV, 1×10^{13} cm^{-2}), the Cr was depleted from 5×10^{16} cm^{-3} to $\sim$2-3×10^{16} cm^{-3} in the surface layer following thermal annealing. The low Cr concentration could reduce compensation and allow low dose activation with higher mobility. Related experimental results are described later.

D. MULTIPLE IMPLANTATIONS - DOPING PROFILE CONTROL

1. Formation of a Flat High-Doped n-Type GaAs Layer

Implant conditions have been worked out for forming $\sim$1-μm-deep layers of Si in GaAs with nearly constant doping throughout the layer. Five implants,

ranging from 40 to 900 keV, are used to construct the layer. Table 8 shows the calculated implant conditions for achieving flat profiles at two different impurity concentration levels: 1×10^{20} cm^{-3} for sample H23 and 1×10^{18} cm^{-3} for sample H27.

TABLE 8. CALCULATED MULTIPLE-IMPLANT PARAMETERS

H23		H27	
Energy (keV)	Dose (cm^{-2})	Energy (kev)	Dose (cm^{-2})
40	4.7×10^{14}	40	4.7×10^{12}
120	1.4×10^{15}	120	1.4×10^{13}
280	1.9×10^{15}	280	1.9×10^{13}
500	2.7×10^{15}	500	2.7×10^{13}
900	4.3×10^{15}	900	4.3×10^{13}

A comparison of the calculated plot* and the actually measured SIMS profile is given in Fig. 35 (log plot) and Fig. 36 (linear plot). Actual implantation data are shown in Table 9. It is evident from the plot in Fig. 36 that a discrepancy exists between the calculated profile and the actual profile produced by the implant machine. It should be pointed out that these implants were made before the 4° beam deflection system was installed in the Van de Graaff machine.

Figure 37 shows the profile of a multiple-implanted sample (H27) designed to produce a 1-μm flat profile with a maximum impurity concentration of 1×10^{18} cm^{-3}. The implant parameters are in Table 8. The samples were capless-annealed at 825°C for 20 min in an arsenic overpressure following implantation.

The shape of the profiles determined from the differential C-V measurements show reasonable agreement with the SIMS measurements made on high-dose-implanted, unannealed samples. The differences in range and standard deviation are approximately within 10% on the 1-MeV single-energy implanted samples. The deviations between the multiple-implanted profiles determined by the SIMS and

*The calculated data were made using conventional LSS R_p and ΔR_p values.

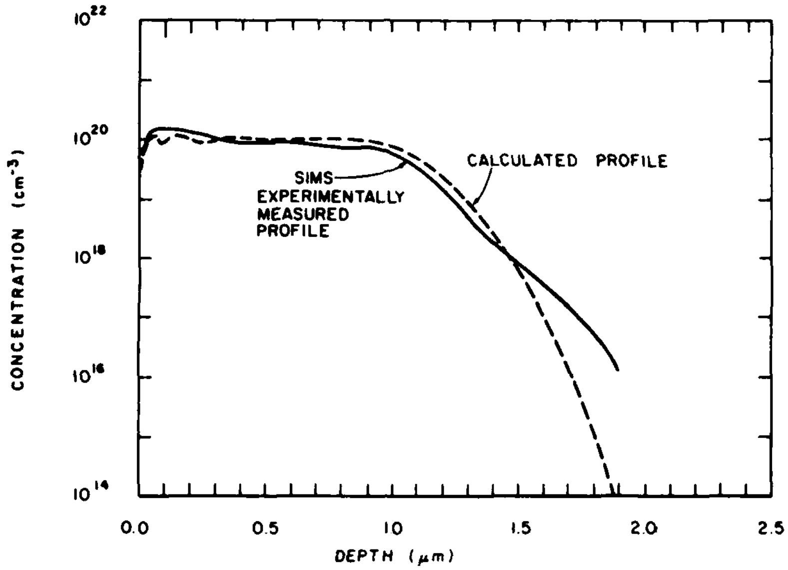

Figure 35. Comparison of calculated and actual SIMS profiles, log plot.

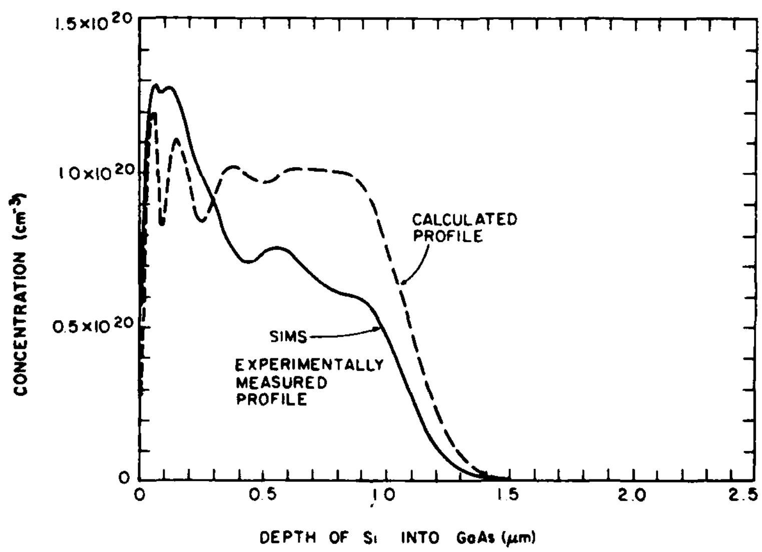

Figure 36. Comparison of of calculated and actual SIMS profiles, linear plot.

TABLE 9. IMPLANT CONDITIONS FOR FLAT PROFILE OF Si IN GaAs

	Energy (keV)				
Parameter	40	120	280	500	900
R_p (μm)	0.0466	0.1375	0.3195	0.5500	0.8860
ΔR_p (μm)	0.0199	0.0600	0.1050	0.1500	0.1900
N_{max} (cm^{-2})	9.47×10^{19}	9.08×10^{19}	7.23×10^{19}	7.26×10^{19}	9.09×10^{19}
N_{dose} (cm^{-2})	4.70×10^{14}	1.35×10^{15}	1.9×10^{15}	2.73×10^{15}	4.33×10^{15}
Dose No.	303.6	872.0	1227	550.2	872.6

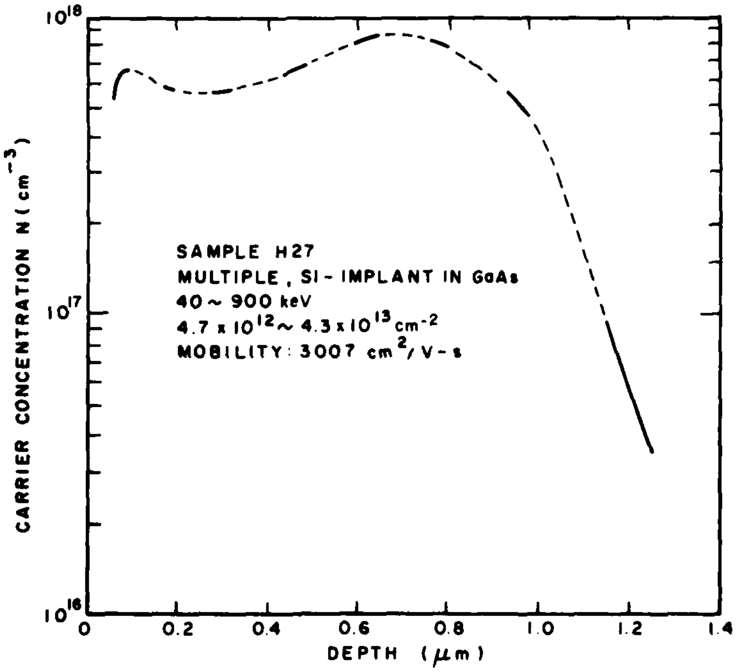

Figure 37. Carrier concentration of a multiple-implanted sample.

C-V measurement are greater. This is expected because the C-V measurement determines the electrically active carrier concentration distribution, while the activation efficiency varies with amount of dose and energy. A better match can be obtained by including the dose-and-energy-dependent activation efficiency in the flat-profile design. The measured mobility of 3000 $cm^2/V\text{-}s$ using van der Pauw measurement compares favorably with published data [54] for n-GaAs, with an electron density close to 1×10^{18} cm^{-3}.

2. Formation of a Medium-Doped n-Type GaAs Layer

We have also investigated producing medium- and low-dose implanted n-layers with controlled electron density profiles to meet the requirement of device (MESFET) fabrication. Based on the range and straggle data deduced from the SIMS profiles made on Si-implanted GaAs samples, we designed multiple-implantation profiles to produce (a) a flat 0.6- to 1.1-μm-thick n-layer at an electron density of $\sim 10^{17}$ cm^{-3} and (b) a high/low (n^+-n) profile which has an n^+-layer at the surface followed by the n-active layer. The n^+-layer is to facilitate good ohmic contacts. A computer program was used for the design. Table 10 shows the calculated implant conditions using four implants for achieving flat and n^+-n profiles at an impurity concentration level of 1.5×10^{17} cm^{-3}.

TABLE 10. CALCULATED MULTIPLE-IMPLANT PARAMETERS FOR FLAT (H51, H52) AND HIGH-LOW (H53) PROFILES OF Si IN GaAs

H51 and H52		H53	
Energy (keV)	Dose (cm^{-2})	Energy (keV)	Dose (cm^{-2})
70	1.7×10^{12}	70	4.0×10^{13}
250	4.3×10^{12}	250	4.3×10^{12}
600	6.5×10^{12}	600	6.5×10^{12}
1000	7.0×10^{12}	1000	7.0×10^{12}

54. S. Sze, Physics of Semiconductor Devices, (John Wiley & Sons, Inc., New York, 1969).

The corresponding implantation data are shown in Table 11. A comparison of the calculated plot, the measured SIMS profile, and carrier concentration profile is given in Fig. 38 for the flat profile and in Fig. 39 for the n^+-n profile.

TABLE 11. IMPLANT CONDITIONS FOR FLAT (AT 1.5×10^{17} cm^{-3}) AND HIGH-LOW PROFILES OF Si IN GaAs

H51 and H52

Energy (keV)	70	250	600	1000
N_{dose} (cm^{-2})	1.7×10^{12}	4.3×10^{12}	6.5×10^{12}	7.0×10^{12}
Dose No.	32.1	27.4	19.3	20.9
Scale	2×10^{-7}	6×10^{-7}	6×10^{-7}	6×10^{-7}

H53

Energy (keV)	70	250	600	1000
N_{dose} (cm^{-2})	4.0×10^{13}	4.3×10^{12}	6.5×10^{12}	7.0×10^{12}
Dose No.	25.8	27.4	19.3	20.9
Scale	6×10^{-6}	6×10^{-7}	6×10^{-7}	6×10^{-7}

Area = 24.19 cm^2 Area = 11.40 cm^2

The agreement among the three profiles in Fig. 38 is reasonably good. The abrupt decrease in carrier concentration at the tail end of the profile, as compared to the calculated and the SIMS profiles, is believed related to the low activation at low dose levels. The dip in the profile around 0.4 μm below the surface is a result of approaching the limit of the two implant machines used (one <300 keV, one >500 keV). These comments are also applicable to Fig. 39. The carrier concentration profile shown in Fig. 39 is measured using a Polaron machine, which performs step chemical etching and C-V profiling automatically.

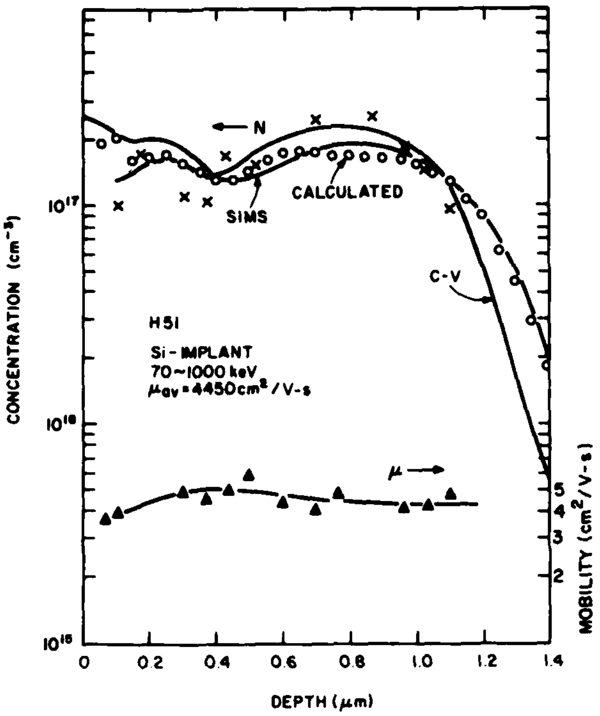

Figure 38. Multiple-implant profiles of H51: SIMS, carrier concentration, and calculated.

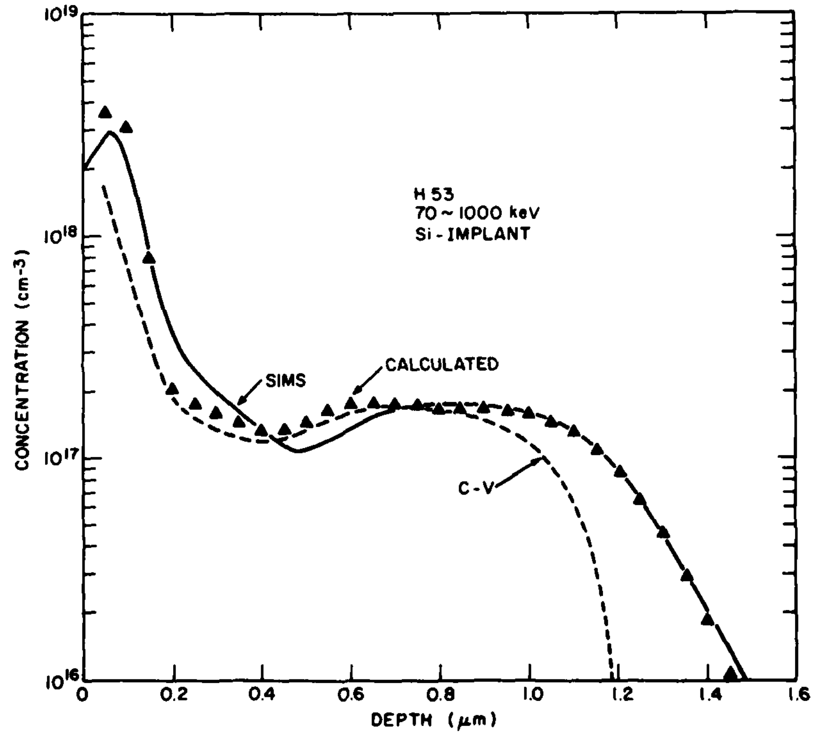

Figure 39. High-low dose multiple-implant profiles: SIMS, carrier concentration, and calculated.

The carrier concentration and the Hall mobility profiles in multiple-implanted thermally annealed sample H51 were also measured using differential van der Pauw measurement. The results are included in Fig. 38. The carrier concentration data are shown as crosses, and the mobility data are shown as triangles. The profile agrees well with that determined from the differential C-V measurement.

For a better approximation of a ~1-μm flat profile, an alternative multiple-implant schedule was utilized. This was done by operating the Van de Graaff machine at a lower energy and the 300-keV implanter at a higher energy. This would eliminate the dip in the implant profiles encountered previously.

The revised implant parameters and implant conditions for wafers H62 and H63 are shown in Tables 12 and 13, respectively; the corresponding calculated Si distribution and measured carrier concentration and mobility profiles of H62 are shown in Fig. 40. Carrier concentration profiles measured using both differential C-V and van der Pauw measurements are included. The wafer using the revised implant schedule indeed showed an improved ~1-μm-thick constant doping profile.

TABLE 12. CALCULATED MULTIPLE-IMPLANT PARAMETERS FOR FLAT PROFILES OF Si IN GaAs (WAFERS H62 AND H63)

Energy (keV)	Dose (cm^{-2})
80	1.6×10^{12}
265	4.3×10^{12}
500	5.8×10^{12}
900	7.2×10^{12}

We also fabricated thinner (~0.5 to 0.7 μm) medium-dose implanted n-GaAs layers using multiple implantation. Table 14 shows the implant parameters of two different designs for wafers H89 and H73. The calculated silicon profile and the measured electron density profile of wafers H89 and H73 are illustrated respectively in Figs. 41 and 42. The electrical characteristics of H89 and H73 measured using the van der Pauw methods are summarized in Table 15. The

TABLE 13. IMPLANT CONDITIONS FOR WAFERS H62 AND H63

Energy (keV)	80	265	500	900
N_{dose} (cm^{-2})	$1.6x10^{12}$	$4.3x10^{12}$	$5.8x10^{12}$	$7.2x10^{12}$
Dose No.	31.0	27.7	20.2	25.1
Scale	$2x10^{-7}$	$6x10^{-7}$	$6x10^{-7}$	$6x10^{-7}$

Area = 24.19 cm^2 Area = 13.07 cm^2

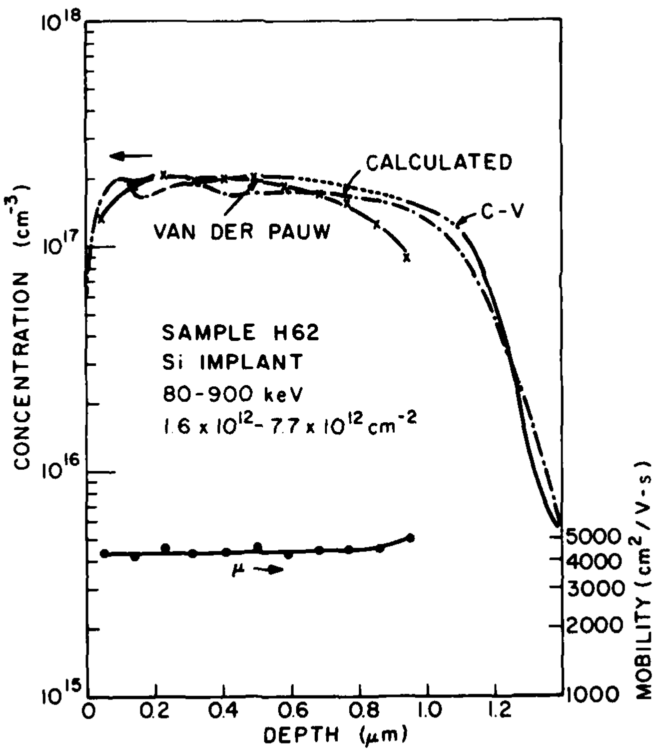

Figure 40. Multiple-implant profiles of H62: calculated and measured. Mobility profile also included.

electron density profiles were measured using a Polaron profiler, which performs step layer removal and plots the result of C-V measurement automatically. The activation is higher in the Ar-implant ($7.5x10^{12}$ cm^{-2}, 750 keV) pretreated sample than in the control. The mobilities of those two samples are comparable.

TABLE 14. CALCULATED MEDIUM-DOSE MULTIPLE-IMPLANT PARAMETERS FOR 0.5-μm-THICK FLAT PROFILE OF Si IN GaAs (WAFERS H89, H73)

H89		H73	
Energy (keV)	Dose (cm^{-2})	Energy (keV)	Dose (cm^{-2})
400	$4.5x10^{12}$	500	$8.0x10^{12}$
180	$2.0x10^{12}$	260	$4.8x10^{12}$
50	$0.5x10^{12}$	80	$1.6x10^{12}$

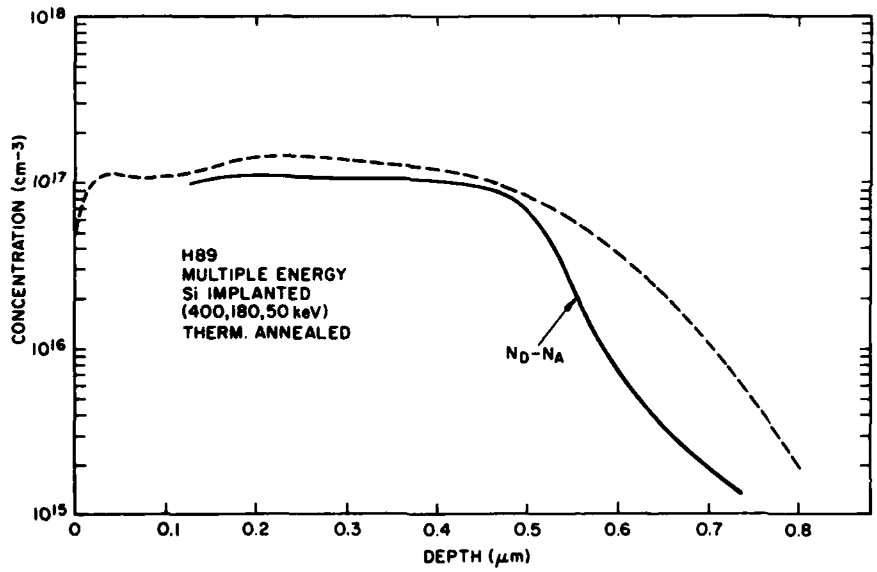

Figure 41. Multiple-implant profiles of H89: calculated (dashed line) and measured.

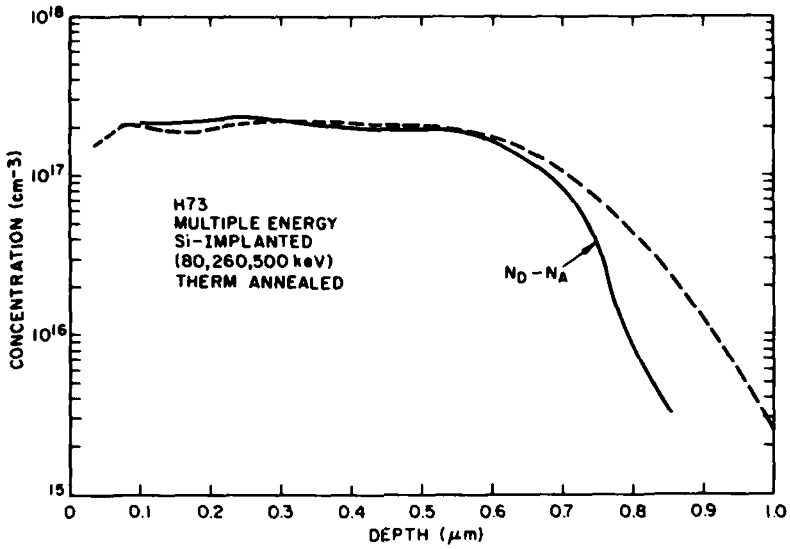

Figure 42. Multiple-implant profiles of H73: calculated (dashed line) and measured.

TABLE 15. ELECTRICAL CHARACTERISTICS OF WAFERS H89 AND H73 MEASURED BY THE VAN DER PAUW METHOD

Sample No.	Substrate	Implant Conditions: Energy (keV)	Implant Conditions: Dose (cm^{-2})	N_s (cm^{-2})	μ (300K) (cm^2/V-s)	η (%)
H89	LEC	400	4.5×10^{12}	4.62×10^{12}	4080	65.9
	Cr doped	180	2.0×10^{12}			
		50	0.5×10^{12}			
H89R	LEC	400	4.5×10^{12}	5.92×10^{12}	4020	84.7
	Cr doped	180	2.0×10^{12}			
	Ar treated	50	0.5×10^{12}			
H73	LEC	500	8.0×10^{12}	1.44×10^{13}	3360	99.7
	Cr doped	260	4.8×10^{12}			
		80	1.6×10^{12}			

Medium-dose multiple implantation studies were also carried out at implant energies below 300 keV for optimization of doping profiles of the implanted n-layers for device (FET) fabrication. High-performance power FETs operating up to 26 GHz were fabricated (in a concurrent program) from a GaAs wafer made by double Si implantation into SI GaAs substrates followed by capless thermal annealing. Power output of ~220 mW at 15 GHz was obtained from a single cell (600-μm gate width) with corresponding gain of 6 dB and power-added efficiency of 27%. The power output and efficiency at 26 GHz are 60 mW and 5%, respectively.

The electron density profiles of representative double Si-implanted thermally annealed samples are shown in Figs. 43 and 44. The profiles were measured by differential C-V technique combined with controlled chemical etching. The wafers were capless-annealed under arsenic overpressure at 825°C for 20 min.

Wafers C77 and C77F, shown in Fig. 44, are identical, except that during annealing two pieces of wafers marked C77F were placed face-to-face on a carrier in the open quartz tube, while wafer C77 was placed face-up in the normal way on a carrier in the same open quartz tube. The wafers annealed under face-to-face conditions showed lower mobility and activation efficiency, as indicated in Fig. 44. The measured peak carrier concentration density is 1.6×10^{17} cm^{-3} for wafer C77F and 2.0×10^{17} cm^{-3} for wafer C77. The lower activation and mobility in the face-to-face annealed wafer indicate that the arsenic overpressure system which we used for thermal annealing is superior. It has been reported in the literature that face-to-face annealing has resulted in good quality n-layers.

3. Formation of a Low-Doped n-Type GaAs Layer

One of the goals of this program is to create a thick, low carrier concentration n-GaAs layer using multiple, high-energy implantation. Since the high-energy Ar-implant treatment has shown substantial improvement for low-dose activation, we have performed multiple implantation of ^{28}Si into a high-energy Ar-treated substrate and compared the results with implants into an untreated substrate.

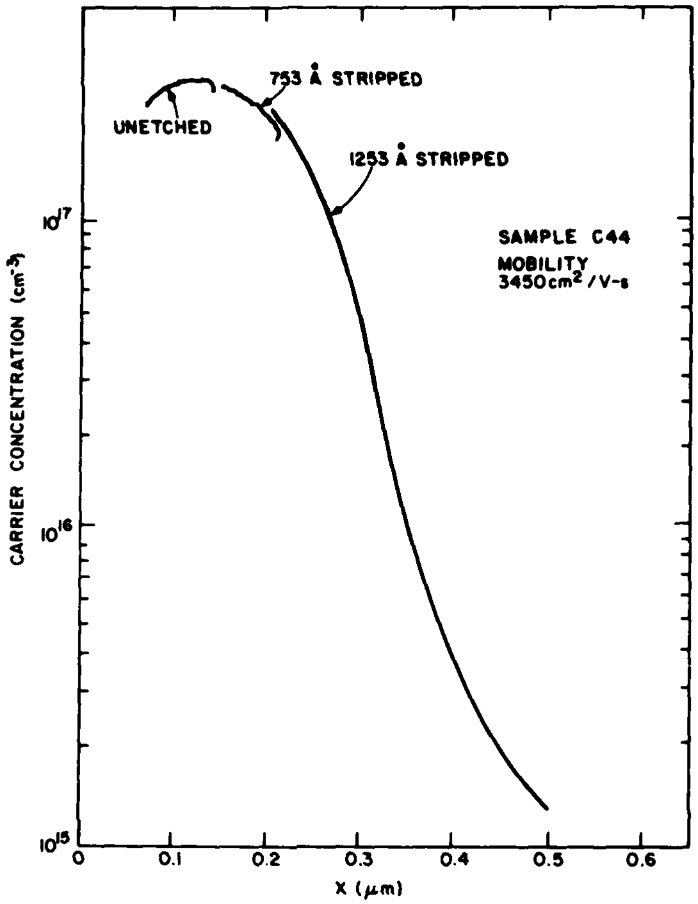

Figure 43. Electron density profile of double-implanted GaAs sample C44.

An implantation schedule to obtain a 0.6-μm-thick, $5x10^{16}$ cm^{-3} n-GaAs layer was designed using three Si implants at energies of 80, 260, and 500 keV into a SI GaAs substrate. An LEC Cr-doped substrate was used for the experiment. Prior to Si implantation, half of the wafer was ^{40}Ar-implanted at 750 keV with a fluence of $5x10^{12}$ cm^{-2}, and half of the wafer was masked from ^{40}Ar implant with an aluminum foil. After Si implant and capless annealing, the two sections of the wafer (designated H80 and H80R) were evaluated using van der Pauw measurement. Table 16 summarizes the implant parameters and the measured results. The Ar-implanted section of the wafer, H80R, shows an improvement in mobility and activation of 9% and 83%, respectively.

Figure 45 shows the electron density profiles of the low-dose multiple Si-implanted wafers, H80 and H80R, where H80R received high-energy Ar-implant

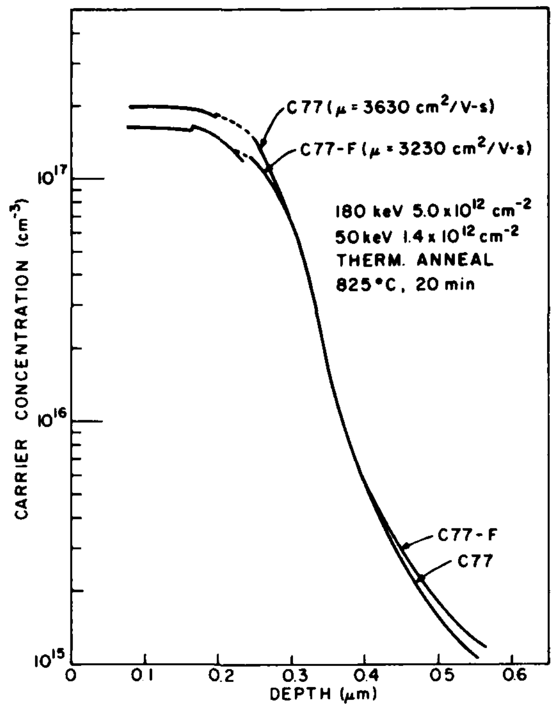

Figure 44. Electron density profiles of double-implanted GaAs samples. C77F is "face-to-face" annealed.

TABLE 16. ELECTRICAL CHARACTERISTICS OF MULTIPLE-ENERGY Si-IMPLANTED n-GaAs IN LEC SI GaAs SUBSTRATES

		Implantation					
Wafer	Substrate	Energy (keV)	Dose (cm^{-2})	N_s (cm^{-2})	μ(300K) (cm^2/V-s)	ρ_s (Ω/□)	η (%)
H80	LEC	500	$3.0x10^{12}$	$2.5x10^{12}$	4300	581	42.2
	Cr doped	260	$2.0x10^{12}$				
		80	$8.4x10^{11}$				
H80R	LEC	500	$3.0x10^{12}$	$4.5x10^{12}$	4700	296	77.2
	Cr doped	260	$2.0x10^{12}$				
	Ar treated	80	$8.4x10^{11}$				

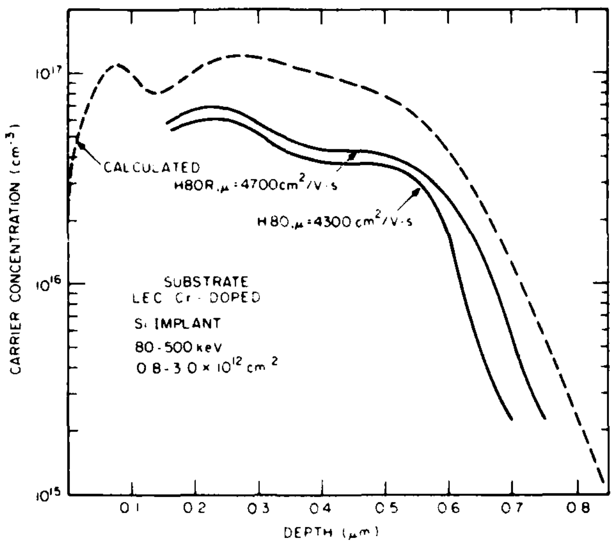

Figure 45. Electron density profiles of multiple Si-implanted n-layers on Si GaAs substrate with (H80R) and without (H80) ^{40}Ar pretreatment. Calculated profile is shown by dashed line.

treatment prior to Si implantation. The average carrier concentration is approximately 5-6x10^{17} cm^{-3}. The Ar-implant-treated wafer has a higher carrier concentration and increased width.

SECTION IV

CHARACTERIZATION OF Si IMPLANTS IN VARIOUS SI GaAs SUBSTRATES - NOT ^{40}Ar-IMPLANT TREATED

A good-quality SI GaAs substrate is crucial for producing high-quality n-layers for device fabrication. The types of substrates obtained for evaluation from various sources were: Metals Research Company (Cr doped, grown by LEC method), Westinghouse Research Laboratories (Cr doped and undoped, grown by LEC method), Crystal Specialties, Inc. (Cr doped, grown by Bridgman method), and Sumitomo Electric Industries (type OA, Cr-O doped).

The substrates were evaluated by implanting ^{28}Si at an energy of 200 keV at two fluence levels; viz., 2×10^{12} cm^{-2}, the typical low-dose threshold for Cr-doped SI GaAs as determined earlier, and 5×10^{12} cm^{-2}, the typical dose for producing the 2×10^{17}-cm^{-3} electron density used in GaAs FET fabrication. Alternative multiple-energy implants were also employed for approximating a constant doping profile. The implanted wafers were annealed at 825°C for 20 minutes under arsenic overpressure. The n-layers were then characterized by measuring the electron *mobility*, *activation efficiency*, and electron density profiles. The measured results indicate that:

(1) Activation of a medium-dose implant is higher than that of a low-dose (near threshold) implant.

(2) Low-dose implant in a Cr-doped Bridgman-grown substrate shows lowest mobility while a similar implant into an LEC undoped substrate shows highest mobility.

A. ELECTRICAL CHARACTERIZATION

1. Bridgman-Grown and LEC SI GaAs Substrates

Table 17 indicates that the implanted n-layers on Cr-doped substrates grown by the LEC method show good mobility but low activation efficiency. (Wafer C101B used substrates purchased from Metals Research Co., and wafers C93C and C93D used substrates obtained from Westinghouse Research Laboratories through M. N. Yoder of ONR).

TABLE 17. CHARACTERISTICS OF SUBSTRATES AT LOW-IMPLANT DOSES

Wafer	Substrate	Implantation Energy (keV)	Implantation Dose (cm^{-2})	N_s (cm^{-2})	μ (cm^2/V-s)	ρ_s ($\Omega/\square$)	η (%)
C93C	LEC Cr-doped	200	$2x10^{12}$	$6.3x10^{11}$	3720	2690	31.3
C93D	LEC Undoped	200	$2x10^{12}$	$5.7x10^{11}$	5250	2360	28.5
C73A	Bridgman Cr-doped	200	$2x10^{12}$	$6.0x10^{11}$	1590	6570	30.0
C101B	LEC Cr-doped Seed	200 70	$1.6x10^{12}$ $4.4x10^{11}$	$5.8x10^{11}$	4280	2520	28.4

Table 18 summarizes the electrical characteristics of medium-dose, Si-implanted n-layers on different GaAs substrates. Sample C94A, which uses an undoped substrate obtained from Westinghouse, gives slightly better mobility and activation than C94B, which uses a Cr-doped substrate obtained from Crystal Specialties, Inc. The substrates used for samples C99A, C99C, and C99D were cut from the center, tail, and seed sections, respectively, of an ingot. These substrates were purchased from Metals Research Co., England.

2. Cr-O-Doped SI Substrates

Table 19 summarizes the electrical characteristics of Si-implanted, capless-annealed wafers using a Cr-O-doped substrate (known as type OA, purchased from Sumitomo Electric Industries in Japan). According to the supplier, the type OA substrate is oxygen dominant, i.e., the deep donor density exceeds the deep acceptor density. Three wafers cut from the front, middle, and tail of an ingot were evaluated at two different fluence levels: (1) low-dose level ($2x10^{12}$ cm^{-2}, 200 keV) near the activation threshold in typical Cr-doped SI GaAs substrates and (2) medium-dose level ($\sim6x10^{12}$ cm^{-2}, dual-energy implanted) for creating a layer of n-GaAs with carrier concentration of $2x10^{17}$ cm^{-3}. For the low-dose implants, all three wafers (D4A, D4B, D4C) showed a mobility (300K) near or greater than 4000 cm^2/V-s.

TABLE 18. CHARACTERISTICS OF SUBSTRATES AT MEDIUM-IMPLANT DOSES

Wafer	Substrate	Implantation Energy (keV)	Implantation Dose (cm^{-2})	N_s (cm^{-2})	μ (cm^2/V-s)	ρ_s ($\Omega/\square$)	η (%)
C94B	Bridgman Cr-doped	200	5.0×10^{12}	2.7×10^{12}	3690	637	53.2
C94A	LEC Undoped	200	5.0×10^{12}	3.0×10^{12}	3800	556	59.2
C99A	LEC Cr-doped (center)	200	5.0×10^{12}	3.2×10^{12}	4020	486	63.6
C99C	LED Cr-doped (tail)	200	5.0×10^{12}	3.3×10^{12}	4070	465	65.2
C99D	LEC Cr-doped (seed)	200	5.0×10^{12}	3.4×10^{12}	4070	449	68.0
D7	Bridgman Cr-doped	180 50	5.2E12 1.4E12	4.0×10^{12}	3100	504	60.5

For medium-dose implants, the three wafers (D5A, D5B, D6A), which received no ^{40}Ar bombardment, showed a mobility between 3580 and 4010 cm^2/V-s and an activation efficiency between 48 and 68%. The differences may indicate the difference in Cr/O concentrations of different sections of the ingot. This remains to be studied further. Note that the substrate cut from the middle of the ingot shows lower activation efficiency both in the case of low-dose implant (D4B) and medium-dose implant (D5B).

B. ELECTRON DENSITY PROFILES

1. Bridgman-Grown and LEC SI GaAs Substrates

The electron density profiles of Si-implanted n-layers depend on substrates and dose levels. Figure 46 shows the profiles of the low-dose, Si-implanted n-layers on Cr-doped (C93C) and undoped (C93D) LEC-grown substrates. These substrates were obtained from Westinghouse Research Laboratories. The Cr-doped

TABLE 19. ELECTRICAL CHARACTERITICS OF Si-IMPLANTED n-GaAs IN A Cr-O-DOPED SUBSTRATE

A. Low-Dose Implant

Wafer	Substrate	Implantation Energy (keV)	Dose (cm^{-2})	N_s (cm^{-2})	μ ($cm^{-2}/V\text{-}s$)	ρ_s ($\Omega/\square$)	η (%)
D4A	Cr-O doped FRONT	200	2×10^{12}	8.1×10^{11}	4090	1890	40.7
D4B	Cr-O doped MIDDLE	200	2×10^{12}	3.6×10^{11}	4220	4120	18.1
D4C	Cr-O doped BACK	200	2×10^{12}	1.2×10^{12}	3990	1310	57.5

B. Medium-Dose Implant

Wafer	Substrate	Implantation Energy (keV)	Dose (cm^{-2})	N_s (cm^{-2})	μ ($cm^{-2}/V\text{-}s$)	ρ_s ($\Omega/\square$)	η (%)
D5A	Cr-O doped BACK	180 50	5.5×10^{12} 1.4×10^{12}	4.7×10^{12}	4010	330	68.4
D5B	Cr-O doped MIDDLE	180 50	5.5×10^{12} 1.4×10^{12}	3.4×10^{12}	3640	511	48.7
D6A	Cr-O doped FRONT	180 50	5.2×10^{12} 1.4×10^{12}	4.4×10^{12}	3580	397	67.2

substrate (WBN 15-10) produces a broader electron density profile which appears closer to the LSS profile than the undoped substrate (WBN 14-20). The mobility of the implanted n-layer (C93D) in the undoped substrate was higher as indicated previously in Table 17.

Figure 47 illustrates the electron density profiles of two medium-dose (5×10^{12} cm^{-2} 200 keV) Si-implanted n-layers (C94A and C94B) using an LEC-grown, undoped substrate (Westinghouse WBN 14-20), and a Bridgman-grown Cr-doped substrate (Crystal Specialties, #3765), respectively. The mobilities are both under 4000 $cm^2/V\text{-}s$.

The profiles of implanted n-layers on three different sections of a Cr-doped GaAs ingot (#A88, LEC-grown, from Metals Research Labs, Inc.) are

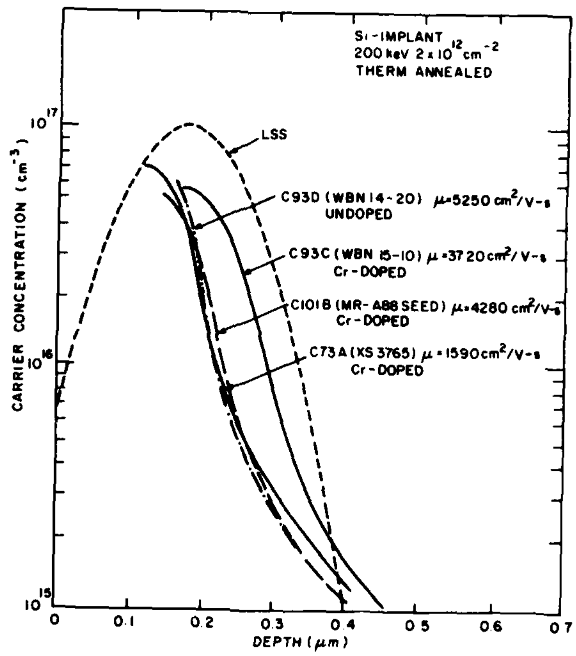

Figure 46. Electron density profiles of C93C, C93D, C101B, and C73A (Westinghouse, Metals Research, and Crystal Specialties substrates).

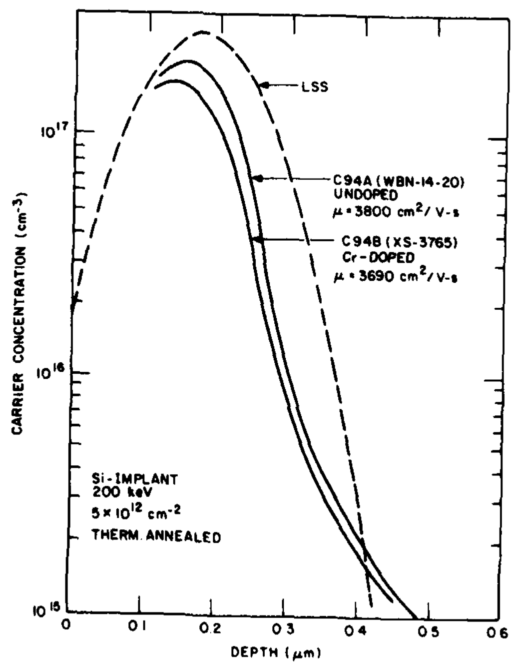

Figure 47. Electron density profiles of C94A and C94B.

shown in Fig. 48. Samples C99A, C99C, and C99D correspond to implantations into wafers from the center, tail, and seed sections of the ingot. All three samples show similar peak carrier concentration values. The Cr concentration in the crystal increases from the seed end toward the tail end. The difference in profile width could be related to the Cr concentration in the substrate.

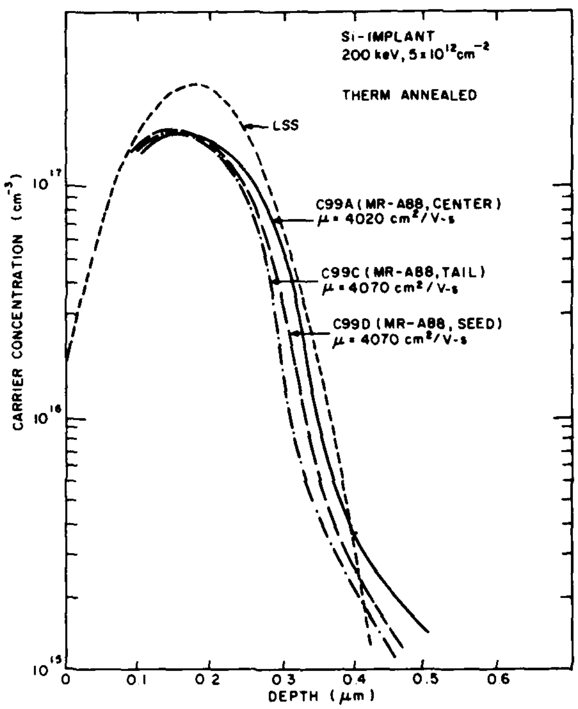

Figure 48. Electron density profiles of C99A, C99C, and C99D.

Calculated LSS doping profiles are includes in Figs. 46, 47, and 48. It should be pointed out that the electron density profile obtained by C-V measurement is inherently limited in reproducing a shallow electron density profile with a steep doping gradient [45]. A perfect match between the measured profile and the LSS profile is not expected even when the activation reaches 100%.

2. Cr-O-Doped SI GaAs Substrates

The electron density profiles of wafers D4A, D4B, and D4C are illustrated in Fig. 49. The measured peak carrier concentration is $5\text{x}10^{16}$ cm^{-3} for D4A and

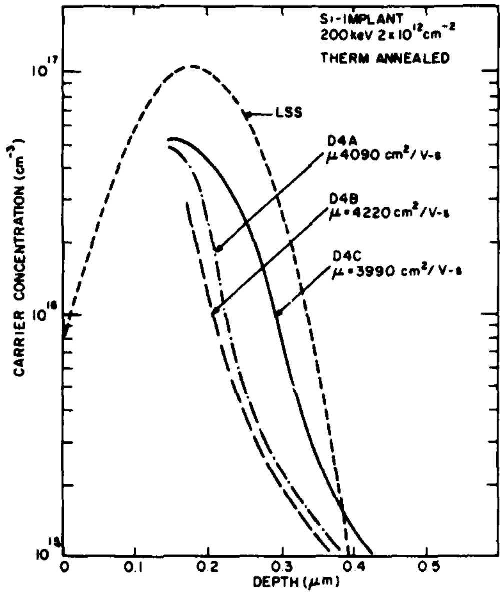

Figure 49. Electron density profiles of capless-annealed, low-dose Si-implanted wafers from the front (D4A), middle (D4B), and back (D4C) of a Cr-O-doped SI GaAs ingot.

D4C and 3x10^{16} for D4B. A large portion of each profile is not obtainable because of zero bias depletion. The variation in shape between each profile may indicate a difference in Cr/O concentration in different sections of the ingot. The range of variation is similar to that measured in LEC Cr-doped and undoped substrates as described previously.

SECTION V

Si-IMPLANTATION STUDY IN ^{40}Ar PRETREATED SI GaAs SUBSTRATES - ACTIVATION AND MOBILITY ENHANCEMENT

Implantation of Si into SI GaAs substrates exhibits a low-dose threshold [1,9]. Below this threshold, the implanted layer either shows no electrical activation or shows activation with very poor mobility after the implanted wafer is thermally annealed. The dose threshold depends on the substrate material and is typically $\sim$1-2x10^{12} cm^{-2} at an implant energy of 200 keV which corresponds to an impurity concentration peak of

$$N_m = \frac{N}{\sqrt{2\pi}\ \Delta R_p} \approx 4\text{-}8\times10^{16}\ \mathrm{cm}^{-3}$$

This carrier concentration corresponds approximately to the Cr concentration in most of the Cr-doped SI GaAs substrates used.

During this program, we developed a technique for generation of n-GaAs layers with higher activation efficiency and/or electron mobility of ^{28}Si implantation into SI GaAs substrates pretreated by a 750-keV, ^{40}Ar implantation. The ^{40}Ar pretreatment has greatly improved the low-dose Si-implant threshold in Cr-doped Bridgman substrates.

In this section, experimental results on activation and mobility enhancement in three different types of substrates will be presented, viz., Bridgman-grown Cr-doped; LEC-grown, Cr-doped and undoped; and Cr-O-doped substrates. The experimental data are analyzed using two probable mechanisms: (1) redistribution of Si atoms from acceptor sites to donor sites and (2) reduction of Cr acceptors.

A. BRIDGMAN-GROWN Cr-DOPED SUBSTRATES

Low-dose (2x10^{12} cm^{-2}, 200 keV) Si-implantation studies were made in a number of Ar-implanted capless-annealed SI GaAs samples that were cut from a Bridgman-grown SI GaAs substrate. The substrate, when not ^{40}Ar treated, had given poor performances at this low-dose level, as described previously in Section IV. Sample C73A gave a mobility of 1590 cm^2/V-s, an activation efficiency of 30% (Table 17), and a carrier density profile (Fig. 46) substantially deviating from LSS.

The fluences of Ar implants in this study were varied between 5×10^{12} cm^{-2} and 1×10^{15} cm^{-2}, and these implantations were made at 750 keV using a Van de Graaff machine. The Ar implantation and subsequent thermal annealing resulted in a redistribution of Cr in the GaAs substrate. The high-energy implantation caused Cr redistribution to a greater depth. Details of Cr redistribution are discussed in Section VI.

After capless annealing, three of the Si-implanted samples were activated with mobilities of greater than 4000 $cm^2/V\text{-}s$, as shown in Table 20. The three samples were pretreated with ^{40}Ar implant at 750 keV with doses of 5×10^{12}, 1×10^{13}, and 5×10^{13} cm^{-2} and followed by thermal annealing at 825°C for 20 min. Notice the substantial increase in activation and mobility for samples pretreated with ^{40}Ar dose. The increase in activation is smallest in sample R7 which was treated with high-dose Ar implant. Sample C73A without ^{40}Ar treatment is included in Table 20 for comparison.

TABLE 20. PROPERTIES OF A LOW-DOSE (2×10^{12} cm^{-2}, 200 keV) Si-IMPLANTED n-LAYER IN Ar-TREATED AND UNTREATED Cr-DOPED BRIDGMAN-GROWN SI GaAs SUBSTRATES

Sample	Ar Dose (cm^{-2}) at 750 keV	μ ($cm^2/V\text{-}s$)	η (%)
R5	5×10^{12}	4410	67.4
R6	1×10^{13}	4010	74.5
R7	5×10^{13}	4080	41.0
C73A	None	1590	30.0

The other samples that received high-dose Ar implants (1×10^{14} and 1×10^{15} cm^{-2}) did not activate. Instead, a conductive layer, which is an indication of conversion, was measured on the surface of one of the wafers (1×10^{15} cm^{-2} implanted).

Figure 50 illustrates the electron density profiles measured by the differential C-V method on the three electrically activated samples. An LSS

profile is included for reference. Note that: (1) The three profiles are much closer to the LSS than that of sample C73A illustrated previously in Fig. 46); C73A had the same Si-implant conditions but without ^{40}Ar pretreatment and (2) sample R7, which was implanted with ^{40}Ar at the highest dose (5×10^{13} cm^{-2}) among the three, showed a much lower peak carrier density.

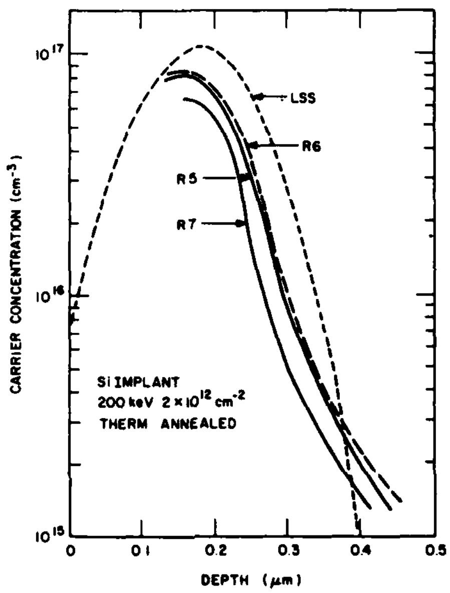

Figure 50. Electron density profiles of R5, R6, and R7, three Si implants in substrates pretreated with ^{40}Ar implant plus anneal; the ^{40}Ar doses are 5×10^{12}, 1×10^{13}, and 5×10^{13} cm^{-2}, respectively.

The effect of ^{40}Ar pretreatment on two higher-dose Si-implanted Bridgman-grown Cr-doped substrates is illustrated in the electron density profiles shown in Figs. 51 and 52. A substantial increase in peak carrier concentration and mobility is obtained in D7R and D8R, which were processed identically to D7 and D8, respectively, with the exception that the substrates were pretreated with 5×10^{12}-cm^{-2} ^{40}Ar implant at 750 keV. The electrical properties of D7, D7R, D8, and D8R and the implant conditions are tabulated in Table 21.

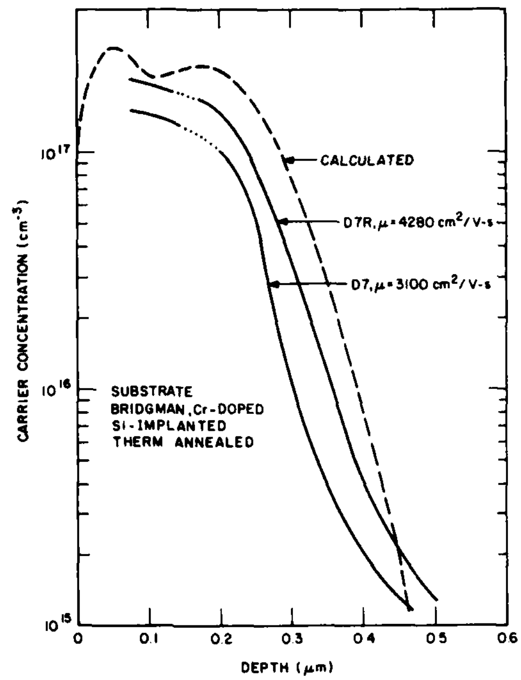

Figure 51. Electron density profiles of D7 and D7R, Si-implanted n-GaAs in a Cr-doped Bridgman-grown substrate. D7R also received high-energy ^{40}Ar implant.

B. LEC Cr-DOPED SUBSTRATES

In our previous studies (see Table 17) the n-GaAs layer created by Si implant and thermal anneal using the LEC Cr-doped substrates has shown a good mobility but a low activation at low implant fluence levels. Wafer C101B, for example, resulted in a mobility of 4280 $cm^2/V\text{-}s$ at a low activation of 28.4% at a total implant dose of $2.4x10^{12}$ cm^{-2}. We were interested to find out whether further improvement could be made if the substrate were first bombarded with high-energy ^{40}Ar.

Table 22 summarizes the implant schedules and measured results of low-dose Si-implanted, thermally annealed n-layers in an LEC Cr-doped SI GaAs substrate. The substrate was cut into four sections. Each section except one was pre-treated with ^{40}Ar implant at 750 keV with doses of $5x10^{12}$, $7.5x10^{12}$, and $1.0x10^{13}$ cm^{-2}. The wafers were then implanted with Si and capless-annealed at 825°C for 20 min. The Si-implant schedules are included in Table 22.

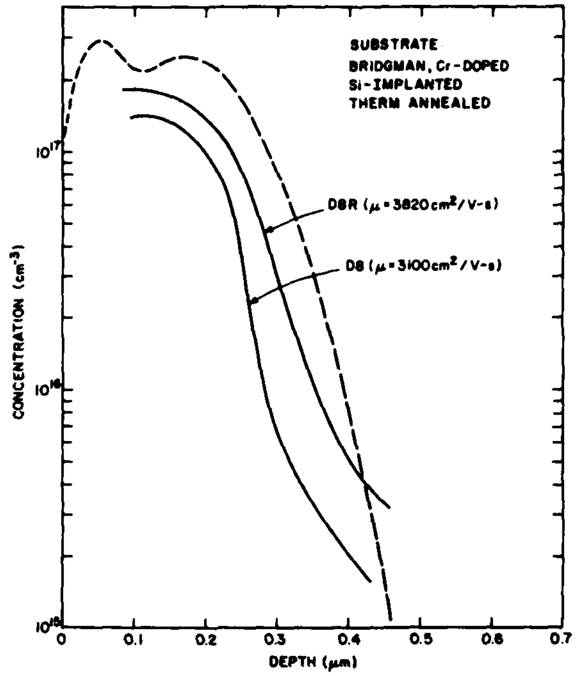

Figure 52. Electron density profiles of D8 and D8R, Si-implanted n-GaAs in a Cr-doped Bridgman-grown substrate. D8R also received high-energy ^{40}Ar implant.

TABLE 21. PROPERTIES OF MEDIUM-DOSE Si-IMPLANTED n-LAYER IN Ar-TREATED AND UNTREATED, Cr-DOPED, BRIDGMAN-GROWN SI GaAs SUBSTRATES

Sample	Ar Dose (cm^{-2}) at 750 keV	Si Implant Energy (keV)	Si Implant Dose (cm^{-2})	μ (cm^2/V-s)	η (%)
D7	None	180	5.2×10^{12}	3100	60.5
		50	1.4×10^{12}		
D7R	5×10^{12}	180	5.2×10^{12}	4280	71.2
		50	1.4×10^{12}		
D8	None	180	5.5×10^{12}	3100	58.6
		50	1.4×10^{12}		
D8R	5×10^{12}	180	5.5×10^{12}	3820	79.0
		50	1.4×10^{12}		

TABLE 22. COMPARISON OF ELECTRICAL PROPERTIES OF Si-IMPLANTED n-GaAs IN LEC GaAs SUBSTRATES WITH AND WITHOUT ^{40}Ar PRETREATMENT

Wafer	Substrate	Implantation Energy (keV)	Implantation Dose (cm^{-2})	N_s (cm^{-2})	μ ($cm^2/V\text{-}s$)	ρ_s ($\Omega/\square$)	η (%)
C101B	LEC Cr doped (Not Ar treated)	200 70	1.6×10^{12} 4.4×10^{11}	5.8×10^{11}	4280	2520	28.4
C101A	LEC Cr doped (Ar treated 5×10^{12} cm^{-2}, 750 keV)	200 70	1.6×10^{12} 4.4×10^{11}	1.2×10^{12}	4070	1280	58.7
D9A	LEC Cr doped (Ar treated 7.5×10^{12} cm^{-2}, 750 keV)	200 70	1.6×10^{12} 3.5×10^{11}	2.1×10^{12}	4220	704	109
D10A	LEC Cr doped (Ar treated 1.0×10^{13} cm^{-2}, 750 keV)	200	2×10^{12}	1.8×10^{12}	4430	784	90.7

The activation efficiencies in the ^{40}Ar-pretreated wafers were 58.7%, 90.7%, and 109%, considerably higher than the 28.4% for the untreated control wafer. The difference in the amount of increment in activation may be due to different doses of ^{40}Ar treatment. The differences in mobility between the ^{40}Ar-treated and the untreated wafers shown in Table 22 are small.

The electron density profiles in the four wafers described in Table 22 were measured using the differential C-V method and are plotted in Fig. 53. The calculated LSS curves for single implant (200 keV, $2x10^{12}$ cm^{-2}) and double implants (200 keV, $1.6x10^{12}$ cm^{-2}; 70 keV, $4.4x10^{11}$ cm^{-2}) are also included. The three ^{40}Ar-pretreated wafers (C101A, D9A, D10A) as a group are closer to the LSS profiles than the untreated wafer (C101B) except for the high carrier concentration of D9A toward the surface of the sample. It should be cautioned, however, that one should not expect the carrier concentration profile measured by the C-V technique to reproduce the implant profile with a steep slope. To investigate the concentration peak at the surface of D9A, Si distribution in D9A was measured by SIMS. The profile (Fig. 54) illustrates an accumulation of Si toward the sample surface. This may have caused the anomalous concentration peak in this sample. The accumulation of Si in this sample is not understood and will be further studied.

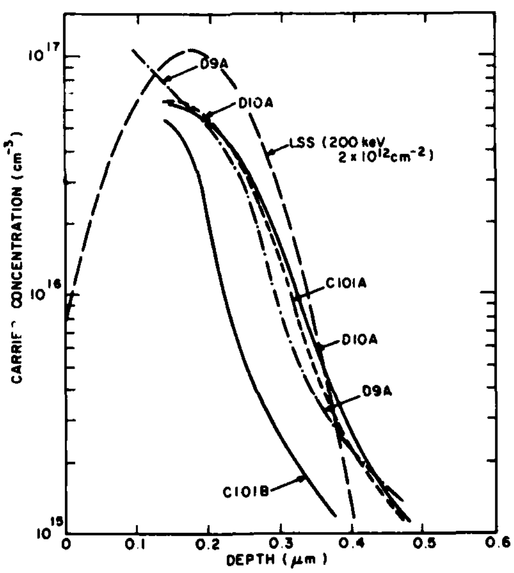

Figure 53. Electron density profiles of four Si-implanted n-layers on an LEC Cr-doped substrate. C101B is not ^{40}Ar treated; the other three are ^{40}Ar pretreated.

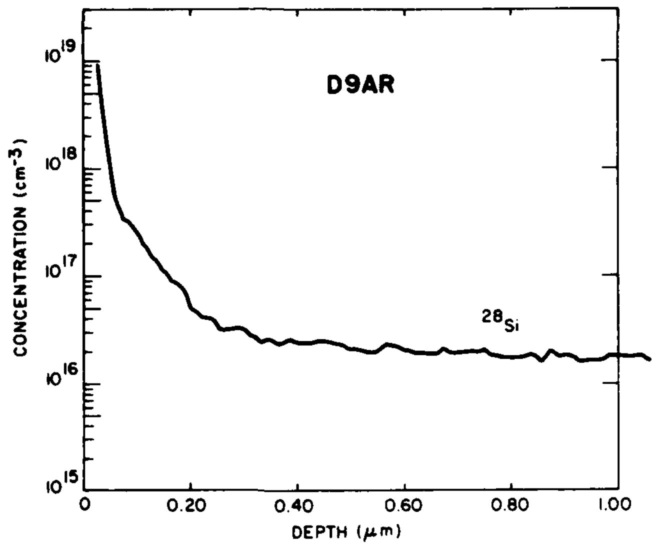

Figure 54. SIMS profile of Si distribution in D9AR which shows an anomalous electron density profile in Fig. 53.

C. LEC UNDOPED SUBSTRATES

The effect of ^{40}Ar treatment on electrical properties of an implanted n-layer in an LEC undoped substrate was studied. Silicon implant in the wafer was done at 200 keV with a fluence of 5×10^{12} cm^{-2}. Part of the substrate was then implanted with ^{40}Ar at 750 keV with a dose of 5×10^{12} cm^{-2}. The substrate (WBN 14-27) was obtained from Westinghouse Research and Development Center through M. N. Yoder. The electrical properties of the implanted/annealed wafers are given in Table 23 where C95CR and C95C designate, respectively, the wafers with and without ^{40}Ar-implant treatment.

Data in Table 23 show that the activation efficiency and mobility are, respectively, 13.5% and 12.5% higher in the ^{40}Ar-treated wafer than in the wafer without ^{40}Ar treatment. The enhancement in activation is moderate compared with that in Cr-doped Bridgman-grown substrates.

The electron density profiles of wafers C95C and C95CR are shown in Fig. 55 where the calculated LSS profiles are included for reference. The higher peak carrier concentration for wafer C95R is consistent with the higher activation measured by the van der Pauw method (Table 23). It is also interesting to note that the ^{40}Ar-pretreated wafer, C95CR, shows a steeper profile than C95C, the untreated wafer, near the tail end of the profile.

TABLE 23. COMPARISON OF ELECTRICAL PROPERTIES OF MEDIUM-DOSE Si IMPLANTS IN UNDOPED LEC SUBSTRATES WITH AND WITHOUT ^{40}Ar PRETREATMENT

		Implant					
Sample	Substrate	Energy (keV)	Dose (cm^{-2})	N_s (cm^{-2})	μ (cm^2/V-s)	ρ_s (Ω/□)	η (%)
C95C	LEC undoped (WBN 14-27)	200	$5x10^{12}$	$2.8x10^{12}$	3690	605	56.4
C95CR	LEC Undoped (WBN 14-27) Ar treated	200	$5x10^{12}$	$3.2x10^{12}$	4150	471	64.0

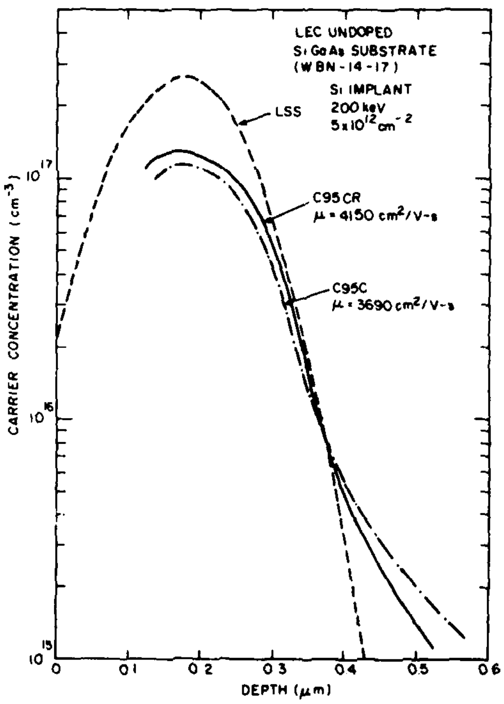

Figure 55. Electron density profiles of Si-implanted n-layers in LEC undoped substrates with (C95CR) and without (C95C) ^{40}Ar pretreatment.

D. Cr-O-DOPED SUBSTRATES

The effect of high-energy Ar implant on the electrical properties of Cr-O-doped substrates is illustrated by samples D6A and D6AR. Both samples were from the same wafer and were processed identically, except that D6AR received an additional ^{40}Ar implant at 750 keV with a fluence of 5×10^{12} cm^{-2}. During the ^{40}Ar implant, part of the wafer (D6A) was masked using an aluminum foil.

Table 24 compares the measured electrical properties of D6A and D6AR. These data were obtained using van der Pauw measurements after the implanted wafers were annealed thermally. Both the mobility and activation efficiency increased in the Ar-treated sample. The 5% increase in activation efficiency, however, is low in comparison with that in Cr-doped Bridgman-grown substrates.

TABLE 24. COMPARISON OF ELECTRICAL PROPERTIES OF Si-IMPLANTED n-GaAs IN Cr-O-DOPED SUBSTRATES WITH AND WITHOUT ^{40}Ar PRETREATMENT

Wafer	Substrate	Energy (keV)	Dose (cm^{-2})	N_s (cm^{-2})	μ (cm^2/V-s)	ρ_s (Ω/□)	η (%)
D6A	Cr-O doped	180	5.2×10^{12}	4.4×10^{12}	3580	397	67.2
		50	1.4×10^{12}				
D6AR	Cr-O doped	180	5.2×10^{12}	4.6×10^{12}	4010	339	70.2
	Ar treated	50	1.4×10^{12}				

Figure 56 illustrates the electron density profiles of the implanted n-layers in samples D6 and D6R. The small amount of enhancement in carrier concentration in the ^{40}Ar-pretreated sample, D6R, is consistent with the van der Pauw measurement.

E. Si IMPLANTATION INTO HIGH-ENERGY ^{31}P-IMPLANTED PRETREATED SI GaAs

Chromium-doped GaAs substrates bombarded appropriately with the inert ^{40}Ar ions have consistently shown improved electrical activation and mobility for n-layers subsequently created on the substrate using Si implant and thermal

AD-A108 777 RCA LABS PRINCETON NJ F/G 7/4
HIGH-ENERGY ION IMPLANTATION FOR MULTIGIGABIT-RATE GAAS INTEGRA--ETC(U)
OCT 81 S G LIU, E C DOUGLAS, C P WU N00014-78-C-0367
UNCLASSIFIED PRRL-81-CR-32 NL

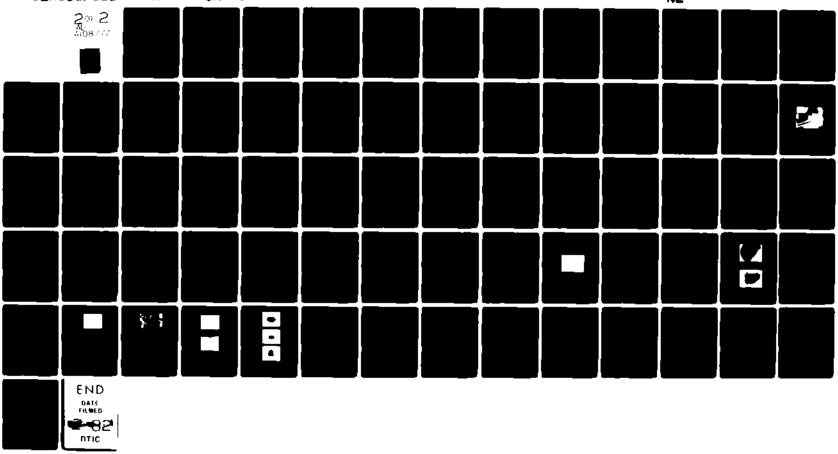

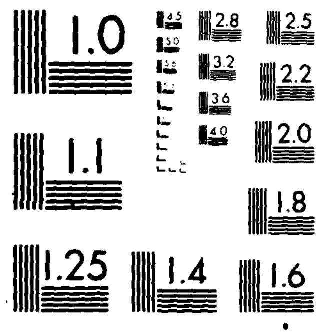

MICROCOPY RESOLUTION TEST CHART
NATIONAL BUREAU OF STANDARDS-1963-A

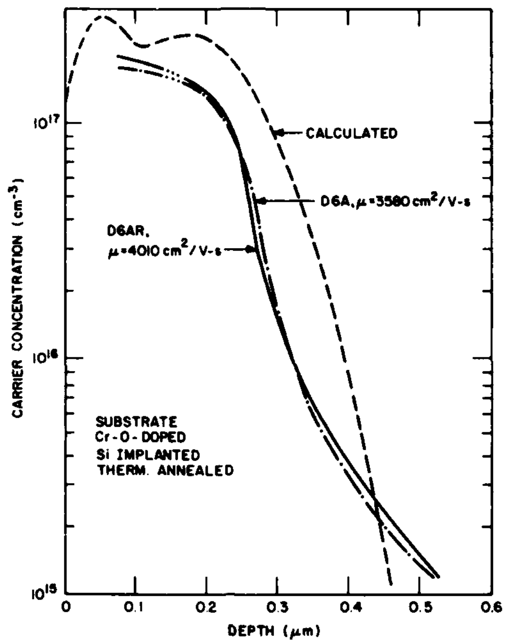

Figure 56. Electron density profiles of D6A and D6AR, Si-implanted n-GaAs in a Cr-O-doped substrate. D6AR also received high-energy ^{40}Ar implant.

annealing. . ›tivated by the idea of testing a different ion which is inactive in GaAs, we have implanted ^{31}P into SI GaAs to see its effect on the electrical properties of the n-layer formed subsequently by Si implantation and thermal annealing.

A Cr-doped LEC substrate from Metals Research Corp. was used in the experiment. Experimental details were the same as described previously. The fluence and energy values for the ^{31}P implant were chosen to be 1×10^{13} cm^{-2} and 900 keV. Since the projected range and straggle of ^{31}P in GaAs at 900 keV are 0.696 μm and 0.155 μm, respectively, we expect a deeper Cr-depletion region is the redistribution mechanism is similar to that produced by Ar bombardment and thermal anneal.

The electrical properties of the n-GaAs layers on wafers D4F and D4F-P were evaluated and are summarized in Table 25. The mobility and activation of

TABLE 25. ELECTRICAL CHARACTERISTICS OF Si-IMPLANTED n-GaAs IN LEC Cr-DOPED SUBSTRATES WITH AND WITHOUT ^{31}P-IMPLANT TREATMENT

		Implantation					
Wafer	Substrate	Energy (keV)	Dose (cm^{-2})	N_s (cm^{-2})	μ(300K) (cm^2/V-s)	ρ_s (Ω/□)	η (%)
D4F	LEC Cr doped	200	$2x10^{12}$	$5.8x10^{11}$	3250	3320	29.0
D4F-P	LEC Cr doped P treated	200	$2x10^{12}$	$7.3x10^{11}$	4230	2030	36.3

the P-treated wafer are 4230 cm^2/V-s and 36.3%, respectively. Both are considerably higher than the corresponding data, 3250 cm^2/V-s and 29% for the wafer without high-energy P implantation.

F. DATA ANALYSIS - POSSIBLE MECHANISMS FOR ACTIVATION/MOBILITY ENHANCEMENT BY ^{40}Ar PRETREATMENT

The carrier concentration and mobility data measured using van der Pauw and differential C-V measurements were analyzed to yield information on the ratio of acceptors to donors [55]. This ratio of acceptor to donor, N_A/N_D, in samples with Ar-implant pretreatment is found to be consistently less than that in samples without pretreatment. This improved result is analyzed below in terms of two possible mechanisms: (1) more Si going to Ga sites than to As sites and (2) a reduction in compensation due to reduced Cr concentration in the substrate. Other effects such as impurity complexes [56] are not included in the models.

55. W. Walukiewicz et al., "Electron Mobility & Free Carrier Absorption in GaAs: Determination of the Compensation Ratio," J. Appl. Phys. 50, 899 (1979).
56. M. N. Yoder, "Complexes and Their Effects on III-V Compounds," in Semi-Insulating III-V Materials, (Shiva Publishing Ltd., Nottingham, 1980), pp. 281-287.

1. Si Occupancy in Ga and As Sites

Let k_1 and k_2 represent the acceptor-to-donor ratios in untreated and ^{40}Ar-pretreated samples, respectively:

$$k_1 = \frac{N_{A1}}{N_{D1}} \tag{15}$$

$$k_2 = \frac{N_{A2}}{N_{D2}} \tag{16}$$

Values of k_1 and k_2 can be estimated from measured carrier concentration and mobility data using calculations made by Walukiewicz et al. [55]. The acceptors, N_A's, and donors, N_D's, can be expressed as:

$$N_A = (N_A)_{Si} + (N_A)_{Cr} \tag{17}$$

$$N_D = (N_D)_{Si} + (N_D)_i \tag{18}$$

where $(N_A)_{Si}$ and $(N_D)_{Si}$ are acceptors and donors due to the presence of Si in As and Ga sites, respectively. $(N_A)_{Cr}$ represents acceptors due to Cr compensation. The chromium atoms are identified as double acceptors [57] in Cr- and Si-doped Bridgman-type substrates. The $(N_D)_i$ represents donors due to residual impurities, mostly Si, presented in the substrate. $(N_D)_i$ will be neglected in the following discussions as they are much fewer in comparison with $(N_D)_{Si}$ in adequately Cr-doped substrates. The subscripts 1 and 2, which refer, respectively, to untreated and Ar-pretreated substrates, are omitted in Eqs. (17) and (18) for simplicity.

Assuming that by Ar pretreatment a fraction x of the Si atoms move from acceptor (As) sites to donor (Ga) sites, we then obtain from Eqs. (15-18) the following:

$$x = \frac{k_1 - k_2}{1 + k_2} \tag{19}$$

57. M. R. Brozel et al., "Electrical Compensation in Semi-Insulating Gallium Arsenide," J. Phys. C., Solid State Phys. 11, 1857 (1978).

The activation of Si-implanted n-layers in untreated substrates is given by:

$$a_1 = \frac{N_{D1}-N_{A1}}{N_d t_1}$$

$$= \frac{N_{D1}}{N_d t_1} \left(1-k_1\right) \tag{20}$$

where N_d is the implanted Si fluence, k_1 is as defined in Eq. (15), and t_1 is the thickness of the n-layer.

The activation of a Si-implanted n-layer in an Ar-pretreated substrate is given by:

$$a_2 = \frac{N_{D2}}{N_d t_2} \left(1-k_2\right) \tag{21}$$

where k_2 is defined in Eq. (16) and t_2 is the thickness of the n-layer in Ar-pretreated samples. As previously seen, we define x by

$$N_{D2} = (1 + x)\ N_{D1} \tag{22}$$

where xN_{D1} denotes the excess number of Si atoms going to Ga sites because of ^{40}Ar treatment, in which case Eq. (21) reduces to

$$a_2 = \frac{N_{D1}(1+x)(1-k_2)}{N_d t_2} \tag{23}$$

Combining Eqs. (21) and (23), we obtain the activation ratio

$$\frac{a_2}{a_1} = \frac{t_1}{t_2}\ \frac{(1+x)(1-k_2)}{(1-k_1)} \tag{24}$$

As an example, consider measured data described in Section V.

a. Cr-O-Doped Substrate

Data for samples D6A and D6AR are reproduced as follows:

	(N_D-N_A)Av. (cm^{-3})	μ(300K) (cm^2/V-s)	$k(=N_A/N_D)$
D6A (Not ^{40}Ar treated)	$1.5x10^{17}$	3580	0.42
D6AR (^{40}Ar treated)	$1.6x10^{17}$	4010	0.30

where N_A/N_D's are estimated from calculations by Walukiewicz et al. [55] for a given carrier concentration and mobility data. Then x is obtained from Eq. (19) to be 0.092, which means that 9.2% of the Si, a relatively small amount, changes occupancy from As sites to Ga sites, as a result of ^{40}Ar pretreatment in this Cr-O-doped substrate.

b. Cr-Doped Bridgman-Grown Substrate

Data for samples D7A and D7R are reproduced as follows:

	(N_D-N_A)Av. (cm^{-3})	μ(300K) (cm^2/V-s)	$k(=N_A/N_D)$
D7A (Not ^{40}Ar treated)	$1.2x10^{17}$	3100	0.58
D7AR (^{40}Ar treated)	$1.6x10^{17}$	4280	0.22

The x is obtained from Eq. (19) to be 0.29, which means that by ^{40}Ar pretreatment, 29% more Si goes to Ga sites (and not to As sites) in this substrate. The activation-increase ratio by Ar-implant treatment in this substrate is calculated from Eq. (24) to be:

$$\frac{a_2}{a_1} = \frac{0.30}{0.32} \text{ x } \frac{(1+0.29)(1-0.22)}{0.58} = 1.63$$

which compares well with 1.2 obtained from van der Pauw measurements.

2. Cr Compensation Model

One may also assume that the ^{40}Ar pretreatment does not alter the Si atom occupancy of Ga and As sites, but only causes a change in compensation due to a redistribution of Cr in the substrate. Under this assumption,

$$N_{D1} = N_{D2} = (N_D)_{Si} \tag{25}$$

$$[(N_A)_{Si}]_1 = [(N_A)_{Si}]_2 \tag{26}$$

we obtain from Eqs. (15-18) the changes in Cr-produced acceptors:

$$\frac{(N_{CR})_1 \ -(N_{Cr})_2}{(N_D)_{Si}} = k_1 - k_2 \tag{27}$$

This means that the difference between k_1 and k_2 is equal to the difference in Cr acceptors normalized to the Si-produced donors.

The activation-increase ratio by Ar-implant treatment under this assumption is given, from Eqs. (20, 21, and 25), by:

$$\frac{a_2}{a_1} = \frac{t_1}{t_2}\frac{(1-k_2)}{(1-k_1)} \tag{28}$$

Taking the same examples considered for the previous model, we calculated the following: (a) For samples D6A and D6AR, the decrease in Cr acceptors (normalized to Si donors) in ^{40}Ar-treated D6AR is calculated from Eq. (27) to be 0.42-0.30 = 0.12 or 12%, and the activation-increase ratio is calculated from Eq. (28) to be 0.70/0.58 = 1.21; (b) for samples D7 and D7R, the decrease in Cr acceptors as a result of ^{40}Ar pretreatment is calculated from Eq. (27) to be 0.58-0.22 = 0.36 or 36%, and the activation increase ratio is calculated from Eq. (28) to be 1.74.

Based on the analysis of experimental results, it appears that either the increase of occupancy of Si in Ga sites or the decrease of Cr-created acceptors could lead to the observed mobility and/or activation enhancement as a result of ^{40}Ar pretreatment of SI GaAs substrates. The displacement of Ga and As

atoms in the substrate [58] as a result of energetic impinging Ar ions could contribute to changes of Si occupancy in Ga sites.* In essence, the Ga and As atoms are knocked deeper into the Ga and As crystal by the energetic impinging Ar ion. The region between the substrate surface and the projected range is relatively devoid of Ga and As; the region immediately deeper than R_p is relatively enriched in Ga, and this is followed by an excess of As. When the subsequent silicon implant is confined to the shallow region where a large number of Ga and As vacancies exist, the activation of Si increases. On the other hand, the Cr redistribution occurred in the GaAs substrate as a result of ^{40}Ar implant and annealing could contribute to the reduction in acceptors, as described in Section VI. The true mechanism is not clearly understood at present. The potential impact of Ar pretreatment on improving the yield of GaAs integrated circuits makes it worthwhile to continue this investigation.

58. L. A. Christel and J. F. Gibbons; to be published.

*M. N. Yoder, private communication.

SECTION VI

IMPURITY REDISTRIBUTION IN GaAs

A number of recent publications [21-24] have reported diffusion or redistribution of Cr in thermally annealed SI GaAs substrates with or without implanted impurities. We have studied the dependence of Cr redistribution on fluence [9,10] in thermally annealed SI GaAs substrates that were implanted with Si at energies of 200 and 600-1000 keV. Similar studies were made on ^{40}Ar-implanted and thermally annealed GaAs. The implant of ^{40}Ar has produced Cr-redistribution profiles similar to those of ^{28}Si implants. The Cr-redistribution profiles were measured on samples co-implanted with high-energy ^{40}Ar and low-energy ^{28}Si in an attempt to shed some light on the mechanism of activation/mobility enhancement described in Section V.

A. Cr DISTRIBUTION IN Si-IMPLANTED GaAs WITHOUT ^{40}Ar TREATMENT

1. Furnace Annealing

Chromium profiles of Si-implanted SI GaAs were investigated using SIMS measurements. The SIMS system at RCA is capable of detecting atomic Cr density of $<5\times10^{15}$ cm^{-3}. Some of the Cr profiles presented in this section were measured by Charles Evans & Assoc., San Mateo, CA.

Studies on the redistribution of Cr in the SI GaAs substrate due to the implantation and annealing operations indicate that the redistribution of Cr is a strong function of implant dose and the annealing method.

Figures 57(a) and 57(b) show, respectively, SIMS profiles of low-dose (4×10^{12} cm^{-2}, 200 keV) Si implants before and after the wafers were capless-annealed under arsenic overpressure. These substrates were Cr doped with (100) orientation and were grown by Crystal Specialties, Inc. The background Cr concentration was $\sim5\times10^{16}$ cm^{-3}. After capless thermal annealing, a very slight depletion of Cr occurred toward the surface. This low implant dose level is typically used to obtain $\sim10^{17}$-cm^{-3} carrier concentration for the active layers of microwave FETs.

At a higher fluence level (e.g., 3×10^{14} cm^{-2}, 200 keV), the Cr-redistribution effect is enhanced. Figures 58 and 59 show SIMS profiles of Cr redistribution in two capless-annealed wafers that were implanted at 1 MeV with

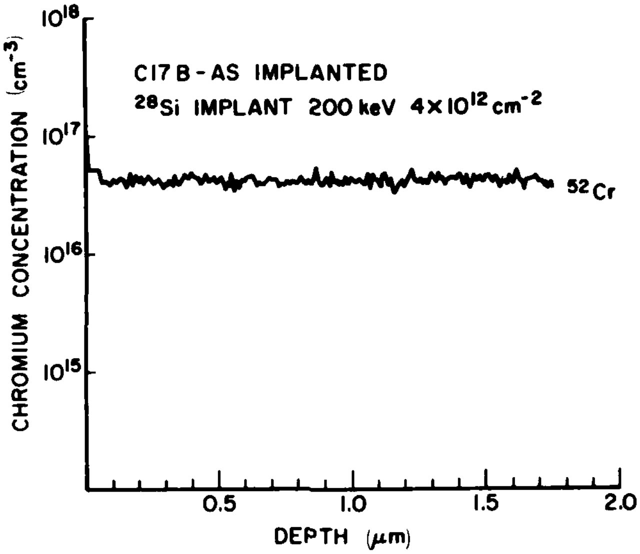

(a)

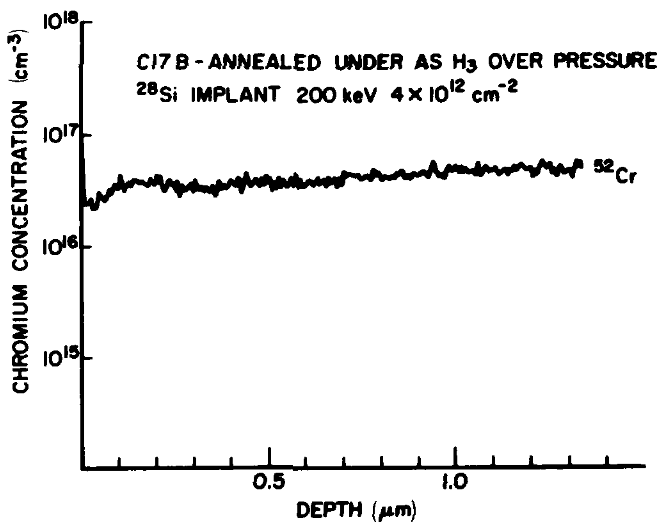

(b)

Figure 57. (a) SIMS profile of Cr concentration in low-dose, Si-implanted, unannealed GaAs; (b) SIMS profile of Cr concentration in low-dose, Si-implanted capless-annealed GaAs.

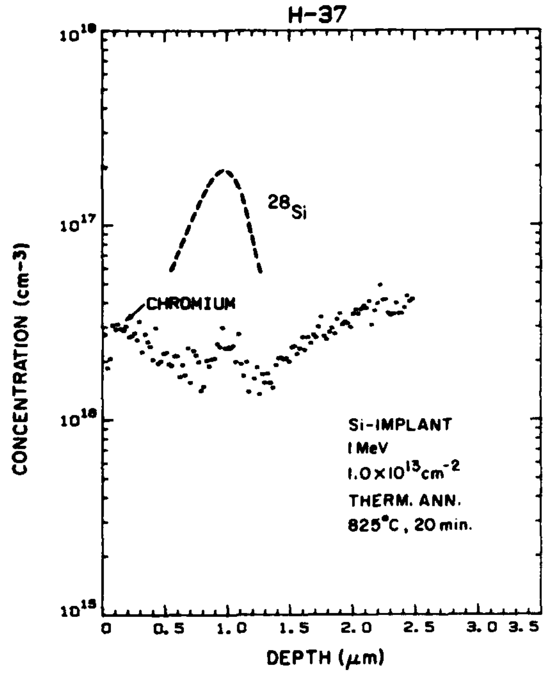

Figure 58. SIMS profile of ^{52}Cr in low-dose, 1-MeV, Si-implanted, capless-annealed GaAs.

fluences of $1\text{x}10^{13}$ and $3\text{x}10^{15}$ cm^{-2}. The Cr distribution in these wafers shows a broad dose-dependent Cr depletion toward the surface, plus local Cr accumulations in the vicinity of R_p, the projected range of Si implant. The position of local Cr accumulation coincides with R_p in the case of medium-dose ($1\text{x}10^{13}$ cm^{-2}) Si implant (Fig. 58), but shifts to a position immediately deeper than R_p in the case of high-dose ($3\text{x}10^{15}$ cm^{-2}) Si implant (Fig. 59). A similar shift in Cr accumulation position was observed in ^{40}Ar-implanted and annealed GaAs and will be discussed later.

2. Laser Annealing

The Cr redistribution in laser-irradiated high-dose Si-implanted GaAs has also been investigated. Figure 60 shows a $3\text{x}10^{15}$-cm^{-2}, 200-keV Si-implanted 1.0-J/cm^2 pulsed ruby-laser-irradiated GaAs sample, and Fig. 61 shows a $2.5\text{x}10^{15}$-cm^{-2}, 600-keV Si implant irradiated with a 1.5-J/cm^2 pulsed Nd:glass

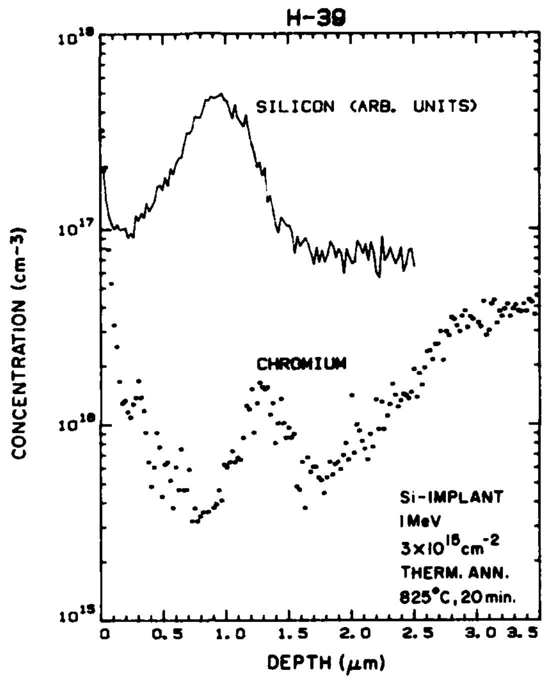

Figure 59. Cr-concentration profile of high-dose, 1-MeV, Si-implanted, capless-annealed GaAs; Si profile in arbitrary units is also shown.

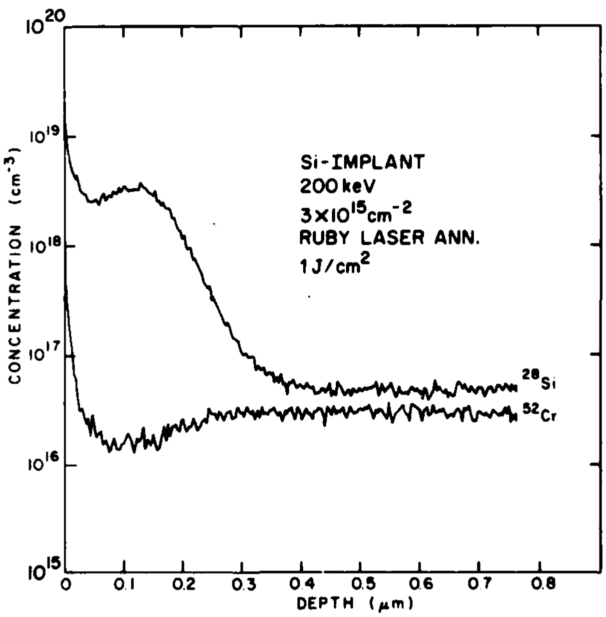

Figure 60. Cr distribution of Si-implanted ($3x10^{15}$ cm^{-2}, 200 keV) 1.0-J/cm^2 pulsed ruby-laser-irradiated GaAs.

laser beam. The pulse width of the laser beam was 25 ns (FWHM). Note that the Cr redistribution in each case consists of a small amount of Cr depletion plus an accumulation at the surface up to mid-10^{17} cm^{-3}. The Cr depletion is much less than that in thermally annealed GaAs implanted at similar dose levels (Fig. 59). The measured sheet carrier concentration of 7.4×10^{14} cm^{-2} for the activated n-layer of sample N7 (Fig. 61) after laser irradiation is much higher than that for thermally annealed control samples.

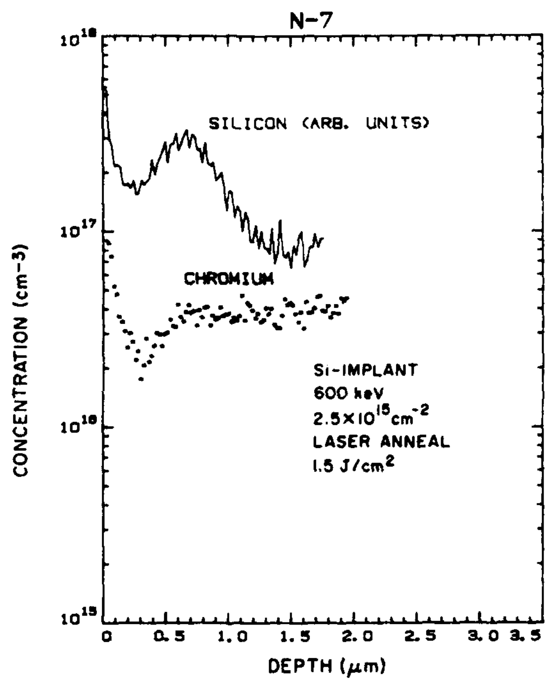

Figure 61. Cr-concentration profile of 600-keV, Si-implanted, laser-annealed GaAs. Si profile in arbitrary units is also shown.

B. Cr DISTRIBUTION IN ^{40}Ar-IMPLANTED/ANNEALED SI GaAs SUBSTRATES

We have observed that the measured SIMS profiles of Si-implanted, thermally annealed SI GaAs show strong dependence of ^{52}Cr redistribution on the ^{28}Si dose. To shed more light on this effect, we implanted inert ^{40}Ar ions into SI GaAs at high energies and studied the Cr-redistribution behavior in these samples. Measured SIMS profiles at high fluences ($\geq 5 \times 10^{13}$ cm^{-2}) show characteristics similar to those observed in Si-implanted samples; namely, (1) there was

a constant Cr level before the sample was thermally annealed, (2) a "double-valley" depletion of Cr existed in a layer near the surface after the sample was thermally annealed, and (3) the amount of Cr redistribution depended on the implant dose level. SIMS profiles of a 750-keV, 5×10^{13}-cm^{-2} Ar-implanted GaAs wafer, before and after thermal anneal, are shown in Fig. 62. An accumulation of Cr, which approximately coincides with the projected range of the implant, exists in the Cr-depletion layer. At a higher implant fluence the Cr depletion increases and broadens, and the Cr-accumulation peak shifts from the position of R_p deeper into the substrate; also the Cr accumulation is enhanced at the surface. This result is illustrated in Fig. 63, where the Cr profile of a 1×10^{15}-cm^{-2} Ar-implanted capless-annealed SI GaAs sample is shown.

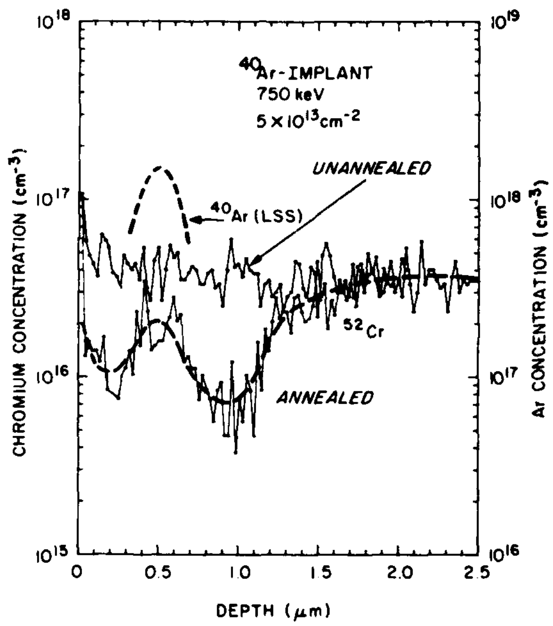

Figure 62. SIMS profile of Cr concentration in ^{40}Ar-implanted GaAs (5×10^{13} cm^{-2}, 750 keV) before and after capless annealing (825°C, 20 min).

SIMS profiles at medium fluence ^{40}Ar-implanted/annealed SI substrates show a moderate and well-defined Cr-depletion region. Figure 64 illustrates the SIMS profile of Cr concentration in an Ar-implanted, thermally annealed SI GaAs substrate (Bridgman grown, Cr doped). The profile shows a broad, flat Cr-depletion channel toward the surface as a result of Ar treatment. An LEC

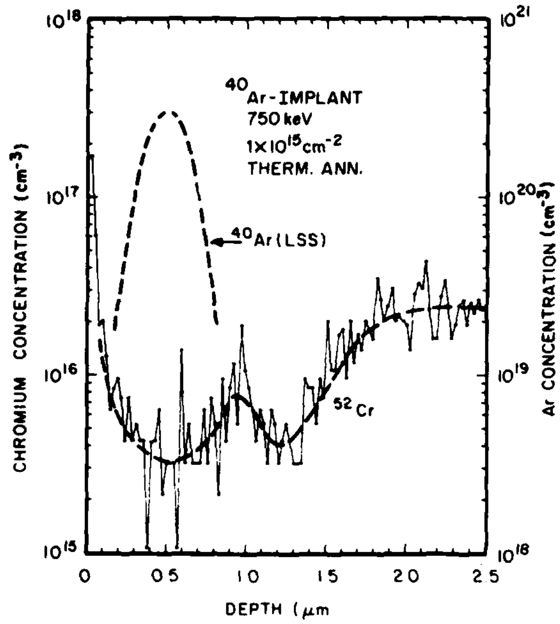

Figure 63. SIMS profile of ^{40}Ar-implanted (1×10^{15} cm^{-2}, 750 keV) capless-annealed (825°C, 20 min) GaAs.

Cr-doped substrate shows a similar Cr depletion after Ar implantation and annealing, as illustrated in Fig. 65. To confirm that the broad depletion of Cr is a result of Ar implant and thermal anneal, and not due to thermal anneal alone, a SIMS profile was measured on a nonimplanted, capless-annealed control sample from the same substrate. The profile is also included in Fig. 64. It shows only a small amount of Cr depletion near the sample surface. Furthermore, the substrate does not show any improvement in low-dose activation for subsequent Si implantation.

C. CHROMIUM DISTRIBUTION IN Si-IMPLANTED/ANNEALED GaAs WITH PRETREATMENT

1. ^{40}Ar-Pretreated Substrates

In this section, we will present a number of SIMS profiles of ^{52}Cr concentration in ^{40}Ar-pretreated substrates followed by Si implant and thermal

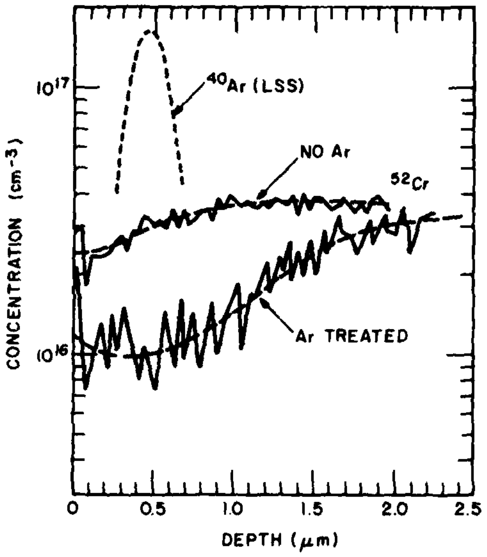

Figure 64. SIMS profiles of Cr concentration in a thermally annealed Bridgman Cr-doped substrate with and without prior ^{40}Ar implant ($5x10^{12}$ cm^{-2}, 750 keV).

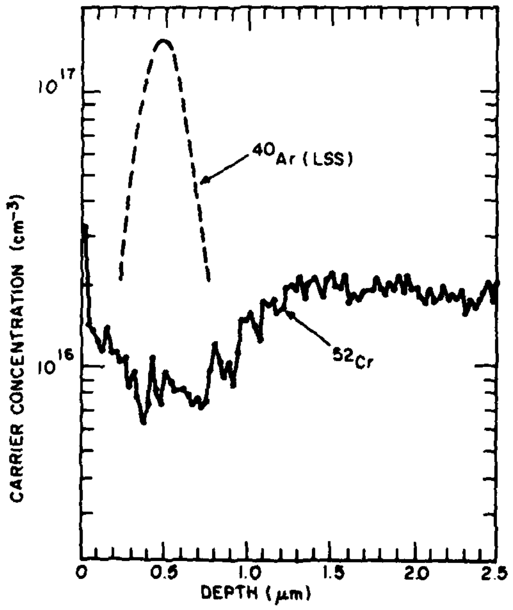

Figure 65. SIMS profile of Cr concentration in a ^{40}Ar-implanted ($5x10^{12}$ cm^{-2}, 750 keV) capless-annealed LEC Cr-doped SI GaAs substrate.

annealing. The ^{52}Cr-concentration measurement was made in an attempt to shed some light on the mechanism of activation/mobility enhancement. The substrates investigated were Bridgman/Cr doped, LEC/Cr, and LEC/undoped. The ^{40}Ar implant was carried out at 750 keV with doses ranging from $5x10^{12}$ to $1x10^{15}$ cm^{-2}. The subsequent Si implant for the n-layer was carried out at 200 keV or lower with medium ($\sim 5x10^{12}$-cm^{-2}) and low ($\sim 2x10^{12}$-cm^{-2}) doses. The ^{40}Ar-pretreated samples with appropriate fluence showed enhanced activation and/or mobility for the subsequently Si-implanted n-layer as described in Section V.

a. Bridgman/Cr-doped Substrates

Figure 66 shows the SIMS profile of Cr concentration in sample R5, an Ar-(750-keV, $5x10^{12}$-cm^{-2}) and Si-(200-keV, $2x10^{12}$-cm^{-2}) implanted, thermally annealed SI GaAs substrate. The substrate (Bridgman Cr-doped) is the same as that used for Fig. 65. The addition of a low-dose ($2x10^{12}$-cm^{-2}) Si implant at 200 keV to the $5x10^{12}$-cm^{-2} ^{40}Ar implant at 750 keV does not significantly change the Cr-concentration profile. A well-defined Cr-depletion channel near the surface exists in both Figs. 65 and 66.

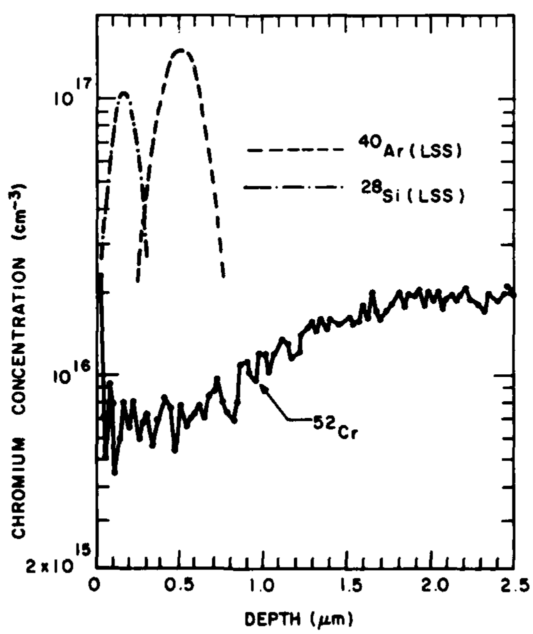

Figure 66. SIMS profile of Cr concentration in ^{40}Ar ($5x10^{12}$ cm^{-2}, 750 keV) and ^{28}Si ($2x10^{12}$ cm^{-2}, 200 keV) implanted capless-annealed SI GaAs.

Figure 67 shows the SIMS profiles of Cr concentration in samples R6 and R7, which were Ar implanted at a higher dose followed by Si implant (2×10^{12} cm^{-2}, 200 keV) and thermally annealed. The ^{40}Ar implant for samples R6 and R7 were, respectively, 1×10^{13} cm^{-2} and 5×10^{13} cm^{-2} at 750 keV. As the ^{40}Ar dose increases, the Cr profile shows a deeper depleted channel near the surface and also shows an accumulation following the depletion forming a W-shaped Cr-redistribution pattern. The accumulation presumably takes place in the area where maximum implant damages and crystal imperfections occur; the accumulation peak being deeper than the Ar-implant range could be a result of disturbance [58] in the stoichiometry produced by implantation. The electrical characteristics of the Si-implanted n-layers of R5, R6, and R7 are given previously in Table 20. It should be pointed out that all three Ar-pretreated samples have shown substantially enhanced activation and mobility as compared with the control sample which receives no Ar pretreatment.

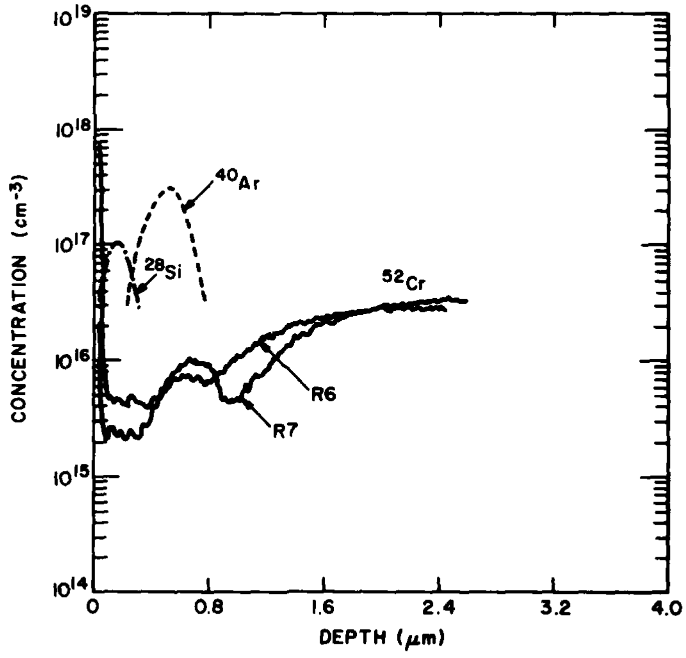

Figure 67. SIMS profiles of Cr concentration in low-dose Si-implanted, capless-annealed GaAs (Bridgman Cr-doped substrate) pretreated with high-energy ^{40}Ar implant of doses 1×10^{13} (R6) and 5×10^{13} cm^{-2} (R7), respectively. Dashed lines show LSS profiles of R6.

Figures 68 and 69 illustrate the Cr-concentration profiles of sample pairs D7R and D7, and D8R and D8, respectively. Implanted Si fluences are higher in these two pairs of samples. (For details, refer to Table 21.) Samples D7R and D8R were pretreated with 5×10^{12}-cm^{-2} ^{40}Ar at 750 keV. Samples D7 and D8 were not Ar treated. The profiles show a Cr depletion to a depth of about 1.4 μm below the surface and an accumulation at 0.2 μm, which is near the peak of Si implantation. The accumulation appears due to the combined effects of Si and Ar implantation. Samples D7 and D8 which received no ^{40}Ar implant showed little variation in Cr distribution.

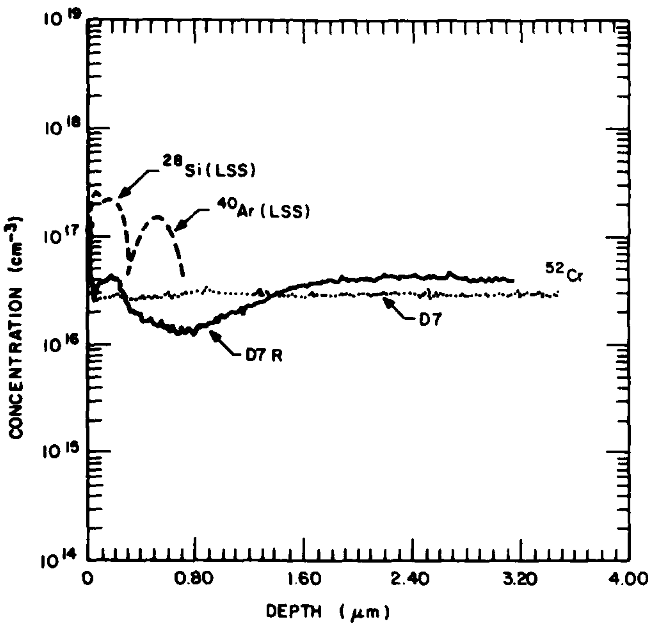

Figure 68. SIMS profiles showing Cr concentration of medium-dose, Si-implanted, capless-annealed GaAs with (D7R) and without (D7) high-energy ^{40}Ar implantation.

b. LEC Cr-Doped Substrates

Figure 70 shows the SIMS profiles of Cr concentration in three implanted samples, C101B, C101A, and D10A, using an LEC Cr-doped GaAs substrate. The implant conditions and the electrical characteristics of the implanted/annealed

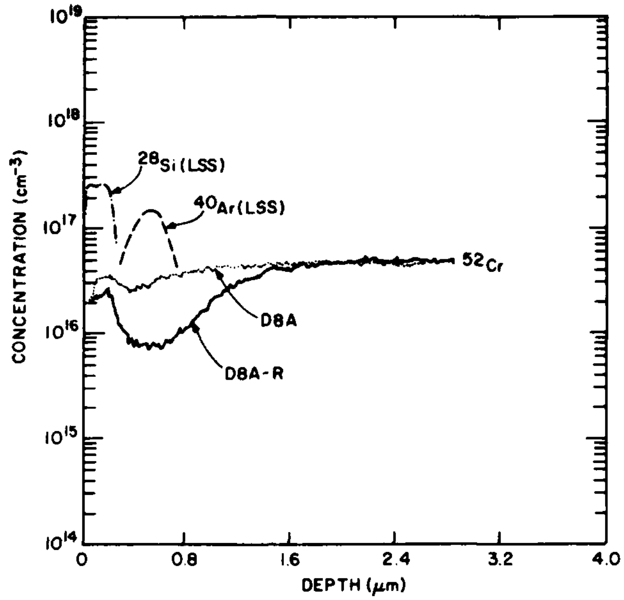

Figure 69. SIMS profiles showing Cr concentration of medium-dose, Si-implanted, capless-annealed GaAs with (D8AR) and without (D8A) high-energy ^{40}Ar implantation.

n-layers were summarized previously in Table 22. Sample C101B was not Ar treated; samples C101A and D10A were pretreated with Ar implantation. All samples were Si implanted (either singly or doubly with a total dose of $\sim 2\times 10^{12}$ cm^{-2}) followed by thermal annealing.

The Cr-redistribution profiles illustrated in Fig. 70 are similar to those (Fig. 67) produced by implants into a Bridgman Cr-doped substrate. A well-defined Cr-depletion channel was formed below the surface, the depth of the channel increasing with the ^{40}Ar-implant dose. The background Cr concentration in the LEC/Cr substrate, however, is 1.5×10^{16} cm^{-3}, which is substantially lower than that in the Bridgman/Cr substrate (3.5×10^{16} cm^{-3}). The difference in the background Cr concentration may account for the difference in mobility in samples C101B and C73A (given in Tables 22 and 20, respectively). This is because both samples were implanted with a low Si dose ($\sim 2\times 10^{12}$ cm^{-2}), which corresponds to a Si atomic concentration of $\sim 4\times 10^{16}$ cm^{-3}. This concentration is higher than the Cr concentration in sample C101B, while it becomes comparable to the Cr concentration in sample C73A.

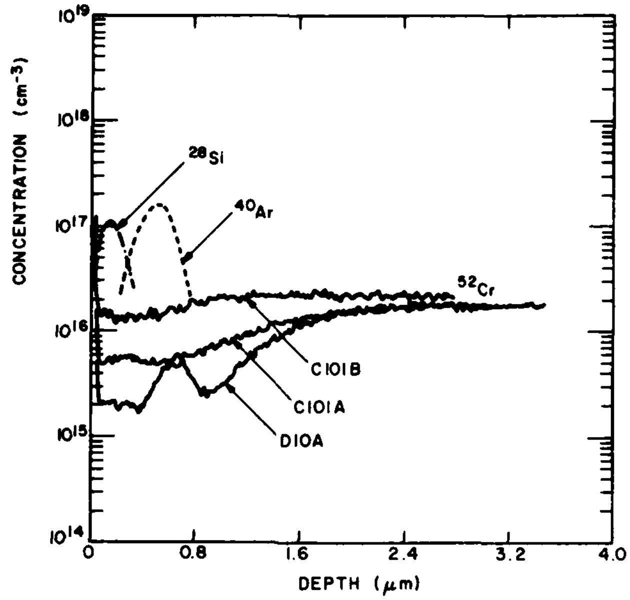

Figure 70. SIMS profiles of Cr concentration in low-dose Si-implanted capless-annealed GaAs (LEC Cr-doped substrate). C101A and D10A were pretreated with high-energy ^{40}Ar implant of doses $5x10^{12}$ and $1x10^{13}$ cm^{-2}, *respectively; C101B was not* ^{40}Ar pretreated. Dashed lines show LSS profiles of C101A.

Figure 71 shows the Cr-distribution profiles of D9A and C96F. Sample C96F was ^{40}Ar implanted with a much higher dose ($1x10^{15}$ cm^{-2}, 750 keV) than was D9A ($7.5x10^{12}$ cm^{-2}, 750 keV) before both samples were implanted with low-dose ^{28}Si and thermally annealed. Both profiles show a Cr accumulation within the broad depleted channel. The Cr accumulation of D9A peaks approximately at the projected range of ^{40}Ar implant, while that of C96F peaks deeper than the projected range. This may be associated with the stoichiometry disturbance [58] resulting from ion implantation, as mentioned previously. Accumulation of Cr also occurs at the surface for samples implanted with high-dose ^{40}Ar ions, which may account for the spurious conversion effect observed in C96F, the high-dose ^{40}Ar implanted/annealed sample.

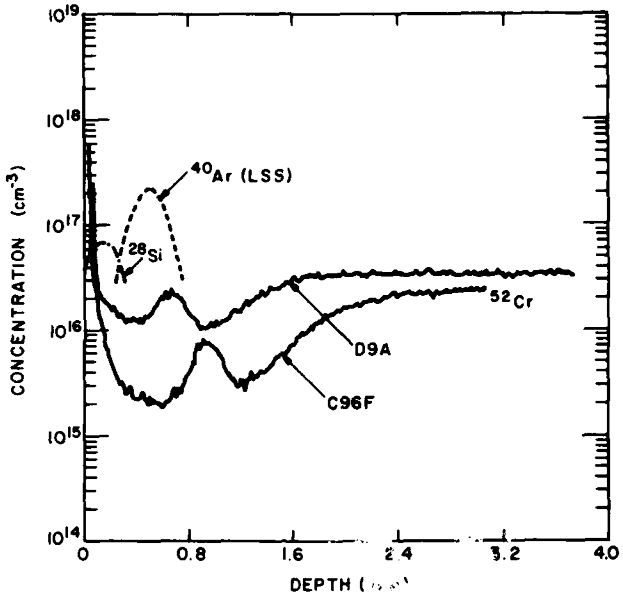

Figure 71. SIMS profiles of Cr concentration in low-dose, Si-implanted, capless-annealed GaAs (LEC Cr-doped substrate) pretreated with high-energy ^{40}Ar implant of doses 7.5×10^{12} (D9A) and 1×10^{15} cm^{-2} (C96F). Dashed lines show LSS profiles of D9A.

c. LEC Undoped Substrates

Figure 72 shows the SIMS profiles of Cr concentration in two samples, C95C and C95CR, using an LEC undoped GaAs substrate. The implant conditions and the electrical characteristics of the implanted annealed n-layers were summarized previously in Table 23. Sample C95C was not ^{40}Ar pretreated; sample C95CR was pretreated with ^{40}Ar implantation followed by Si implant and thermal annealing.

The background Cr concentration of the undoped sample is $2\text{-}4 \times 10^{15}$ cm^{-3}, which is about an order of magnitude lower than that in Cr-doped substrates. The scattering of background concentration rises from the accuracy of SIMS measurement. A Cr depletion channel is also present in the profile, but the amplitude is much smaller than that in Cr-doped substrates.

2. ^{31}P-Pretreated Substrate

Figure 73 shows the Cr redistribution profile for wafer D4F-P, a 900-keV ^{31}P-implant substrate followed by Si implant (2×10^{12} cm^{-2}, 200 keV) and thermal anneal. A control section of the same wafer, designated D4F, which received

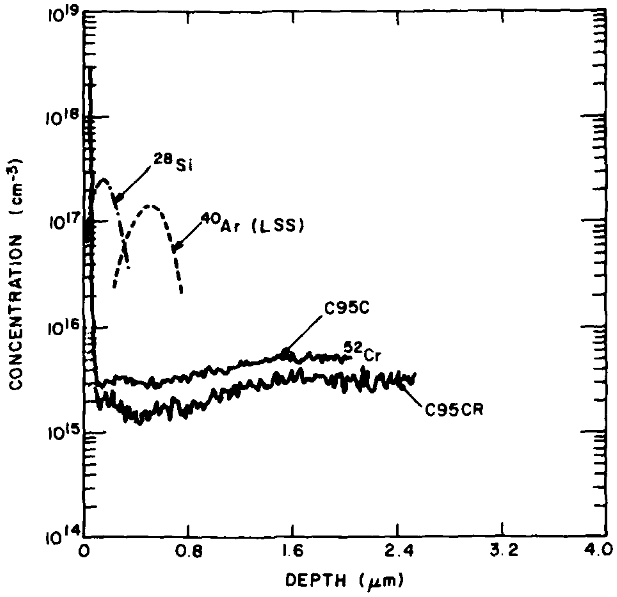

Figure 72. SIMS profiles of Cr concentration in medium-dose, Si-implanted, capless-annealed GaAs (LEC undoped substrate), with (C95CR) and without (C95C) high-energy ^{40}Ar implantation (750 keV, $5x10^{12}$ cm^{-2}).

only Si implant and thermal anneal, is included for reference. The Cr-concentration profile of D4F-P, the ^{31}P-bombarded wafer, clearly shows a nearly flat Cr reduction region that extends to a depth of about 1.2 μm. The Cr level was reduced to $\sim 2x10^{16}$ cm^{-3} from the original $\sim 3.5x10^{16}$ cm^{-3}. The mobility and activation of D4FP, the P-treated wafer, are higher than that of D4F, as previously described in Section V.

D. DISTRIBUTION OF OTHER IMPURITIES (Fe, Mn) IN ^{40}Ar-TREATED GaAs

We have also looked at the effect of high-energy ^{40}Ar implant and anneal upon the distribution of other impurities in SI GaAs substrates. SIMS profiles of Fe, Mn, and Cr were measured on sample R20, a ^{40}Ar-implanted (750-keV, $1x10^{13}$ cm^{-2}), Cr-doped substrate before and after thermal annealing. Figures 74 and 75 shows the SIMS profiles measured before and after the wafer was annealed.

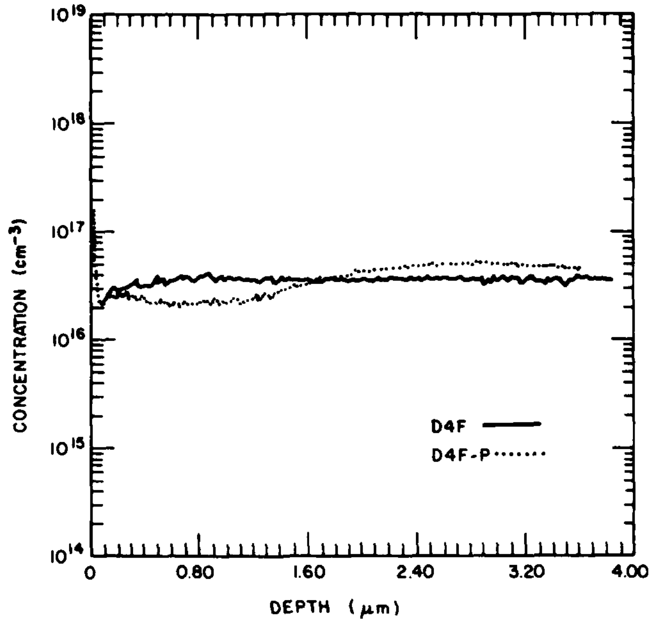

Figure 73. SIMS profiles showing Cr concentration in low-dose, Si-implanted, capless-annealed GaAs with (D4F-P) and without (D4F) high-energy ^{31}P implantation.

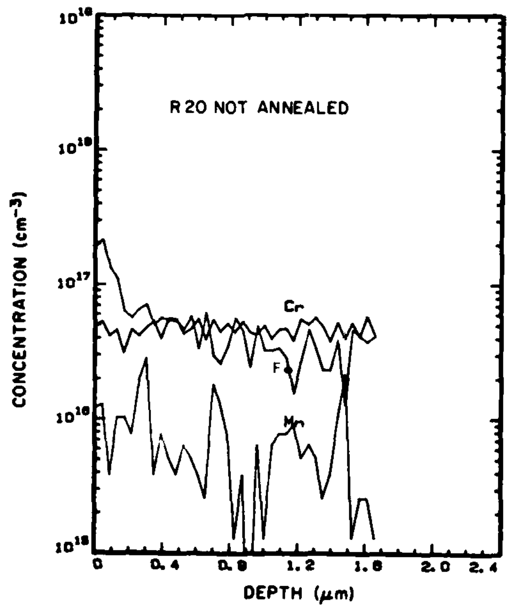

Figure 74. SIMS profiles showing Mn, Cr, and Fe concentrations in R20 before thermal annealing.

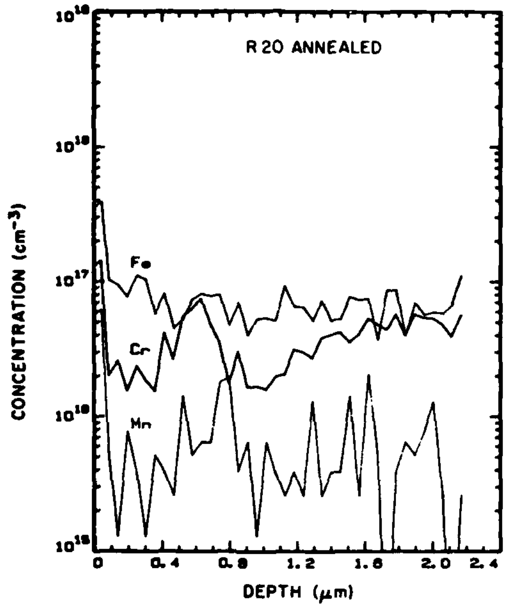

Figure 75. SIMS profiles showing Mn, Cr, and Fe concentrations in R20 after thermal annealing.

Regardless of the low sensitivity of the SIMS measurement, the profiles do show that the Cr distribution is similar to that in Fig. 65. The Mn seems to follow a similar distribution, although it is not conclusive. The low sensitivity is partially due to the fact that the measurement for three profiles was done simultaneously, each profile receiving only one-third of its number of counts. The sensitivity of the impurity profiles can be improved.

SECTION VII

LASER, ELECTRON-BEAM, AND RADIATION ANNEALING

During this program we have studied annealing of Si-implanted GaAs using (1) a high-power Q-switched Nd:glass laser [18] (λ = 1.06 µm), (2) a high-power Q-switched ruby laser [20] (λ = 0.694 µm), (3) a pulsed dual-frequency laser, (4) a pulsed electron beam, and (5) a high-power halogen lamp. In contrast to the ruby laser, the photon energy of the Nd:glass laser (1.17 eV) is less than the bandgap of GaAs (1.4 eV at 300 K). The optical absorption at the Nd:glass laser wavelength is therefore strongly dependent upon the amount of impurities and lattice defects produced by implantation. This section describes studies made on as-implanted and laser-annealed samples using van der Pauw measurements and secondary ion-mass spectrometry (SIMS). The results are compared with those obtained using thermal annealing. Other subjects studied include optical absorption measurements in Nd:glass-laser-irradiated GaAs, surface morphology and crystallinity of a laser-annealed GaAs layer, and unalloyed ohmic contacts made onto laser-(or electron beam)-annealed GaAs.

A. HIGH-POWER PULSED LASER SYSTEM

The laser system used is the Korad Model K-1500 gigawatt laser system* (Fig. 76), consisting of the oscillator, the amplifier, and the Pockel cell unit for Q-switching the oscillator output. The oscillator ruby rod is 10.16x0.95 cm (4x3/8 in.) in diameter and is wrapped around by a helical xenon flashlamp, which serves to optically pump the laser material and produce a population inversion of the chromium ions in the ruby when at least half the chromium ions are excited. Lasing occurs when the round-trip gain between parallel mirrors placed at opposite ends of the oscillator ruby rod is greater than unity. The Pockel cell Q-switch prevents the threshold for lasing from being attained by effectively reducing the reflectivity of the rear cavity mirror to zero. This allows the ruby rod to achieve a maximum energy storage, which corresponds to a high value for the gain coefficient. The cell is then

*Hadron, Inc., Korad Div., Santa Monica, CA.

triggered to "insert" the cavity mirror, at which time a high cavity gain occurs. This results in a "giant pulse" with high power density and short pulse duration, typically 25 to 30 ns. This giant pulse is then further amplified by an amplifier stage. The amplifier ruby rod is 22.9x1.9 cm (9x3/4 in.) in diameter and works by stimulated light emission triggered by the giant pulse from the oscillator stage and the Pockel cell. Amplification by a factor as high as 20X can be achieved. Maximum laser output power is 1 GW/pulse at 2 pulses/min.

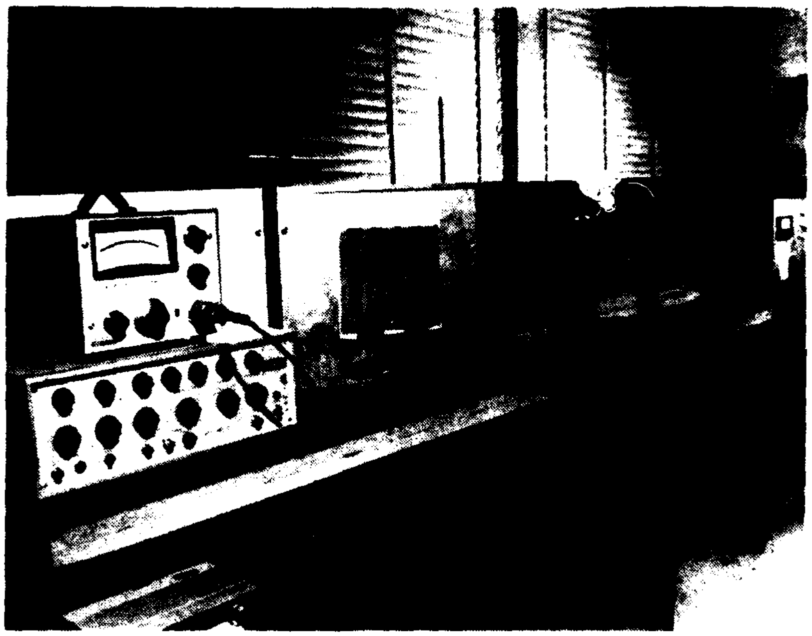

Figure 76. High-power pulsed laser system.

At a given oscillator-rod high voltage above the threshold value of 3.98 kV, the laser-output pulse width is a function of two parameters, namely, Q-switch shutter delay and Pockel cell bias voltage. These two parameters are independent of each other so that they can be optimized separately. The laser-output pulse width was measured with a photodiode and a Tektronix* 7704 fast oscilloscope. The photodiode used was a silicon avalanche photodiode, type C30902E from RCA Electro Optics and Devices.** The rise time was specified

*Tektronix, Inc., Beaverton, OR.
**RCA Electro Optics and Devices, Lancaster, PA.
†Polaroid Corp., Cambridge, MA.

to be 0.4 ns which was adequate for this application. The Tektronix 7704 oscilloscope was set up to operate in the triggered single sweep mode, and a camera with ultrafast Polaroid† film (Type 410, ASA 10,000) was used to photograph the pulse. The optimum pulse shape recorded had a Gaussian distribution with a FWHM of 30 ns. The same laser system was modified for Nd:glass-laser experiments with replacement of the laser rod and associated optical devices. The double-frequency laser beam was produced by the Q-switched Nd:glass laser with a frequency doubler. The energy density of the laser output pulse was measured with a calibrated (±5%) ballistic thermopile.

B. ANNEALING Si-IMPLANTED GaAs USING LASER-BEAM IRRADIATION

1. Pulsed Nd:Glass Laser

Semi-insulating GaAs substrates of (100) orientation were implanted under high vacuum with $^{28}Si^+$ at energies between 70 and 200 keV, and fluence between $3x10^{12}$ and $3x10^{15}$ cm^{-2}. The wafers were polished and chemically etched prior to implantation as previously described. Some wafers were polished on both sides to facilitate optical absorption studies. Following implantation, the 0.04-cm-thick wafer was cleaved to samples approximately between 0.5 and 2 cm^2 for laser-annealing experiments.

The Nd:glass laser was operated with an output energy density of between 0.2 and 2.5 J/cm^2 per pulse (25 ns FWHM). The corresponding power density lies between 8 and 100 MW/cm^2. The diameter of the laser beam is 2 cm. The thermally annealed samples used for comparison were either annealed at 825°C for 20 min under an arsenic overpressure without encapsulation or annealed at temperatures up to 1000°C using samples encapsulated with a 2000-Å-thick sputtered Si_3N_4 layer.

Figure 77 shows comparative results of sheet carrier concentration density for Nd:glass-laser and thermally annealed samples with implanted ^{28}Si doses between $3x10^{12}$ and $3x10^{15}$ cm^{-2}. The energy density of each laser pulse used in the annealing is indicated by crosses in the figure; they vary between 0.5 and 1.17 J/cm^2. All experiments were performed with single pulses. At the low-energy density level, the implanted layers are only partially annealed. Figure 77 also shows that the electrical activation is greatly enhanced by laser annealing for samples implanted with doses higher than $3x10^{14}$ cm^{-2}. The sheet carrier concentration density N_s as determined by van der Pauw measurement is

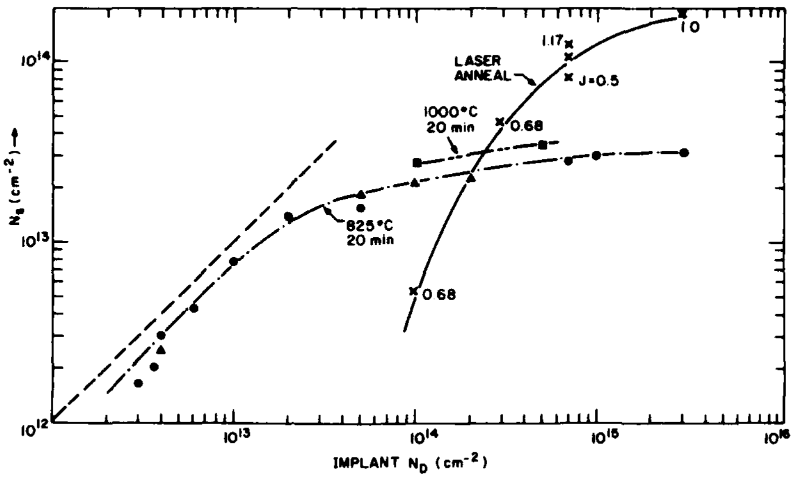

Figure 77. Comparison of thermal and laser annealing; a 1.06-μm, 25-ns single-pulse (Nd:glass) laser was used. The 1000°C anneal used sputtered Si_3N_4 encapsulant; the 825°C anneal was capless.

two to five times higher than that of samples thermally annealed at 825 or 1000°C for 20 min. The 825°C anneal was done under arsenic overpressure with no encapsulant; the 1000°C anneal was done under N_2 atmosphere with sputtered Si_3N_4 encapsulant. The low electrical activation at a lower dose level for a given pulsed laser energy may be attributed to the reduction in enhanced optical absorption. The enhanced absorption is dependent on the amount of dose of the implantation as studied by the optical absorption measurements.

Table 26 lists some measured results on the mobility, the sheet carrier concentration, and the activation efficiency of Si-implanted GaAs samples annealed by a Nd:glass laser and by thermal anneal (825°C, 20 min). The fluences listed in the table are greater than 3×10^{14} cm^{-2}. The laser-annealed samples showed higher activation efficiencies. The mobilities for laser-annealed samples are comparatively lower even considering the difference in carrier concentration. For example, mobilities for laser-annealed samples are 253 cm^2/V-s at a sheet carrier concentration of 1.91×10^{14} cm^{-2} and 529 cm^2/V-s at 1.25×10^{14} cm^{-2}, compared with a mobility of 1392 cm^2/V-s at 2.9×10^{13} cm^{-2} and 1881 cm^2/V-s at 2.8×10^{13} cm^{-2} for similar samples annealed thermally.

TABLE 26. COMPARISON OF Nd:GLASS-LASER ANNEALING AND THERMAL-ANNEALING DATA

Si Implantation		Nd:Glass Laser Annealing				Thermal Annealing		
Dose (cm^{-2})	Energy (keV)	Energy (J/cm^2)	N_s (cm^{-2})	μ ($cm^2/V\text{-}s$)	η (%)	N_s (cm^{-2})	μ ($cm^2/V\text{-}s$)	η (%)
3.0×10^{15}	70	1.00	1.91×10^{14}	253	6.4	5.1×10^{13}	1392	1.7
3.0×10^{15}	200	2.25	1.45×10^{14}	1017	4.8	3.3×10^{13}	1909	1.1
1.0×10^{15}	70	0.34	6.55×10^{13}	254	6.6	3.2×10^{13}	1770	3.2
$5/2 \times 10^{14}$	200/70	1.17	1.25×10^{14}	529	17.9	2.8×10^{13}	1881	4.0
3.0×10^{14}	200	0.68	4.60×10^{13}	522	15.3	3.0×10^{13}	1540	10.0

The optical absorption in the samples, which were polished on both sides, were measured by spectrophotometry. The transmission through the sample and the reflection from the sample were measured on a Cary spectrometer in the 7000- to 12000-Å wavelength range. The absorption at a given wavelength (e.g., 1.06 μm) is calculated by the expression:

$$A = 1 - T - R \tag{29}$$

where A, T, and R are, respectively, absorption, transmission, and reflection which are all absolute values and are expressed in percentages. The enhanced absorption due to implantation damage is equal to $A-A_0$, where A_0 is the absorption through the unimplanted sample. At 1.06-μm wavelength, the measured value of A_0 was typically 0.1. The reflectance was measured with reference to an aluminum mirror, and the absolute value is obtained through calibration. At 1.06 μm, the reflectance of aluminum on glass is 0.862.

Figure 78 shows the reflectance measured on an as-implanted wafer and on the same wafer irradiated with a Nd:glass laser pulse at an energy density of 0.34 J/cm^2. Because of the enhanced absorption in the high-dose implanted layer, the reflection is affected only by the front (implanted) surface. Consequently, the reflectance forms a continuous line as it passes through the absorption edge as shown in Fig. 78(a). In the case of the annealed sample, restored lattice order reduces the enhanced absorption in the implanted layer. As a result, the reflectance spectrum forms a step [Fig. 78(b)] as the optical wavelength passes through the band edge of GaAs, because the reflection is enhanced in the long wavelength range due to multiple reflection from the polished sample back surface. The multiple reflection dominates over the change in surface reflectivity which occurs as a result of implantation.

The transmittance through an ion-implanted sample before and after annealing is shown in Fig. 79. The gradual increase in absorption from the long-wavelength side toward the absorption edge in the as-implanted sample is a band-tailing effect produced by impurities [59]. The transmittance at 1.06-μm wavelength changes from 0.170 for the as-implanted sample to 0.457 after laser

59. See, for example, J. Pankove, Optical Processes in Semiconductors, (Prentice-Hall, Inc., Englewood Cliffs, NJ, 1971), p. 10.

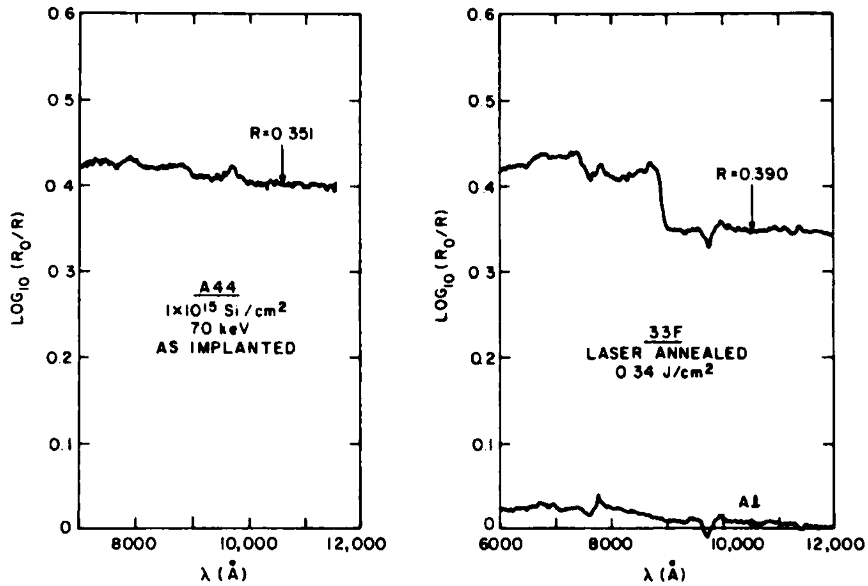

Figure 78. Reflectance measured on an as-implanted wafer (a) and after laser annealing (b).

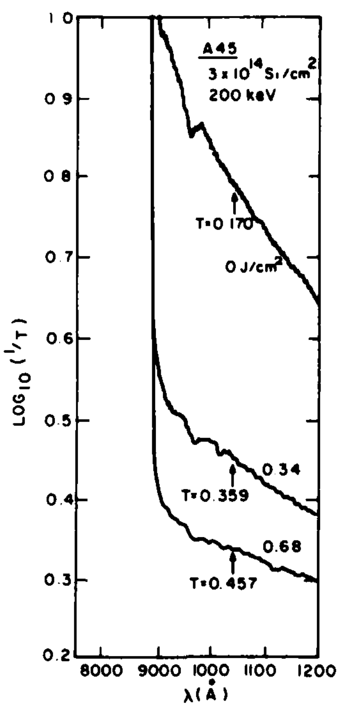

Figure 79. Optical transmission from a Si-implanted GaAs sample annealed at different laser energy densities.

annealing at 0.68 J/cm^2. The enhanced absorption ($A-A_0$) can be evaluated from Eq. (29). Figure 80 shows the measured values of transmittance, reflectance, and enhanced absorption for as-implanted samples at different dose levels.

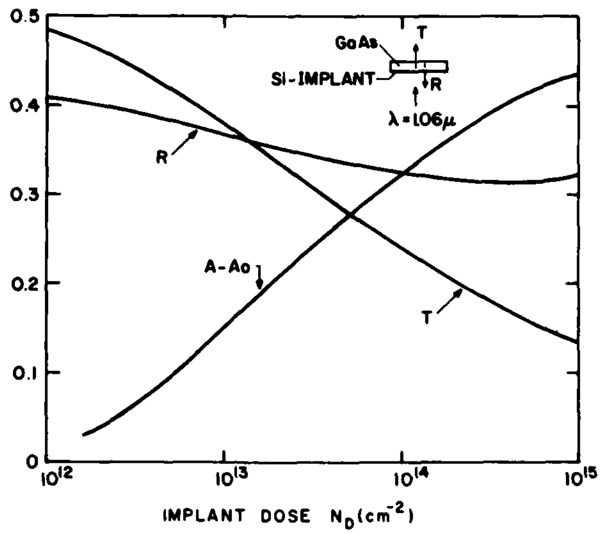

Figure 80. Measured values of transmittance (T), reflectance (R), and enhanced absorption ($A-A_o$) for different dose levels.

Optical absorption measurements show that the implantation-enhanced absorption at a given wavelength (e.g., 1.06 μm) below the band edge increases with implant dose. This enhanced absorption is greatly reduced following annealing as a result of lattice re-ordering. Such optical measurement may thus be used as a diagnostic technique for optimizing the required laser energy while maintaining good surface morphology.

The photon energy of the Nd:glass laser of 1.17 eV (λ = 1.06 μm) is lower than the bandgap of GaAs (1.4 eV at 300 K). The optical absorption at 1.06 μm is therefore dependent upon the amount of impurities and lattice defects produced by implantation. The Nd:glass laser may therefore be suitable for deep impurity distribution such as that produced by MeV Si implantation in GaAs.

Annealing of high-energy (>600 keV) Si-implanted GaAs wafers was investigated using a high-power pulsed Nd:glass laser. The electrical characteristics were evaluated using van der Pauw measurements. The results are tabulated in Table 27. Two samples were single-energy implanted and two were multiple implanted. Samples N6A and N6B were multiple-implanted using five energies between 40 and 900 keV with corresponding fluences between 1.4×10^{14} and 1.30×10^{15} cm^{-2} and were designed to produce a uniform 1-μm Si concentration of $1/3 \times 10^{20}$ cm^{-3}. The fact that high-energy-implanted samples can be activated with the irradiation of an Nd:glass laser is encouraging.

TABLE 27. ELECTRICAL PROPERTIES OF HIGH-ENERGY Si-IMPLANTED Nd:GLASS-LASER-IRRADIATED GaAs

Sample No. (Implant No.)	Implantation Energy (keV)	Implantation Dose (cm^{-2})	Laser Energy (J/cm^2)	N_s (cm^{-2})	μ (cm^2/V-s)	ρ_s (Ω/□)	η (%)
N7(H7)	600	2.52×10^{15}	1.5	7.88×10^{13}	734	108.0	3.1
N8(H8)	700	2.70×10^{15}	1.5	2.23×10^{14}	1027	27.0	8.2
N6A(H24)	40 to 900	1.41×10^{14} to 1.30×10^{15}	1.5	7.14×10^{14}	488	17.9	22.0
N6B(H24)	40 to 900	1.41×10^{14} to 1.30×10^{15}	1.2	3.58×10^{14}	464	37.6	11.0

Figures 81 and 82 show the depth distribution of carrier density and mobility of the multiple-implanted samples, N6A and N6B, respectively. The samples were evaluated using differential van der Pauw measurements. The measurements show that the carrier density reached $\sim 2 \times 10^{19}$ (N6A) and $\sim 9 \times 10^{18}$ cm^{-3} (N6B) 1 μm below the sample surface. The corresponding mobilities were ~ 300 cm^2/V-s. Much lower carrier concentrations with higher mobilities were measured toward the sample surface. The significance of the depth profile of carrier concentrations and mobilities is that pulsed Nd:glass-laser beams can

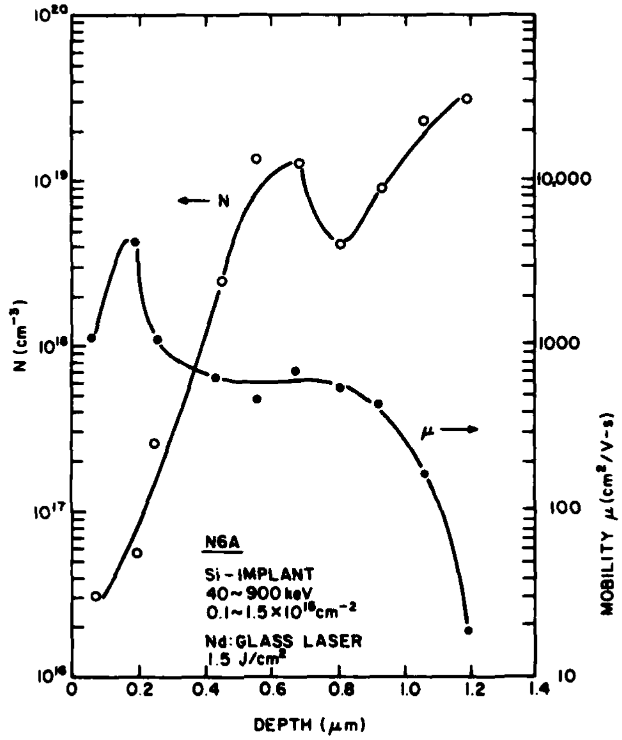

Figure 81. Depth distribution of carrier concentration and mobility of multiple-implanted GaAs; laser-irradiated at 1.5 J/cm^2.

be used to activate 1-μm-deep MeV implanted GaAs. The lower carrier concentration at the sample surface may be related to (1) the lower dose at the low-energy end of the multiple implants and (2) the decrease in carrier concentration at the surface in laser-irradiated GaAs following a subsequent thermal treatment [60]. Ohmic contacts for differential van der Pauw measurements were formed at an elevated temperature of 450°C for 1 min.

60. P. A. Pianetta, C. A. Stolte, and J. L. Hauser, "Pulsed E-Beam and Ruby Laser Annealing of Ion-Implanted GaAs," Symp. Proc. on Laser and Electron Beam Processing of Materials, Academic Press, 1980.

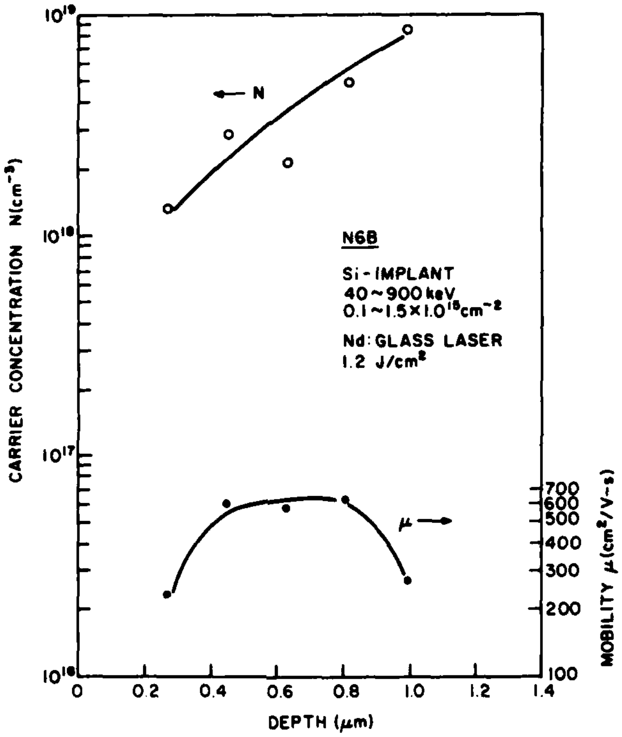

Figure 82. Depth distribution of carrier concentration and mobility of multiple-implanted GaAs; laser-irradiated at 1.2 J/cm^2.

2. Pulsed Ruby Laser

Laser-annealing experiments were also carried out using a ruby laser on a Si-implanted (100)-oriented SI GaAs substrate. The wafers were implanted at 70, 100, and 200 keV, with doses ranging between 1×10^{14} and 1×10^{16} cm^{-2}. The Q-switched ruby laser was operated with an output energy density of between 0.2 and 2.3 J/cm^2 per 30-ns (FWHM) pulse. The electrical characteristics of the laser-annealed samples were studied using the van der Pauw measurements.

Tables 28 and 29 summarize electrical properties of 200- and 70-keV Si-implanted ruby-laser-irradiated GaAs compared with similar samples annealed thermally. The data was tabulated in terms of sheet resistance ρ_s, mobility μ, and activation efficiency η, which is defined as the ratio of the electrically activated sheet carrier concentration N_s to the implanted fluence. The thermal annealing was carried out under arsenic overpressure at 825°C for 20 min. The higher activation efficiency of 200-keV implants compared with that of 70-keV

TABLE 28. ELECTRICAL PROPERTIES OF 200-keV Si-IMPLANTED RUBY-LASER-IRRADIATED GaAs

Si Implantation		Ruby-Laser Annealing				Thermal Annealing		
Energy (keV)	Dose (cm^{-2})	E (J/cm^2)	ρ_s ($\Omega/\square$)	μ (cm^2/V-s)	η (%)	ρ_s ($\Omega/\square$)	μ (cm^2/V-s)	η (%)
200	$1x10^{14}$	2.3	104	1300	46.3			
200	$1x10^{14}$	1.7	91	1350	51.0	132	2200	21.5
200	$1x10^{14}$	0.6	1600	454	8.6			
200	$5x10^{14}$	2.3	27	1030	45.5			
200	$5x10^{14}$	1.7	27	830	55.6	112	1738	6.4
200	$5x10^{14}$	1.0	320	280	14.0			
200	$3x10^{15}$	2.3	27	370	20.8			
200	$3x10^{15}$	1.8	31	355	18.9	130	1938	0.8
200	$3x10^{15}$	1.0	57	250	14.5			

TABLE 29. ELECTRICAL PROPERTIES OF 70-keV Si-IMPLANTED RUDY-LASER-IRRADIATED GaAs

Si Implantation		Ruby-Laser Annealing				Thermal Annealing		
Energy (keV)	Dose (cm^{-2})	E (J/cm^2)	ρ_s ($\Omega/\square$)	μ (cm^2/V-s)	η (%)	ρ_s ($\Omega/\square$)	μ (cm^2/V-s)	η (%)
70	$1x10^{15}$	2.3	39	693	23.0			
70	$1x10^{15}$	1.7	29	745	29.4	170	1712	2.1
70	$1x10^{15}$	0.8	156	314	12.8			
70	$3x10^{15}$	2.3	24	564	15.1			
70	$3x10^{15}$	1.7	29	496	14.6	72	1387	2.1
70	$3x10^{15}$	1.3	52	300	13.3			
70	$3x10^{15}$	0.8	148	172	8.2			
70	$1x10^{16}$	2.3	21	481	6.3			
70	$1x10^{16}$	1.3	93	210	3.2	90	1727	0.4

implants at a given fluence is believed due to the lower atomic Si concentration associated with the broader straggle of 200-keV implants.

Tables 28 and 29 show that the activation efficiency and hence the sheet carrier concentration is considerably higher in laser-irradiated samples than in thermally annealed samples. The mobility of laser-irradiated GaAs, however, is lower than that of thermally annealed samples, even taking into consideration the expected lower mobility as a result of higher carrier density. The net effect of a much higher activation and a lower mobility results in a lower sheet resistance in high-energy laser-irradiated GaAs as shown in Tables 28 and 29.

The atomic profiles of high-dose implanted laser-irradiated GaAs were investigated previously. The amount of impurity profile broadening depends on the energy density of the laser beam. A substantial broadening was observed in samples irradiated with a high-energy-density beam. The SIMS profile of a 1-J/cm^2 pulsed ruby-laser-irradiated GaAs ($3x10^{15}$-cm^{-2}, 200-keV implanted) .ows no significant broadening as compared with profiles of the as-implanted and the thermally annealed samples (Fig. 83). The same sample, however, has shown high electrical activation (Table 28). This result indicates that, under proper conditions, Si-implanted GaAs can be electrically activated using a pulsed laser beam without melting the implanted layer. Rapid diffusion in a

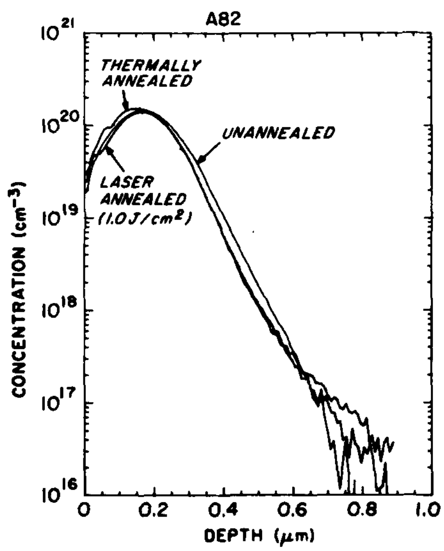

Figure 83. SIMS profiles showing Si-implanted GAs samples that are as-implanted, 1.0-J/cm^2 ruby-laser annealed, and thermal annealed.

liquid state has been regarded [61] as the cause for substantial impurity profile broadening observed in ion-implanted laser-annealed silicon.

Figure 84 shows results of sheet carrier concentration densities as a function of the implantation dose level for samples annealed by high-power pulsed ruby laser and for samples annealed thermally. The thermal annealing was done at 825 and 900°C for 20 min, and the energy used for implantation was at 200 keV, as described previously. The energy densities used for laser anneal shown in Fig. 84 were 1.7 and 2.3 J/cm^2, which were higher than that plotted in Fig. 77. It is interesting to note that samples implanted at 200 keV show higher activation efficiencies than those implanted at 70 keV, at the high implant dose level. This may relate to the fact that the impurity density in the implanted layer is higher in the 70-keV implanted sample than in the 200-keV implanted sample because of the smaller straggle associated with the 70-keV implantation. Lower activation efficiencies were observed with increased fluence above 5x10^{14} cm^{-2} as shown in Fig. 84.

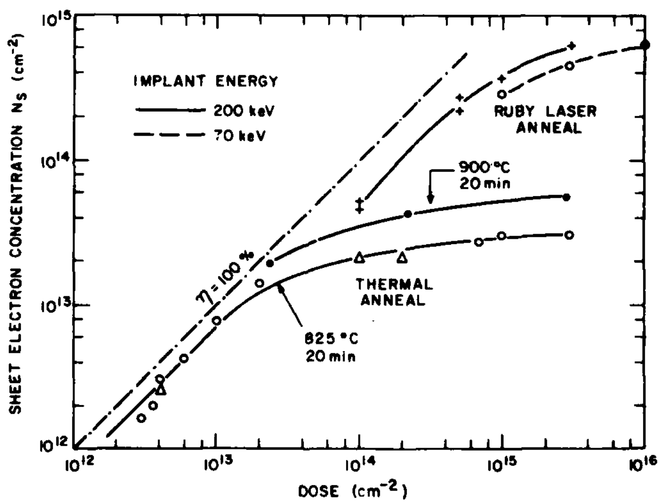

Figure 84. Sheet electron concentration as a function of dose for ruby-laser and thermally annealed samples.

61. J. C. Wang, R. F. Wood, and P. P. Pronko, "Theoretical Analysis of Thermal and Mass Transport in Ion-Implanted Laser-Annealed Silicon," Appl. Phys. Lett. 33, 445 (1978).

The sheet carrier concentration density of up to 6.25×10^{14} cm^{-2} with an activation efficiency of 20.8% was measured on high-dose implanted samples. These results are more than an order of magnitude higher than that for similar samples annealed thermally. Figure 85 shows a plot of the mobility μ, the acivation efficiency η, and the sheet resistance ρ_s for 200-keV Si-implanted GaAs wafers implanted with three different fluences and followed by a ruby-laser irradiation at 2.3 J/cm^2. Higher activation efficiencies (45 to 60%) and higher mobilities (930 to 1350 $cm^2/V\text{-}s$) were measured in wafers implanted at a dose level ranging from 1×10^{14} to 5×10^{14} cm^{-2}. The sheet resistances are lower and show little variations when the implant dose is higher than about 5×10^{14} cm^{-2}. The sheet resistances at the high-dose region shown in Fig. 85 are typically 4 to 5 times lower than similar thermally annealed wafers. The lowest sheet resistance obtained was 20.8 Ω/□, which was measured on samples implanted at 70 keV with a dose of 3×10^{15} cm^{-2} and annealed by ruby-laser irradiation at 2.3 J/cm^2.

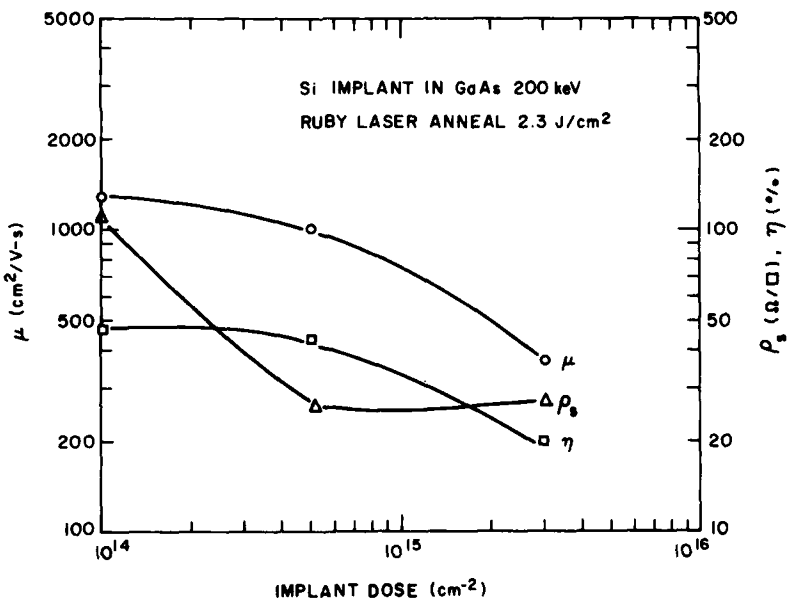

Figure 85. Mobility (μ), activation efficiency (η), and sheet resistance (ρ_s) as a function of dose.

The electrical characteristics of ion-implanted laser-annealed samples depend on the implantation energy and fluence, and the energy density of the laser irradiation on the sample surface. Figure 86 shows the measured mobility, the sheet resistance, and activation efficiency of Si-implanted GaAs wafers irradiated by a ruby laser operated at different energy densities. The wafers were implanted at 200 keV with fluences of 5×10^{14} and 3×10^{15} cm^{-2}.

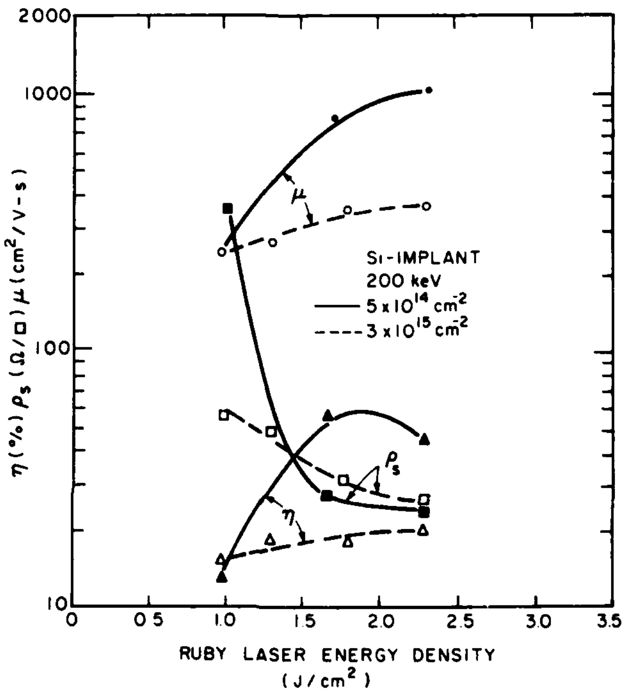

Figure 86. Mobility (μ), activation efficiency (η), and sheet resistance (ρ_s) as a function of energy density.

The data points indicate that in the wafer implanted with the 5×10^{14} cm^{-2} dose, the mobility and activation efficiency are much higher for samples irradiated at a higher surface energy density (1.7 to 2.3 J/cm^2) than that irradiated at a lower surface energy density (1 J/cm^2). The sheet resistance drops substantially from 360 $\Omega/\Box$ at 1 J/cm^2 to 27 $\Omega/\Box$ at 1.7 to 2.3 J/cm^2. The sheet resistance starts to reach the low level at a laser energy density of about 1.5 J/cm^2, which may be considered as a threshold for full activation in this sample.

3. Pulsed Nd:Glass Laser with Frequency Doubler

Annealing of high-dose-implanted GaAs samples was studied using a double-frequency laser beam (Nd:glass laser, λ = 1.06 μm, with a doubler, λ = 0.53 μm). The output power of the doubler, which is made from a CD*A crystal, is 15% of the total power. The samples irradiated with double-frequency laser beam show good surface morphology at irradiated energy densities of 0.9 to 1.2 J/cm^2. Unalloyed ohmic contacts with Ti/Pt/Au metallization were successfully made onto the double-frequency laser-irradiated surface. Table 30 shows the electrical properties measured by van der Pauw methods on samples implanted with different doses and irradiated with laser beams at different energy densities.

TABLE 30. ELECTRICAL PROPERTIES OF 70-keV Si-IMPLANTED GaAs

Sample	Implant Energy (keV)	Implant Dose (cm^{-3})	Laser Energy (J/cm^{-2})	ρ_s (Ω/□)	μ (cm^2/V-s)	η (%)
L-16	200	3×10^{15}	1.2	24.8	403	15.6
	70	1×10^{15}				
L-17	200	1×10^{15}	1.2	51.9	442	18.1
	70	5×10^{14}				
L-15	250	2×10^{14}	1.0	373.0	504	11.0
	70	1×10^{14}				
L-19	200	4×10^{14}	1.1	168.0	518	14.4
	50	1×10^{14}				
L-3	200	3×10^{15}	0.88	144.0	247	5.9

Figure 87 illustrates the atomic Si profiles of Si-implanted Cr-doped GaAs before and after irradiation with a 1.7-J/cm^2 double-frequency laser beam and

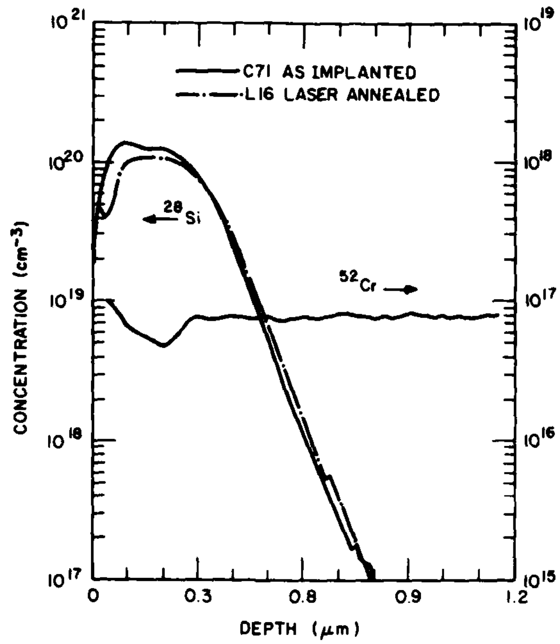

Figure 87. SIMS profiles of Si-implanted GaAs showing Si distribution before and after irradiation with double-frequency pulsed laser beam and Cr distribution after irradiation.

the corresponding Cr-concentration profile after laser irradiation. The flat top of the Si profile is a result of multiple Si implant in the sample (3×10^{15} cm^{-2}, 200 keV; 1×10^{15} cm^{-2}, 70 keV). There is no major broadening either in the Si or in the Cr profile. Some structures appearing on the SIMS profiles are not clearly understood.

4. Scan-Pulsed Laser

Annealing experiments with the 0.53-µm laser were performed using the Quantronix Corporation (Smithtown, NY) Model 610 Epitherm which is a Q-switched Nd:YAG laser with a second harmonic generator. The laser pulse width is 100 ns, repetition rate is 7 kHz, and beam spot size is ~5 mil in diameter.

Preliminary results on scan-laser experiments using an energy density of 1.8 J/cm^2 were not very encouraging. All samples showed scan marks on the surface, which may be an indication of dissociation at the surface. Probing the surface showed no activation except for one sample which has light scanning

marks. After cleaning in HCl, that sample ($3x10^{15}$ cm^{-2}, 70 keV Si-implanted) showed a sheet carrier concentration of $9.1x10^{13}$ cm^{-2}, a mobility of 479 cm^2/V-s, and a sheet resistance of 144 Ω/□. A similar sample irradiated with a 1-J/cm^2 pulsed ruby laser had a sheet carrier concentration of $2.9x10^{14}$ cm^{-2}, a mobility of 273 cm^2/V-s, and a sheet resistance of 77 Ω/□. The irradiated layer was activated without requiring HCl treatment.

C. ANNEALING Si-IMPLANTED GaAs USING ELECTRON-BEAM IRRADIATION

The pulsed electron-beam experiments were carried out at Spire Corporation, Bedford, MA. The pulse width is 100 ns, and each sample is annealed with a single pulse.

Results on samples annealed with pulsed electron beams were quite encouraging. The electrical activation is comparable to that annealed with high-power pusled laser beams. For example, a $3x10^{15}$-cm^{-2}, 200-keV Si-implanted GaAs sample following electron-beam annealing gave a sheet electron density of $5.6x10^{14}$ cm^{-2}, a sheet resistance of 45 Ω/□, a mobility of 246 cm^2/V-s, and an activation efficiency of 18.7%. These results are comparable to similar samples irradiated with ∿1.2-J/cm^2 pulsed ruby laser. Unalloyed ohmic contacts were formed by depositing either Ti/Pt/Au or AuGe/Ni/Au on electron-beam-irradiated samples.

SIMS profiles on a Si-implanted GaAs sample before and after electron-beam annealing are shown in Fig. 88. A slight redistribution in impurity density is detected. The sample was implanted at 200 keV with a fluence of $3x10^{15}$ cm^{-2} and irradiated with a 100-ns pulse at 0.7 J/cm^2 at 20 keV.

D. ANNEALING Si-IMPLANTED GaAs USING RADIATION ENERGY FROM A HALOGEN LAMP

We have recently investigated a fast annealing process, using the radiant energy from an incoherent light source in an attempt to minimize the unwarranted impurity (e.g., Cr) redistribution associated with the regular slow furnace anneal. It is known that problems such as surface conversion of annealed wafers can be caused by excessive Cr depletion and the presence of residual impurities in SI GaAs substrates. Preliminary annealing experiments gave encouraging results: Si-implanted GaAs layers have been annealed with good mobility and activation in a time interval of less than 10 seconds. Both high-(∿$3x10^{15}$ cm^{-2}) and low-(∿$7x10^{12}$ cm^{-2})-dose-implanted samples were successfully

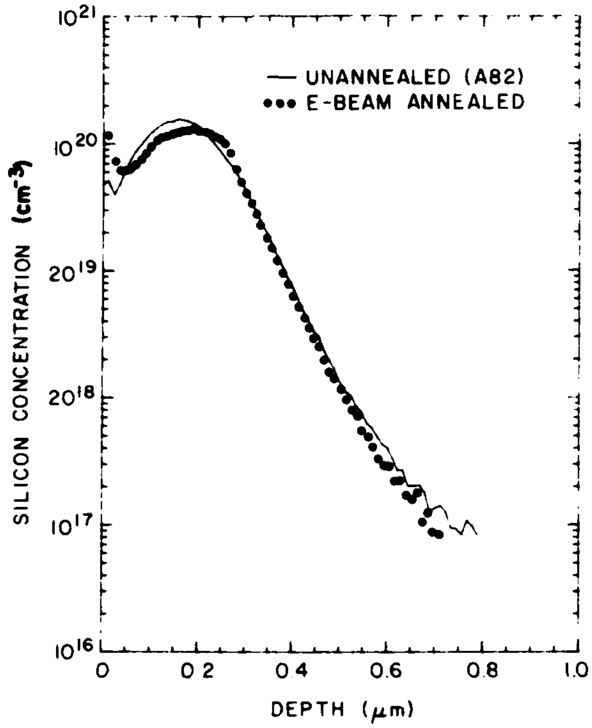

Figure 88. Impurity profiles of a Si-implanted sample before and after electron-beam annealing at 0.7 J/cm^2.

annealed. (High-power pulsed laser annealing was successful only on high-dose-implanted GaAs.)

The anneal was done in a quartz tube using a 600-W halogen lamp. The samples were annealed without encapsulation in a nitrogen atmosphere. The annealing system provided a controlled transient temperature at the position of the wafer. A typical generated transient-temperature pulse, when the lamp is turned on for 10 seconds, is illustrated in Fig. 89. The temperature was monitored by a fine thermal couple, and it reached 800°C in about 5 seconds. Controlled peak temperature up to 1070°C has been measured in 5 seconds using a 1000-W halogen lamp. Annealing experiments were performed with the lamp energized between 5 and 10 seconds.

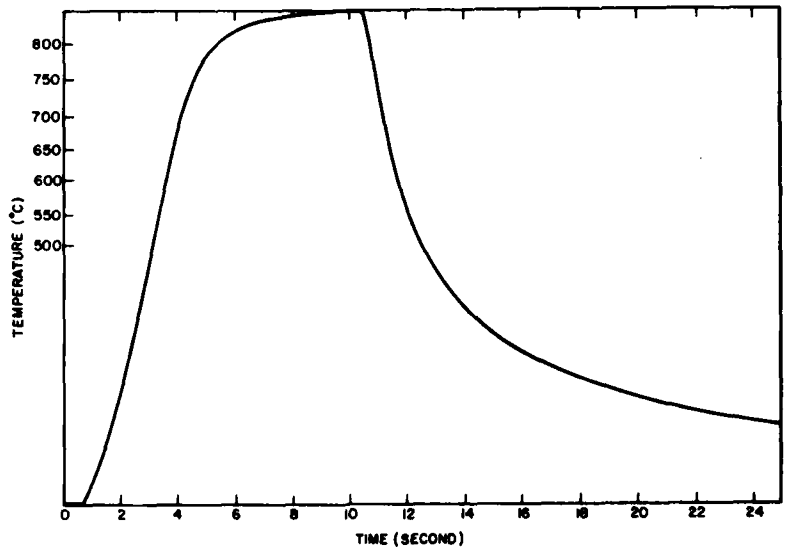

Figure 89. Temperature-time characteristics of a wafer in the radiant-energy furnace.

Table 31 shows the characteristics of a number of Si-implanted wafers annealed using a halogen lamp. Three samples (D37-1, D37-2, D37-3) were medium-dose implanted, and two samples (D70-1, D77-2) were high-dose implanted. The data indicate that the electrical characteristics of the annealed n-GaAs layer are dependent on pulse duration. The optimum annealing conditions, the doping profiles, and the impurity distributions are being further investigated.

E. SIMS MEASUREMENTS

Impurity distribution in as-implanted, Nd:glass-laser-annealed, ruby-laser-annealed, and electron-beam-annealed samples have been investigated with the SIMS technique. Depth profiles were obtained by bombarding the samples with 5-keV Cs^+ ions while detecting the implanted ^{28}Si atoms as a molecular ion $^{75}As^{28}Si^-$ at mass 103. Ultrahigh vacuum (4×10^{-10} Torr) in the sample chamber during the analysis prevented interference from the molecular ion $^{71}Ga^{16}O_2$ which is also at mass 103.

TABLE 31. CHARACTERISTICS OF Si-IMPLANTED GaAs ANNEALED BY PULSED RADIATION FROM A HALOGEN LAMP

Sample	Implant Energy (keV)	Implant Dose (cm^{-2})	Time Lamp Energized (s)	Sheet Carrier Concentration (cm^{-2})	Mobility (cm^2/V-s)
D37-1	180	$6.5x10^{12}$	10	$2.72x10^{12}$	3590
	50	$0.5x10^{12}$			
D37-2	180	$6.5x10^{12}$	6.5	$4.26x10^{12}$	3700
	50	$0.5x10^{12}$			
D37-3	180	$6.5x10^{12}$	5.0	$4.95x10^{12}$	3285
	50	$0.5x10^{12}$			
D70-1	200	$3.0x10^{15}$	6.0	$4.80x10^{13}$	1660
	70	$1.0x10^{15}$			
D77-2	200	$3.0x10^{15}$	6.0	$4.04x10^{13}$	1950
	70	$1.0x10^{15}$			

The SIMS analyses show that the amount of impurity redistribution depends upon the energy and dose of implantation and upon the energy density of the laser pulse used to anneal the sample. No redistribution occurred after irradiation with a low energy-density pulse, but a substantial impurity broadening was observed in high-dose-implanted samples irradiated with a high energy-density pulse ($\sim$2 J/cm^2). The broadening is believed to be associated with a diffusion in the liquid GaAs created by the high-energy laser pulse.

Figure 90 shows the SIMS profile of a sample implanted at 70 keV with a dose of $1x10^{15}$ cm^{-2} (peak impurity concentration $\sim10^{20}$ cm^{-3}) before and after irradiation with a low energy-density (0.3 J/cm^2) pulse (25 ns) from a Nd:glass laser. The profile shows no redistribution in impurity after irradiation with a single laser pulse up to about 1 J/cm^2 in energy density.

Figure 91 shows three SIMS profiles: one is the profile of a GaAs wafer as-implanted at 70 keV with a dose of $3x10^{15}$ cm^{-2}; the other two are samples

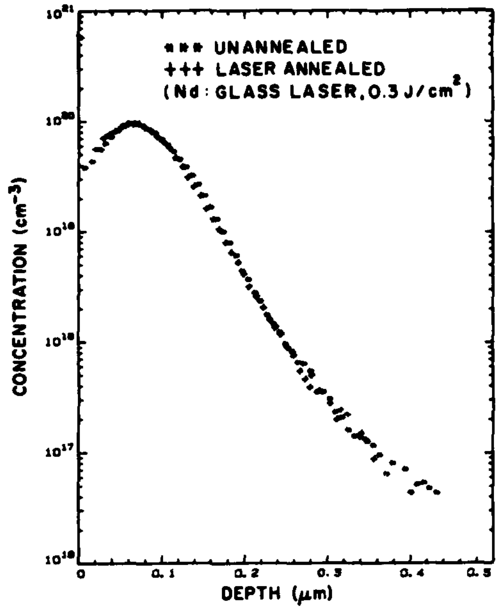

Figure 90. SIMS profile of a Si-implanted GaAs sample before and after laser annealing, 70 keV, 1×10^{15} cm^{-2}.

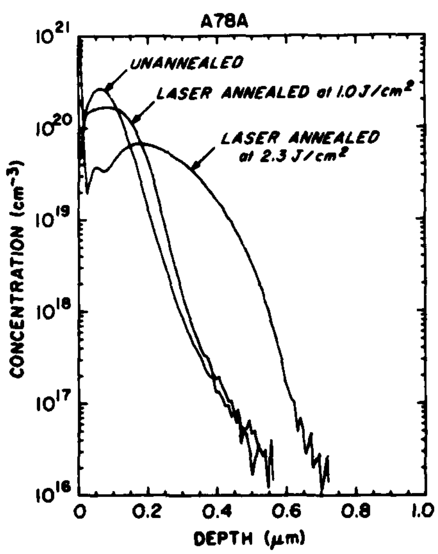

Figure 91. SIMS profiles of an unannealed GaAs wafer, a laser-annealed wafer at 1 J/cm^2, and a laser-annealed wafer at 2.3 J/cm^2.

from the same wafer after being irradiated with single ruby-laser pulses at energy densities of 1.0 and 2.3 J/cm^2, respectively. A redistribution in impurity density was observed in the laser-irradiated samples. The impurity profile broadening associated with the short-duration, high-energy, laser-pulse irradiation suggests that melting occurs near the surface region, and the substantial broadening in impurity distribution is a result of diffusion in liquid GaAs.

Figure 92 shows the SIMS profiles of a GaAs sample implanted at 70 keV with a very high dose of $1x10^{16}$ cm^{-2}. The impurity density of the as-implanted sample peaks at $1x10^{21}$ cm^{-3}. After thermal annealing (825°C, 20 min), the impurity profile does not vary except for a shoulder broadening at an impurity concentration of $2x10^{19}$ cm^{-2}. After irradiation with a 2.3-J/cm^2 ruby-laser pulse, the peak impurity concentration drops by an order of magnitude to about $1x10^{20}$ cm^{-2}, and the impurity penetrates to a depth of about 0.8 μm. The deeper penetration depth associated with the higher impurity concentration further suggests the occurrence of diffusion in the melted GaAs surface layer.

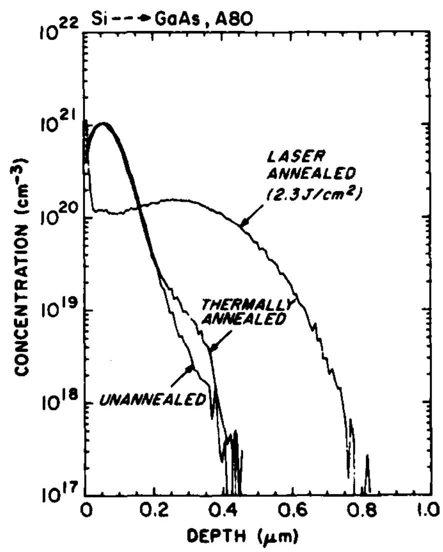

Figure 92. SIMS profiles of unannealed, thermally annealed, and laser-annealed samples.

F. UNALLOYED OHMIC CONTACTS

The contact resistivity of ohmic contacts made onto GaAs has been reported to be inversely proportional to the carrier density of GaAs [62,63]. Contact resistivities of Au-Ge ohmic contacts on ion-implanted GaAs with different dose levels were studied using the TLM technique [64]. Since the laser-annealed heavily implanted GaAs layer shows a much higher activation than does the thermally annealed layer, one expects a superior ohmic contact formed onto such a surface.

To form ohmic contacts on n-type GaAs, a thermal alloying step is normally required after the metal is deposited onto the GaAs surface. Metallizations conventionally used are AuGe/Ni/Au, and alloying is normally done at 400 to 450°C for approximately 1 min. Unalloyed ohmic contacts on n-GaAs have been reported by evaporation of metal onto high-concentration ($\sim 1 \times 10^{19}$ cm^{-3}) n^{++}-GaAs produced by molecular beam epitaxy (MBE) [65], or high fluence implants irradiated by electron [66] or laser [20] beams. Recent developments in ohmic contacts and their correlations with theory were discussed in a paper by Yoder [67].

We have demonstrated unalloyed ohmic contacts made by evaporation of AuGe or Ti-Pt-Au directly onto high-dose implanted, high-power pulsed-laser or electron-beam-irradiated GaAs. The use of refractory metallization allows one to form ohmic contacts over n^{++} regions and Schottky contacts over n-regions concurrently. This may be used to simplify device processing. Not all laser-irradiated GaAs samples were successful in forming unalloyed ohmic contacts

---

62. W. D. Edward et al., "Specific Contact Resistance of Ohmic Contacts to GaAs," Solid State Electron. 15, 388 (1972).
63. Y. Goldberg and B. V. Tsarenkov, "Dependence of the Resistance of Metal GaAs Ohmic Contacts on the Carrier Density," Soviet Phys. Semicond. 3, 1447 (1970).
64. H. H. Berger, "Models for Contacts to Planar Device," Solid State Electron. 15, 145 (1972).
65. P. A. Barnes and A. Y. Cho, "Nonalloyed Ohmic Contacts to n-GaAs by Molecular Beam Epitaxy," Appl. Phys. Lett. 33, 651 (1978).
66. R. L. Mozzi, W. Fabian, and F. J. Piekarcki, "Nonalloyed Ohmic Contacts to N-GaAs by Pulse Electron Beam-Annealed Selenium Implants," Appl. Phys. Lett. 35, 337 (1979).
67. M. N. Yoder, "Ohmic Contacts in GaAs," Solid State Electron. 23, 117 (1980).

using both AuGe and Ti-Pt-Au metallizations. In a number of Si-implanted GaAs samples irradiated with pulsed ruby-laser beams we only succeeded in making unalloyed ohmic contacts with AuGe-based metallization [20]. This is illustrated in Fig. 93, which shows I-V curves between as-evaporated Ti/Pt/Au and Au-Ge/Ni/Au contact pads on laser-irradiated GaAs. The reasons are not fully understood. Unalloyed ohmic contacts using Ti-Pt-Au metallization were made on high-dose-implanted GaAs irradiated with a dual-frequency laser beam.

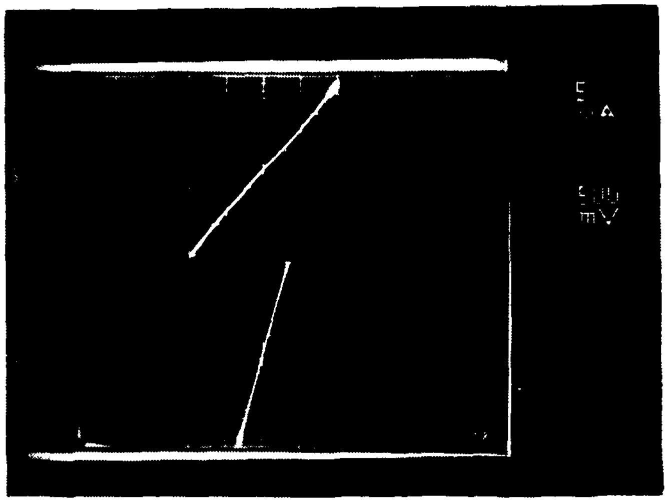

Figure 93. I-V curves between as-evaporated metal contacts on Si-implanted laser-irradiated GaAs. Top: Ti:Pt:Au/500:500:1000 Å; bottom: AuGe:Ni:Au/1500:500:2000 Å.

Table 32 shows electrical performance of unalloyed ohmic contacts using AuGe-based (AuGe/Ni/Au or AuGe/Au) metallization. The sheet resistances, ρ_s, and contact resistivities, ρ_c, were measured by transmission line method (TLM) [64]. The measured resistivities of a number of samples were between 1×10^{-5} and 3×10^{-7} Ω-cm^2. The corresponding sheet resistance measured was between 50 and 140 $\Omega/\square$. The thickness of the Au-Ge layer was 900 to 1500 Å, and the thickness of the Au layer was 2500 Å. The presence of the Ni layer (300 to 500 Å) did not appear to change the ohmic contact characteristics. Figure 94 shows the Auger analysis (performed by J. H. Thomas of RCA Laboratories) of an AuGe/Ni/Au unalloyed ohmic contact on GaAs; it shows little interaction between

TABLE 32. PERFORMANCE OF UNALLOYED OHMIC CONTACTS USING AuGe-BASED METALLIZATION

Sample	Si-Implant Dose (cm^{-2})	Si-Implant Energy (keV)	Energy Density (Ruby Laser) (J/cm^2)	ρ_s ($\Omega/\square$)	ρ_c 10^{-6} (Ω-cm^2)
9D	1×10^{15}	70	0.8	~50	~2.6-6.3
7D	3×10^{15}	70	0.8	137-55	~3.5-9.7
104F	3×10^{15}	70	1.0	95-69	~0.3-3.7

the Ni and other metal layers. It should be pointed out that the 70-keV, high-dose-implanted, ruby-laser-irradiated samples showed "hot spots" in some areas on the surface. The measurements were made on metal patterns located in regions free from hot spots.

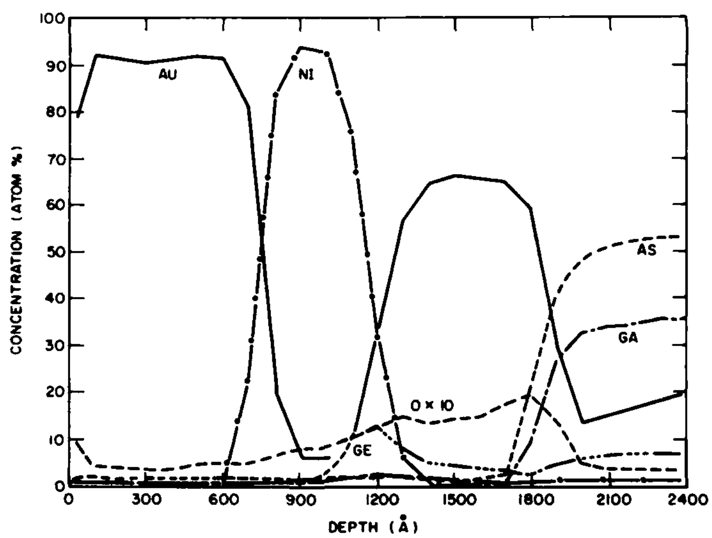

Figure 94. Auger profile of unalloyed AuGe/Ni contacts on a laser-annealed sample.

Table 33 shows electrical performance of unalloyed ohmic contacts using Ti-Pt-Au metallization. The thickness of each metal layer was Ti - 500 Å, Pt - 500 Å, and Au - 2500 Å. The implanted surfaces were irradiated with a dual-frequency laser beam, the output from a Nd:glass laser ($\lambda = 1.06\ \mu m$) plus that from a frequency doubler made from CD*A crystal.

TABLE 33. PERFORMANCE OF UNALLOYED OHMIC CONTACTS USING Ti-Pt-Au METALLIZATION

Sample	Si-Implant Dose (cm^{-2})	Si-Implant Energy (keV)	Energy Density (Ruby Laser) (J/cm^2)	ρ_s ($\Omega/\square$)	ρ_c 10^{-6} (Ω-cm^2)
L3	3×10^{15}	200	0.88	109-80	39-148
L16	1×10^{15} 3×10^{15}	70 200	1.20	35-26	8.7-21

Sample L16, the multiple-implanted dual-frequency laser-beam-irradiated sample, appears to give the best combined unalloyed ohmic contact performance, i.e., low sheet resistance, low contact resistivity, and good surface morphology, among the samples tested. Figures 95 and 96 show Nomarski interference contrast micrographs of sample L16 before and after the evaporation of square Ti-Pt-Au metal patterns. The atomic profiles of L16 were measured by SIMS. There is no significant profile broadening after the sample is irradiated with a double-frequency laser beam at 1.2 J/cm^2.

G. SURFACE MORPHOLOGY AND CRYSTALLINITY STUDY

In the study of laser annealing of Si-implanted GaAs and the formation of unalloyed ohmic contacts on these samples, it is desirable to optimize implant parameters and anneal conditions to achieve low sheet resistance, low contact resistivity, and good surface morphology. The surface morphology and crystallinity of laser-irradiated GaAs implants were investigated using the scanning electron microscopy (SEM) and reflection high-energy electron diffraction

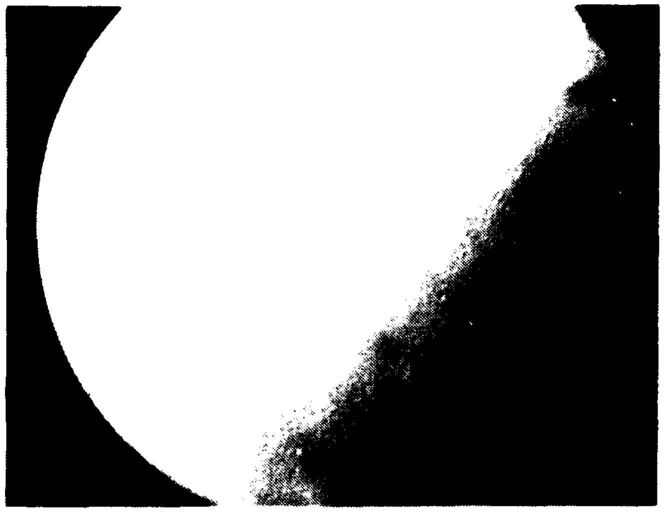

Figure 95. Nomarski interference contrast micrograph of sample L16, 1.2 J/cm^2 double-frequency laser-irradiated.

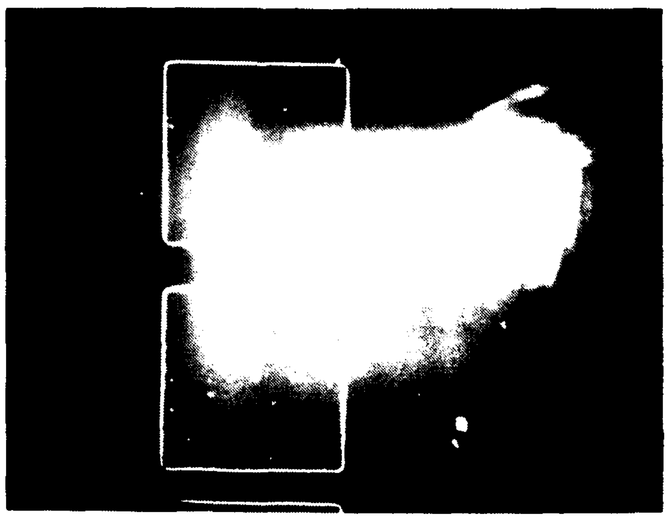

Figure 96. Nomarski interference contrast micrograph of unalloyed Ti-Pt-Au contact pads on laser-irradiated sample L16. Magnification: 200X.

(RHEED) analyses*, respectively. Some correlations between the electrical activation, surface structures, and the crystallinity were observed.

Table 34 lists characteristics of Si-implanted GaAs irradiated with either a laser or an electron beam. The laser beams are either from a ruby laser (λ = 0.69 μm) or a Nd:glass laser with a frequency doubler (λ = 1.06 and 0.53 μm). Both the laser and electron beam are pulse-operated, as described previously. The sheet resistances are obtained from van der Pauw measurements. The surface structures referred to are those measured using SEM or Nomarski interference contrast micrograph. Table 34 indicates the following correlations between the electrical activation, surface structures, and crystallinities.

(1) Under irradiation conditions where the implanted layer turns into single crystal, the sheet resistance is low (24 to 57 Ω/□), and the SEM shows no structures on the surface [Figs. 97(a) and (b)]. The sample (73F) irradiated with a high energy-density laser pulse, however, visually appears wavy on the surface. A Nomarski interference contrast micrograph [Fig. 98(a)] shows an uneven rippled surface. Similar ripples [13] were observed on laser-annealed Si surfaces, and it was suggested that the ripple formation occurs when the melting threshold is periodically exceeded.

(2) Under irradiation conditions where the implanted layer turns polycrystalline, the sheet resistance is high ($\gtrsim$100 Ω/□), and the SEM shows microstructures on the surface [Figs. 99(a) and (b)] although the surface visually (or viewed with the aid of a Nomarski interference microscope) appears smooth.

Table 34 also shows that unalloyed ohmic contacts can be formed onto ion-implanted GaAs layers which become polycrystalline after laser or electron-beam irradiation; this occurs when either the energy densities of the beams or the implanted impurity concentrations are low. These ohmic contacts will not be very practical because of the high sheet resistances of the non-single-crystal (or small grained) GaAs. Samples such as EB1 (electron-beam irradiated) or L16 (dual-frequency laser-beam irradiated) shown in Table 34 are more suitable for unalloyed ohmic contact applications.

*The RHEED analyses were made by J. T. McGinn, RCA Laboratories, Princeton, NJ.

TABLE 34. CHARACTERISTICS OF Si-IMPLANTED GaAs IRRADIATED BY PULSED LASER OR ELECTRON BEAM

Sample	Si-Implant Energy Dose (keV)(cm^{-2})	Crystallinity	Laser or EB Irradiation (J/cm^2)	ρ_s ($\Omega/\square$)	Surface Structure (SEM 20K)
L3*	200 $3x10^{15}$	Both poly and single crystal	0.88 J/cm^2 (λ=1.06& 0.53 μm)	144	yes**
105F	200 $3x10^{15}$	Single crystal	1.0 J/cm^2 (λ=0.69 μm)	57	--
73F	70 $3x10^{15}$	Single crystal	2.3 J/cm^2 (λ=0.69 μm)	24	no†
7D*	70 $3x10^{15}$	Broad rings indicating small grained GaAs	0.8 J/cm^2 (λ=0.69 μm)	148	yes**
EB1*	200 $3x10^{15}$	Single crystal	Elec. Beam 0.7 J/cm^2, 20 keV	45	no**
EB3*	100 $1x10^{15}$	--	Elec. Beam 0.7 J/cm^2 20 keV	--	yes**
L16*	200 $3x10^{15}$ 70 $1x10^{15}$	--	(λ=1.06 & 0.53 μm)	25	no**

Some results of RHEED measurements showing the crystallographic information are given in Fig. 100. Figure 100(a) shows the result of sample 105F which was annealed using a 1.0-J/cm^2 pulsed ruby-laser beam. The diffraction from the surface produces a strong, well-formed diffraction pattern of GaAs. The pattern indicates that the surface of the sample is a (100) plane. Figure 100(b) shows evidence for both poly- and single-crystalline GaAs within 100 Å of the surface for sample L3, which was irradiated with a 0.88-J/cm^2 dual-frequency laser beam (Nd:glass plus frequency doubler). Figure 100(c) shows the diffraction pattern of a single-crystal surface of an electron-beam-irradiated GaAs. The GaAs samples shown in Fig. 100 were Si implanted at 200 keV with fluences of $3x10^{15}$ cm^{-2}.

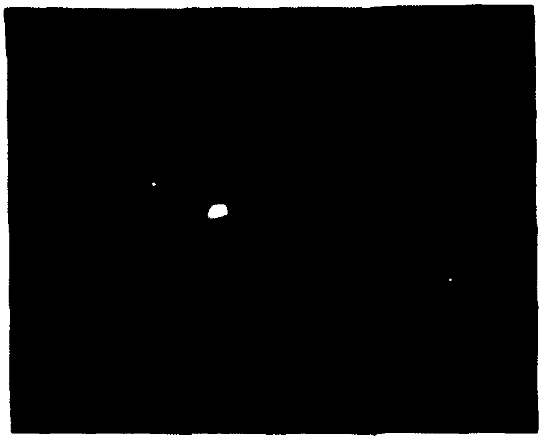

(a)

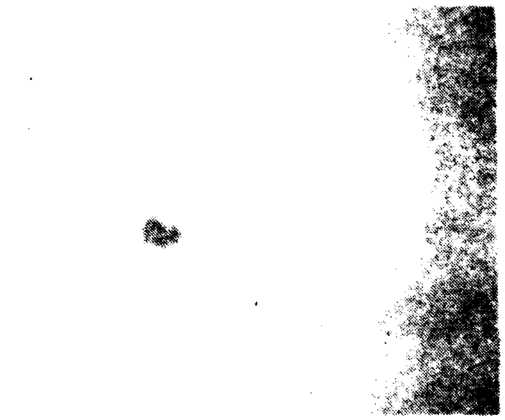

(b)

Figure 97. (a) SEM (10K, 45°) of sample 73F. (b) SEM (20K, 50°) of sample EB1.

(a)

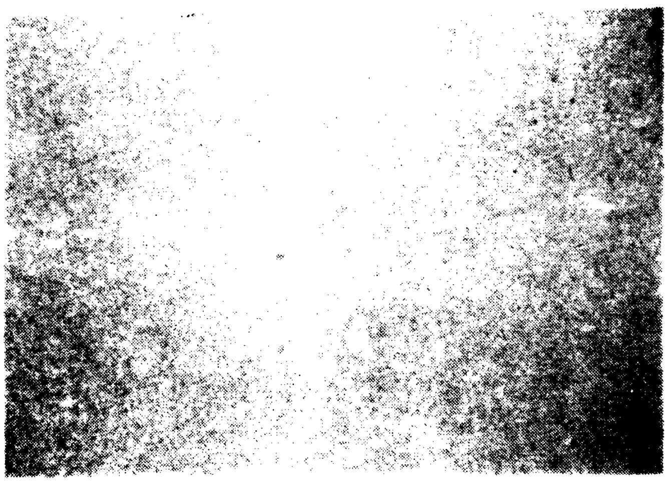

(b)

Figure 98. (a) Nomarski interference contrast micrograph of ruby-laser-annealed (2.3 J/cm^2) sample. (b) SEM of same sample at 20X magnification.

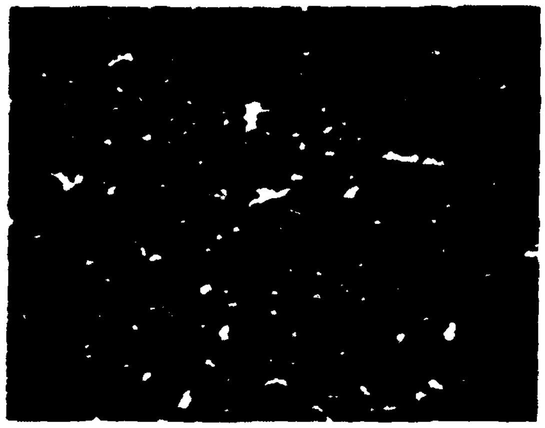

(a)

(b)

Figure 99. (a) SEM (20K, 55°) of sample L3. (b) SEM (20K, 55°) of sample EB3.

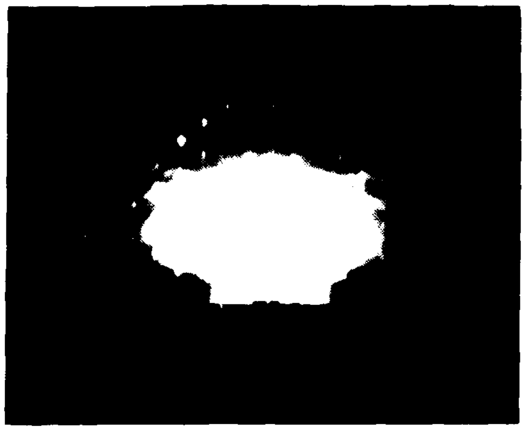

(a)

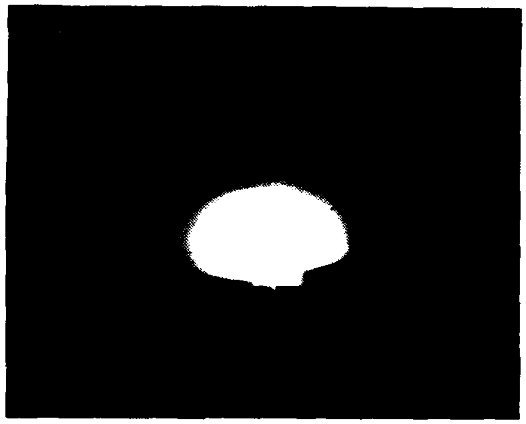

(b)

(c)

Figure 100. (a) RHEED analysis of sample 105F, 1.0 J/cm^2 ruby-laser-irradiated.
(b) RHEED analysis of sample L3, 0.88 J/cm^2 dual-frequency-irradiated.
(c) RHEED analysis of sample EB1, 0.7 J/cm^2 electron-beam-irradiated.

SECTION VIII

SUMMARY

Ion implantation of silicon, sulfur, and selenium in GaAs along with different annealing techniques for producing high-quality n-GaAs layers for microwave and high-speed logic circuit applications were studied. The Si implantations were investigated at energies between 30 and 1200 keV and fluences between $1x10^{12}$ and $5x10^{15}$ cm^{-2} and were measured in various types of SI GaAs substrates including Bridgman Cr doped, LEC Cr doped, LEC undoped, and Cr-O doped. Implantations into these substrates pretreated with high-energy ^{40}Ar implant were investigated in detail and compared with those implants into substrates without the pretreatment. Summarized below are the highlights of this report.

(1) A substrate pretreatment technique has been developed. It consists of ^{40}Ar implantation into SI GaAs substrates at appropriate energy and fluence prior to implantation of ^{28}Si and subsequent thermal anneal. The pretreatment has resulted in enhanced activation and/or mobility for the implanted n-GaAs layer. This effect has, to different extents, been observed in Bridgman and LEC Cr-doped, LEC undoped, and Cr-O-doped SI GaAs substrates.

Silicon-implanted, thermally annealed n-layers in ^{40}Ar-pretreated Bridgman-grown SI GaAs substrates show, for example, greatly enhanced low-dose ($2x10^{12}$-cm^{-2}, 200-keV) activation and mobility. The pretreatment technique reduces the "implant threshold" in the substrate, thus producing n-layers of low doping and high mobility.

This operationally simple pretreatment technique will allow the use of a variety of SI GaAs substrates. Another benefit is that it might be possible to improve the doping and thickness uniformity (hence FET pinch-off voltage uniformity - a major concern of gigabit-rate ICs) across the implanted wafer.

(2) Depth profiles and range statistics of ^{28}Si implantation in GaAs with energies up to 1.2 MeV were studied using SIMS analysis. Based on the information obtained, uniformly doped 0.2- to 1.0-μm n-layers having mobilities of 4700 to 4450 cm^2/V-s with carrier concentrations of 0.5-$2x10^{17}$ cm^{-3} and uniformly doped 1-μm n^+-layers having a mobility of 3000 cm^2/V-s with a carrier concentration of $1x10^{18}$ cm^{-3} were produced by multiple implantation and capless thermal annealing under arsenic overpressure.

(3) An operationally simple capless annealing process was developed. The anneal was performed under an arsenic overpressure produced by a constant flow of H_2 and AsH_3 through an open quartz tube. The arsenic overpressure prevents decomposition of GaAs and results in an excellent surface morphology.

Temperature-dependence studies of the capless annealing process showed that high dose ($>10^{14}$ cm^{-2}, 200 keV) Si-implanted samples annealed at 900°C give a higher electrical activation and lower sheet resistance than those annealed at 825°C.

(4) Cr-redistribution studies using SIMS in thermally annealed Si implants in SI GaAs substrates show a strong dependence of Cr redistribution on implant fluence. No significant redistribution was found for doses typically used for FET fabrication. At higher dose levels, pulsed-laser-irradiated implants show much less Cr redistribution than thermally annealed GaAs. The ^{40}Ar implanted GaAs layers show similar Cr-redistribution effects as in the ^{28}Si implants.

(5) Investigation of $^{28}Si^+$ and $^{32}S^+$ implanted capless-annealed GaAs at the low implant energy (<300 keV) shows that the carrier concentrations are limited at the high dose to about 3×10^{18} cm^{-3} following capless annealing at 825°C for 20 min and limited at the low dose to about 5×10^{16} cm^{-3}. A "cutoff" fluence of about 2×10^{12} cm^{-2} at 200-keV implant was observed in Bridgman Cr-doped GaAs substrates used for implant. The diffusion coefficient at the annealing temperature was deduced from electron density profiles to be $2\text{-}5\times10^{-14}$ cm^2/s for S in GaAs and less than $\sim10^{-15}$ cm^2/s for Si in GaAs.

The surface of the as-implanted SI GaAs substrates exhibits electrical conduction as a result of lattice disorders. The dependence of the sheet conductivity on implantation dose was determined experimentally. The conductivity provides a convenient way of monitoring the as-implanted GaAs.

(6) High-dose Si-implanted GaAs was annealed using high-power pulsed laser and electron beams. Electrical activation of high-dose implanted samples are many times higher in laser-annealed samples than for those thermally annealed. Activation of 1-MeV implanted GaAs with peak electron density over 1×10^{19} cm^{-3} was demonstrated by using a high-power subbandgap Nd:glass laser (λ = 1.06 μm).

(7) Unalloyed ohmic contacts were formed on laser-irradiated GaAs using AuGe/Ni or Ti/Pt/Au metallization. The crystallinity of laser-(or electron-beam) irradiated Si-implanted GaAs was studied using reflection high-energy diffraction (RHEED) analysis. Auger analysis was used to study the ohmic-contact characteristics.

Optical absorption has been studied in Si-implanted GaAs wafers irradiated with high-power Nd:glass laser pulses. Measurements show that the implant-enhanced absorption at a given infrared wavelength increases with implant dose. The enhanced absorption is greatly reduced following annealing as a result of lattice reordering.

(8) Impurity distribution in as-implanted, thermally annealed, and laser-annealed samples has been investigated by SIMS analysis. The amount of impurity redistribution depends upon the energy and dose of implantation and upon the energy density of the laser pulse used to anneal the sample. A substantial impurity broadening was observed in the high-dose-implanted samples irradiated with a high energy-density ($\sim 2\ J/cm^2$) pulse. The broadening is believed to be associated with a diffusion in the liquid GaAs created by the high-energy laser pulse. An uneven ripple observed on such a surface using a Nomarski interference contact micrograph indicated the occurrence of melting at the sample surface.

(9) Si-implanted GaAs samples were successfully annealed with good mobility and activation using a short duration (<10 s) radiant pulse produced by a halogen lamp. This rapid annealing technique could reduce impurity redistribution in the substrate and improve the depth profile of implanted n-GaAs layers.

(10) The success in producing high-quality n-GaAs layers by direct implant of ^{28}Si into SI GaAs was demonstrated in a concurrent company-sponsored program by fabrication of high-performance GaAs power FETs operating up to 26 GHz.

REFERENCES

1. S. G. Liu, E. C. Douglas, and C. P. Wu, "High-Energy Ion Implantation for Multigigabit-Rate GaAs Integrated Circuit," Annual Report, May 15, 1978 to May 14, 1979, also May 15, 1979 to June 30, 1980, under Contract No. N00014-78-C-0367.
2. B. M. Welch, F. H. Eisen, and J. A. Higgins, "Gallium Arsenide Field Effect Transistors by Ion Implantation," J. Appl. Phys. 45, 3685 (1974).
3. E. Stoneham, T. S. Tan, and J. Gladstone, "Fully Ion-Implanted GaAs Power FETs," 1977 IEDM Digest, p. 330.
4. R. A. Murphy et al., 1974 IEEE S-MTT Int. Symp., New York, p. 345.
5. C. O. Bozler et al., "High-Efficiency Ion-Implanted Lo-Hi-Lo GaAs IMPATT Diodes," Appl. Phys. Lett. 29, 123 (1976).
6. T. Mizutani and K. Kurumada, "GaAs Planar Gunn Digital Devices by Sulfur Ion-Implantation," Electron. Lett. 11, 639 (1975).
7. L. C. Upadhyayula, S. Y. Narayan, and E. C. Douglas, "Fabrication of 3-Terminal Transferred-Electron Logic Devices by Proton Bombardment for Device Isolation," Electron. Lett. 11, 201 (1975).
8. B. M. Welch and R. C. Eden, "Planar GaAs Integrated Circuits Fabricated by Ion Implantation," Technical Digest, Int. Elec. Devices Meeting, 1977, p. 205.
9. S. G. Liu, E. C. Douglas, C. P. Wu, C. W. Magee, S. Y. Narayan, S. T. Jolly, F. Kolondra, and S. Jain, "Ion-Implantation of Sulfur and Silicon in GaAs," RCA Review 41, 227 (1980).
10. S. G. Liu, E. C. Douglas, C. W. Magee, F. Kolondra, and S. Jain, "High-Energy Implantation of Si in GaAs," Appl. Phys. Lett. 37, 79 (1980).
11. G. C. Taylor, S. G. Liu, and D. Bechtle, "Ion-Implanted K-Band GaAs Power FET," IEEE/MTT Intnl. Microwave Symp. Digest, June 1981.
12. E. I. Shtyrkov, I. B. Khaibullin, M. M. Zaripov, M. F. Galyatudinov, and R. M. Bayazitov, "Local Annealing of Implantation Doped Semiconductor Layers," Sov. Phys. Semicond. 9, 1309 (1976).

13. W. L. Brown, J. A. Gdovchenko, K. A. Jackson, L. C. Kimerling, H. J. Leamy, G. L. Miller, J. M. Poate, J. W. Rodgers, G. A. Rozgonyi, T. T. Sheng, T. N. C. Venkatesan, and G. K. Celler, "Laser-Annealing of Ion-Implanted Semiconductors," Proc. on Rapid Solidification Proc. - Principles and Technologies, Reston, VA, Nov. 1977.
14. R. T. Young, C. W. White, G. J. Clark, J. Narayan, W. H. Christie, M. Murakami, P. W. King, and S. D. Karmer, "Laser Annealing of Boron-Implanted Silicon," Appl. Phys. Lett. 32, 139 (1978).
15. S. U. Compisano, I. Catalano, G. Foti, E. Rimini, F. Eisen, and M. A. Nicolet, "Laser Reordering of Implanted Amorphous Layers in GaAs," Solid-State Electron. 21, 485 (1978).
16. J. L. Tandon and F. H. Eisen, "Pulsed Annealing of Implanted Semi-Insulating GaAs," AIP Conf. Proc. 50, 616 (1979).
17. M. Arai, K. Nishiyama, and N. Watanabe, "Radiation Annealing of GaAs Implanted with Si," Jpn. J. Appl. Phys. 20, L124 (1981).
18. S. G. Liu, C. P. Wu, and C. W. Magee, "Annealing of Ion-Implanted GaAs with Nd:Glass Laser," AIP Conf. Proc. 50, 603 (1979).
19. B. J. Sealy, M. H. Badawi, S. S. Kular, and K. G. Stephens, "Electrical Properties of Laser-Annealed Donor-Implanted GaAs," Electron. Lett. 14, 720 (1978).
20. S. G. Liu, C. P. Wu, and C. W. Magee, "Annealing of Ion-Implanted GaAs with a Pulsed Ruby Laser," Symp. Proc. on Laser and Elec. Beam Processing of Materials, Academic Press, 1980, p. 341.
21. A. M. Huber, G. Morillot, and N. T. Linh, "Chromium Profiles in Semi-Insulating GaAs after Annealing with a Si_3N_4 Encapsulant," Appl. Phys. Lett. 34, 858 (1979).
22. R. G. Wilson, P. K. Vasuder, D. M. Jamba, C. A. Evans, Jr., and V. R. Deline, "Chromium Concentrations, Depth Distributions and Diffusion Coefficient in Bulk and Epitaxial GaAs and in Si," Appl. Phys. Lett. 36, 215 (1980).
23. J. Kasahara and N. Watanabe, "Redistribution of Cr in Capless-Annealed GaAs Under Arsenic Pressure," Jpn. J. Appl. Phys. 19, L151 (1980).
24. C. A. Evans, Jr. and V. R. Deline, "Redistribution of Cr During Annealing of ^{80}Se-Implanted GaAs," Appl. Phys. Lett. 35, 291 (1979).

25. F. H. Eisen et al., "Sulfur, Selenium, and Tellerium Implantation in GaAs," Inst. Phys. Conf. Proc. 28, 64 (1976).
26. R. K. Surridge and B. J. Sealy, "A Comparison of Sn-, Ge-, and Te-ion-implanted GaAs." J. Phys. D: Appl. Phys. 10, 911 (1977).
27. J. K. Kung, R. M. Melbon, and D. H. Lee, "GaAs FETs with Silicon-Implanted Channels," Election. Lett. 13, 187 (1977).
28. A. G. Foyt, J. P. Donelly, and W. T. Lindley, "Efficient Doping of GaAs by Se^+ Ion Implantation," Appl. Phys. Lett. 14, 372 (1969).
29. W. K. Chu et al., Proc. 3rd. Intnl. Conf. on Ion Imp., Plenum Press, New York, 1973.
30. R. D. Pashley and B. M. Welch, "Tellurium-Implanted N^+ Layers in GaAs," Solid State Electron. 18, 997 (1975).
31. A. Lidow and J. F. Gibbons, "A Double-Layered Encapsulant for Annealing Ion-Implanted GaAs Up to 1100°C," Appl. Phys. Lett. 31, 158 (1977).
32. B. J. Sealy and R. K. Surridge, "A New Thin Film Encapsulant for Ion-Implanted GaAs," Thin Solid Films 26, L19 (1974).
33. A. A. Immorlica and F. H. Eisen, "Capless Annealing of Ion-Implanted GaAs," Appl. Phys. Lett. 29, 94 (1976).
34. D. H. Lee, R. M. Malbon, and J. M. Whelan, "Characteristics of Implanted N-type Profiles in GaAs Annealed in a Controlled Atmosphere," Ion-Implanted Semiconductors, ed. by F. Chernow et al., Plenum Press, New York, 1976.
35. J. Kasahara, M. Arai, and N. Watanabe, "Effect of Arsenic Partial Pressure on Capless Anneal of Ion-Implanted GaAs," J. Electrochem. Soc. 126, 1997 (1979).
36. J. R. Arthur, "Vapor Pressures and Phase Equilibria in the GaAs System," J. Phys. Chem. Solids 28, 2257 (1967).
37. P. Williams, R. K. Lewis, C. A. Evans, and P. R. Hanley, "Evaluation of a Cesium Primary Ion Source on an Ion Microprobe Mass Spectrometer," Anal. Chem. 49, 1399 (1977).
38. C. W. Magee, "Depth Profiling of n-Type Dopants in Si and GaAs Using C_s^+ Bombardment Negative Secondary Ion Mass Spectrometry in Ultra-High Vacuum," J. Electrochem. Soc. 126, 600 (1979).

39. A. Lidow, J. F. Gibbons, V. R. Deline, and C. A. Evans, Jr., "Solid Solubility of Selenium in GaAs as Measured by Secondary Ion Mass Spectrometry," Appl. Phys. Lett. 32, 572 (1978).

40. Y. Kato et al., "Electrical Conductivity of Disordered Layers in GaAs Crystal Produced by Ion Implantation," J. Appl. Phys. 45, 1044 (1974).

41. L. J. van der Pauw, "A Method of Measuring Specific Resistivity and Hall Effect of Discs of Arbitrary Shape," Philips Res. Rep. 13, 1 (1958).

42. J. F. Gibbons et al., Projected Range Statistics, 2nd. ed. (Halsted Press, A Div. of John Wiley and Sons, Inc., 1975).

43. D. L. Rode and S. Knight, "Electron Mobility in GaAs," Phys. Rev. B3, 2534 (1971).

44. C. O. Thomas, D. Kahng, and R. C. Manz, "Impurity Distribution in Epitaxial Silicon Films," J. Electrochem. Soc. 109, 1055 (1962).

45. C. P. Wu, E. C. Douglas, and C. W. Mueller, "Limitations of the CV Technique for Ion-Implanted Profiles," IEEE Trans. Electron Devices ED-22, 319 (1975).

46. A. B. Y. Young and G. L. Pearson, "Diffusion of Sulfur in GaP and GaAs," J. Phys. Chem. Solid 31, 517 (1970).

47. A. Asai and H. Kodera, "Electrical Properties of n-type Layers in GaAs prepared by Solid Sulfur Diffusion," Proc. of the 4th. Int. Symp., Boulder, CO, 1972, p. 130.

48. P. L. Kendall, Semiconductors and Semimetals, vol. 4, (Academic Press, New York, 1968).

49. R. Baron, G. A. Shifrin, and O. J. Marsh, "Electrical Behavior of Group III and V Implanted Dopants in Silicon," J. Appl. Phys. 40, 3702 (1969).

50. J. W. Mayer, L. Eriksson, and J. A. Devices, Ion Implantation in Semiconductors, (Academic Press, New York, 1970), p. 193.

51. M. G. Kendall and A. Stuart, The Advanced Theory of Statistics, (Charles Griffin, London, 1958), vol. 1, p. 148.

52. W. P. Elderton, Frequency Curves and Correlation, 4th ed. (Cambridge Univ. Press, 1953).

53. W. K. Hofker, "Implantation of Boron in Silicon" Philips Research Supplements 8, 1975.

54. S. Sze, Physics of Semiconductor Devices, (John Wiley & Sons, Inc., New York, 1969).

55. W. Walukiewicz et al., "Electron Mobility & Free Carrier Absorption in GaAs: Determination of the Compensation Ratio," J. Appl. Phys. 50, 899 (1979).

56. M. N. Yoder, "Complexes and Their Effects on III-V Compounds," in Semi-Insulating III-V Materials, (Shiva Publishing Ltd., Nottingham, 1980), pp. 281-287.

57. M. R. Brozel et al., "Electrical Compensation in Semi-Insulating Gallium Arsenide," J. Phys. C., Solid State Phys. 11, 1857 (1978).

58. L. A. Christel and J. F. Gibbons; to be published.

59. See, for example, J. Pankove, Optical Processes in Semiconductors, (Prentice-Hall, Inc., Englewood Cliffs, NJ, 1971), P. 10.

60. P. A. Pianetta, C. A. Stolte, and J. L. Hauser, "Pulsed E-Beam and Ruby Laser Annealing of Ion-Implanted GaAs," Symp. Proc. on Laser and Electron Beam Processing of Materials, Academic Press, 1980.

61. J. C. Wang, R. F. Wood, and P. P. Pronko, "Theoretical Analysis of Thermal and Mass Transport in Ion-Implanted Laser-Annealed Silicon," Appl. Phys. Lett. 33, 445 (1978).

62. W. D. Edward et al., "Specific Contact Resistance of Ohmic Contacts to GaAs," Solid State Electron. 15, 388 (1972).

63. Y. Goldberg and B. V. Tsarenkov, "Dependence of the Resistance of Metal GaAs Ohmic Contacts on the Carrier Density," Soviet Phys. Semicond. 3, 1447 (1970).

64. H. H. Berger, "Models for Contacts to Planar Device," Solid State Electron. 15, 145 (1972).

65. P. A. Barnes and A. Y. Cho, "Nonalloyed Ohmic Contacts to n-GaAs by Molecular Beam Epitaxy," Appl. Phys. Lett. 33, 651 (1978).

66. R. L. Mozzi, W. Fabian, and F. J. Piekarcki, "Nonalloyed Ohmic Contacts to N-GaAs by Pulse Electron Beam-Annealed Selenium Implants," Appl. Phys. Lett. 35, 337 (1979).

67. M. N. Yoder, "Ohmic Contacts in GaAs," Solid State Electron. 23, 117 (1980).

DISTRIBUTION LIST

Code 414 Office of Naval Research Arlington, VA 22217	4
Naval Research Laboratory 4555 Overlook Avenue, S.W. Washington, D.C. 20375	
Code 6811	1
6850	1
6820	1
Defense Documentation Center Building 5, Cameron Station Alexandria, VA 22314	12
Dr. Y. S. Park AFWAL/DHR Building 450 Wright-Patterson AFB Ohio 45433	1
ERADCOM DELET-M Fort Monmouth, NJ 07703	1
Texas Instruments Central Research Lab M.S. 134 13500 North Central Expressway Dallas, TX 75265 Attn: Dr. W. Wisseman	1
Dr. R. M. Malbon/M.S. 1C Avantek, Inc. 3175 Bowers Avenue Santa Clara, CA 94304	1
Mr. R. Bierig Raytheon Company 28 Seyon Street Waltham, MA 02154	1
Dr. R. Bell, K-101 Varian Associates, Inc. 611 Hansen Way Palo Alto, CA 94304	1
Dr. Mike Driver Westinghouse Research and Development Center Beulah Road Pittsburgh, PA 15235	1
Dr. D. Richard Decker Rockwell International Science Center P.O. Box 1085 Thousand Oaks, CA 91360	1
Dr. C. Krumn Hughes Research Laboratory 3011 Malibu Canyon Road Malibu, CA 90265	1
Mr. Lothar Wandinger ECOM/AMSEL/TL/IJ Fort Monmouth, NJ 07003	1
Dr. Harry Wieder Naval Ocean Systems Center Code 922 271 Catalina Blvd. San Diego, CA 92152	1
Dr. William Lindley MIT Lincoln Laboratory F124 A, P.O. Box 73 Lexington, MA 02173	1
Commander U. S. Army Electronics Command V. Gelnovatch (DRSEL-TL-IC) Fort Monmouth, NJ 07703	1
RCA Microwave Technology Center Dr. F. Sterzer Princeton, NJ 08540	1

Hewlett-Packard Corporation 1
Dr. Robert Archer
1501 Page Road
Palo Alto, CA 94306

Watkins-Johnson Company 1
E. J. Crescenzi, Jr./
K. Niclas
3333 Hillview Avenue
Stanford Industrial Park
Palo Alto, CA 94304

Commandant 1
Marine Corps
Scientific Advisor (Code AX)
Washington, D.C. 20380

Communications Transistor Corp. 1
Dr. W. Weisenberger
301 Industrial Way
San Carlos, CA 94070

Microwave Associates 1
Northwest Industrial Park
Drs. F. A. Brand/J. Saloom
Burlington, MA 01803

Commander, AFAL 1
AFWAL/AADM
Dr. Don Rees
Wright-Patterson AFB, Ohio 45433

Professor Walter Ku 1
Phillips Hall
Cornell University
Ithaca, NY 14853

Commander 1
Harry Diamond Laboratories
Mr. Horst W. A. Gerlach
800 Powder Mill Road
Adelphia, MD 20783

Advisory Group on Electron 1
Devices
201 Varick Street, 9th Floor
New York, NY 10014

Dr. Ken Weller 1
MS/1414
TRW Systems
One Space Park
Redondo Beach, CA 90278

Professor L. Eastman 1
Phillips Hall
Cornell University
Ithaca, NY 14853

Professor Hauser and 1
Littlejohn
Department of Electrical Engr.
North Carolina State University
Raleigh, NC 27607

Professor J. Beyer 1
Department of Electrical & Computer Eng.
University of Wisconsin
Madison, WI 53706

Professor Rosenbaum & Wolfe 1
Semiconductor Research Laboratory
Washington University
St. Louis, MO 63130

W. H. Perkins 1
Electronics Lab 3-115/B4
General Electric Company
P.O. Box 4840
Syracuse, NY 13221

Bryan Hill 1
AFWAL/AADE
Wright-Patterson AFB, Ohio 45433

H. Willing/Radar Directorate 1
BMD - Advanced Technical Center
P.O. Box 1500
Huntsville, Alabama 35807

DATE
FILMED

2-8